1. Introduction

1.1 Project Objectives

Sandia National Laboratories conducted a research project, funded by the Engineering Research Applications Branch, Office of Nuclear Regulatory Research at the Nuclear Regulatory Commission (NRC), to pursue the following objectives:

1. To investigate the dynamic responses of freestanding dry cask storage systems subjected to a prescribed seismic excitation. Three site-specific analyses and a comprehensive set of parametric analyses were performed using the following procedure:
   a) Develop a coupled finite element model of a freestanding cask/module, a concrete pad, and a foundation.
   b) Apply appropriate sets of prescribed seismic time histories to the model.
   c) Apply appropriately selected material properties to the submodels and coefficients of friction at their interfaces.
2. To provide support to the NRC in revising the regulatory guidelines and facilitate the safety review of licensing applications by the Nuclear Material Safety and Safeguards staff for the dry cask storage systems. The parametric analysis results were compiled in nomograms to assist this process.

1.2 Background

The Spent Fuel Project Office (SFPO) in the Office of the Nuclear Material Safety and Safeguards (NMSS) at the NRC has been involved in investigating technical issues concerning the dry storage and transportation of spent nuclear fuel. Sandia National Laboratories was contracted by the Engineering Research Applications Branch, Office of Nuclear Regulatory Research (RES) at the NRC for investigating the seismic behavior of dry cask storage systems (DCSS) containing spent fuel. The results of this research effort are expected to aid the NMSS staff in performing the safety review of licensing applications of DCSSs by assessing their dynamic response in terms of sliding, tipping, collision of neighboring casks, and the integrity of cask internals under seismic loads.

Dry storage of spent fuel above ground has become an accepted "repository" alternative by installing DCSSs at an Independent Spent Fuel Storage Installation (ISFSI) (which is licensed under 10 CFR Part 72 [1]), consisting of arrays of freestanding storage casks on a concrete pad. Many ISFSIs have been licensed and installed inside operating nuclear power plants, and a few sites are in the licensing application process, as shown in Figures 1.1, and 1.2, respectively.

Most of the casks/modules are freestanding on a concrete pad, rather than anchored like typical civil structures. This results in a rather complicated nonlinear contact problem at the cask/pad interface after the onset of cask rocking, rolling, or sliding motion. Consequently, there are safety concerns about the possibility of a cask tipping over and collision in an earthquake event. Three-dimensional coupled finite element models with explicit time integration were developed to investigate the highly nonlinear dynamic seismic responses of casks. The ABAQUS [2] finite element analysis program, Version 6.4, was used to analyze these coupled models consisting of three submodels: a cylindrical cask or a rectangular module, a flexible concrete pad, and an underlying foundation. Contact constraints were employed at the interfaces between the cask and pad and the pad and the foundation.. The seismic event was described by one vertical and two horizontal components of statistically independent seismic acceleration time histories. A deconvolution procedure was used to adjust the amplitudes and frequency contents of these three-component reference surface motions before applying them simultaneously at the foundation base.

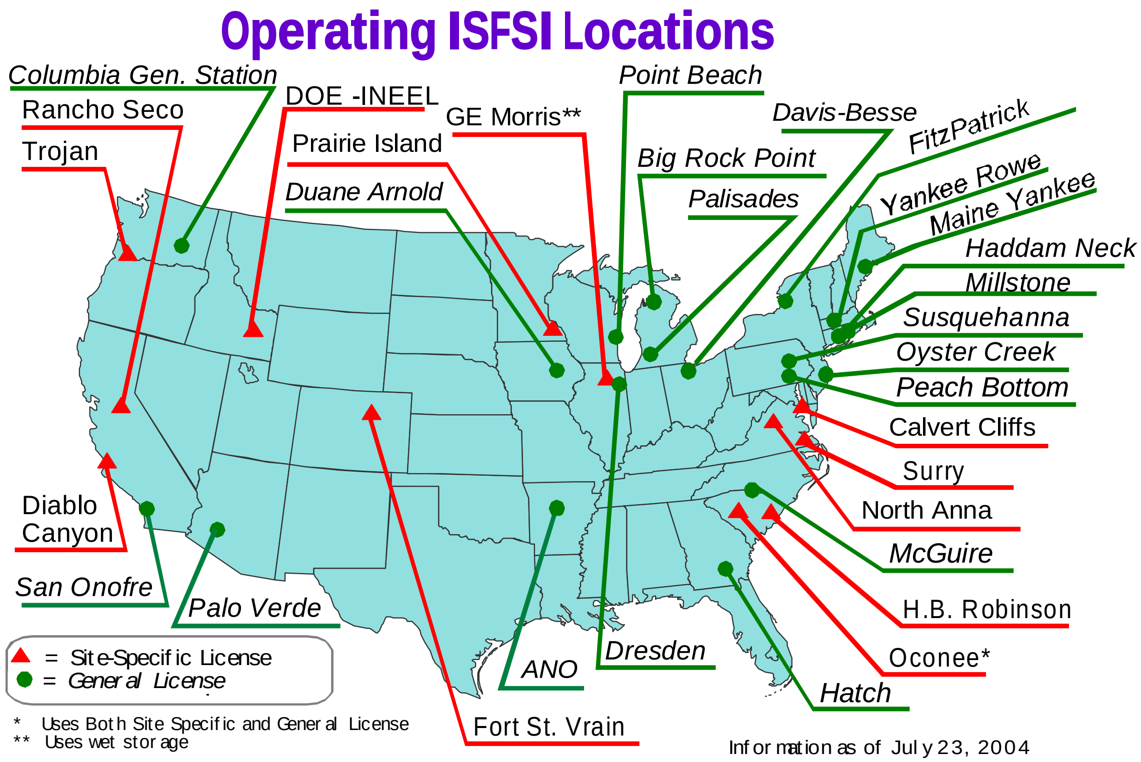

Figure 1.1: Operating Spent Fuel ISFSI Sites

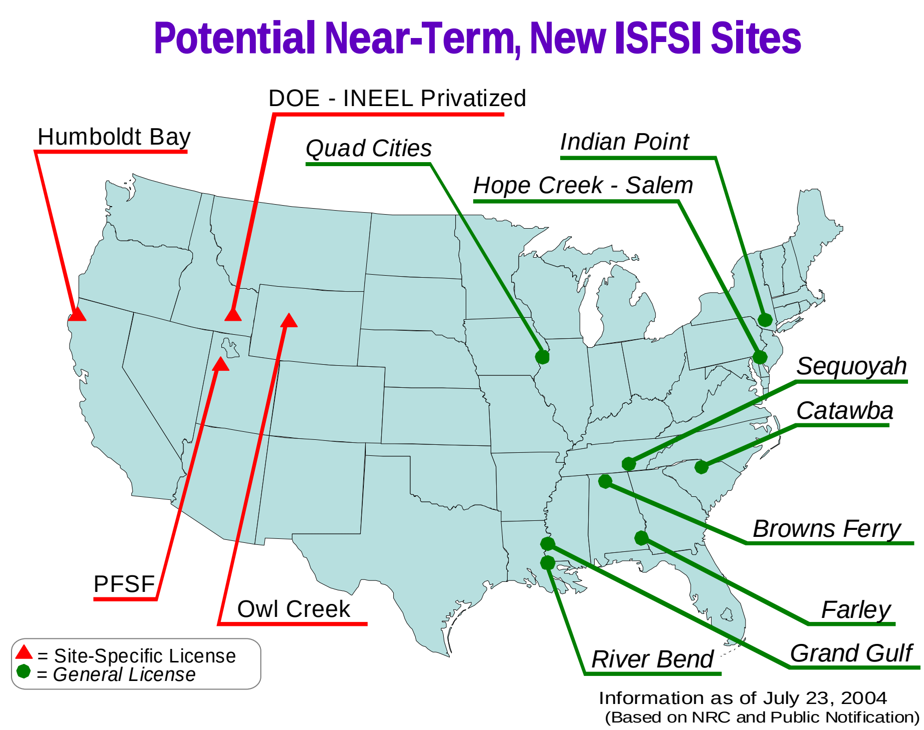

Figure 1.2: Potential New Applications for ISFSI Sites

Coupled models very similar to those used in the parametric study summarized in this report have already been used to perform three site-specific analyses for the three-module rectangular Transnuclear West module/cask [3] and HI-STORM 100 casks at Hatch Nuclear Power Station [4] and at Private Fuel Storage Facility [5]. Most of those analysis results indicated that the cask or module usually experiences higher sliding displacements with a lower coefficient of friction at the cask/pad interface and higher angular rotations with respect to the vertical axis for a higher coefficient of friction. The lessons learned from the site-specific analyses helped guide the much broader parametric analyses summarized in this report. This report documents the details of the coupled models as well as all analysis results from the parametric analyses.

1.3 Report Organization

A variety of modeling approaches have been used to evaluate the nonlinear seismic behavior of casks/modules. Some modeling details and technical merits of these approaches will be discussed in Chapter 2. Chapter 3 is devoted to covering details of the coupled models including the coupled analysis philosophy and methodology as well as model details of vertical cylindrical casks and horizontal rectangular modules. The coupled modeling approach provides a realistic simulation for soil-structure interaction effects and the nonlinear cask behavior associated with the cask rocking or rolling motion. Applying simultaneously a vertical and two horizontal components of surface defined seismic acceleration time histories at the foundation base requires a mathematically based deconvolution procedure that preserves the dynamic characteristics of seismic ground motions. The modeling issues are further complicated by providing justification of simulating a semi-infinite foundation by a finite body with properly prescribed boundary conditions.

The scope of parametric analyses of two selected cask designs, vertical cylindrical casks and horizontal rectangular modules, are discussed in Chapter 4. The characteristics of the seismic input motions are governed by the selection of three spectral curve shapes (NUREG/CR-0098 [6], Regulatory Guide 1.60 [7], and NUREG/CR-6728 [8]), five selected earthquake records for each spectral shape, and five surface peak ground accelerations (PGA) ranging from 0.25 to 1.25 g. Three different foundation types are chosen for analyses including soft soil, stiff soil, and weathered rock foundations. The nonlinear contact at the cask/pad interface is simulated by three coefficients of friction covering the lower bound (0.20), the median (0.55), and the upper bound (0.80).

All parametric analysis results from the coupled models are presented and discussed in Chapter 5. Analysis results are plotted for graphical representation and compiled in nomograms. The parametric analysis findings are summarized in Chapter 6, conclusions are given in Chapter 7, and all relevant references are listed in Chapter 8.

INTENTIONALLY LEFT BLANK

2. Approaches to Evaluate Nonlinear Seismic Behavior of Casks

The research effort in this project focused on investigating the nonlinear dynamic behavior of freestanding dry cask systems in a seismic event. The cask and the pad experience translational and rotational motions relative to each other and to the foundation when subjected to seismic ground motions. The combination of frictional contact at the cask/pad interface and soil-structure interaction results in a highly nonlinear cask response. This chapter is devoted to describing the physical problem under investigation, various modeling approaches to analyze this problem, and the philosophy leading to the development of the coupled models used in this project.

2.1 Problem Description

In most Independent Spent Fuel Storage Installations (ISFSI), dry cask systems have been installed as freestanding structures on a concrete pad. Physically disconnecting the cask and the pad has financial benefits in terms of reduced installation and future decommissioning costs. In addition, it has enabled the U.S. Nuclear Regulatory Commission (NRC) to enunciate a clear regulatory position on storage casks, permitting the holder of a Part 50 license to deploy an NRC-certified storage cask on a concrete pad without further licensing reviews.

Relatively thin concrete pads have been used in most ISFSIs, nominally 0.61 m (2 feet) for the vertical cylindrical casks and 0.91 m (3 feet) for the horizontal rectangular modules. The design limitations of the casks for impact loads due to drop and tip over have dictated the use of thin concrete pads. As pointed out by Moore et al. [9], a flexible pad should be modeled to account for the out-of-plane flexibility of the ISFSI pad.

The parametric analyses performed in this project investigated the nonlinear responses of the vertical cylindrical casks and the horizontal rectangular modules. Figures 2.1 [10] and 2.2 [11] show typical designs of these two storage systems. Since there is a storage space limitation at most ISFSIs, a design goal is to install as many casks as permitted on a concrete pad, resulting in a fairly small separation distance (within allowable design limits) between neighboring casks, as depicted in Figures 2.3 [10] and 2.4 [11]. Consequently, the possible collision of neighboring casks is a concern in the safety review of the stability of casks in a prescribed earthquake event.

2.2 Survey of Analysis Methods

Moore et al. [9] performed a seismic evaluation of the cylindrical HI-STORM 100 casks in support of the ISFSI design at the Hatch Nuclear Power Plant. They analyzed the problem by investigating the soil-structure interaction to demonstrate the importance of including the out-of-plane flexibility of the pad in the models and its effects on the seismic response of casks. Their seismic model of the cask/pad assembly, developed with the SASSI (System for Analysis of Soil-Structure Interaction) code [12], consists of using plate elements to represent the pad, beam elements for the casks, and beam elements with springs to simulate the contact between the cask and the pad. The strain compatible soil profiles used in the models were generated using the program SHAKE91 [13].

Singh et al. [14] also performed dynamic analyses to predict the structural response of the HI-STAR 100 casks under seismic events. They used the computer code DYNAMO [15] to assemble the dynamic model for the cask system, which includes various internal components of the cask. The mechanical interaction between the cask base and the soil foundation was simulated using vertical compression-only gap elements and horizontal piecewise linear friction elements.

In this project, the research effort focused on providing a realistic assessment of the dynamic stability of storage cask systems under seismic events through truly coupled cask/pad/foundation models. The key features of these coupled models included investigating the highly nonlinear friction contact algorithms at the cask/pad interface and the dynamic soil-structure interaction effect by applying the three components of seismic excitation at the foundation base. The details of the coupled models and the analysis results are discussed in the following chapters.

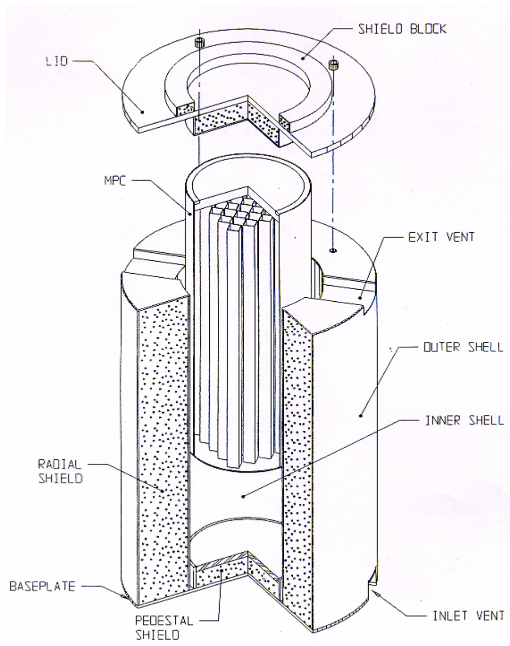

Figure 2.1: Design of a Vertical Cylindrical Cask with Multi-Purpose Canister Partially Inserted

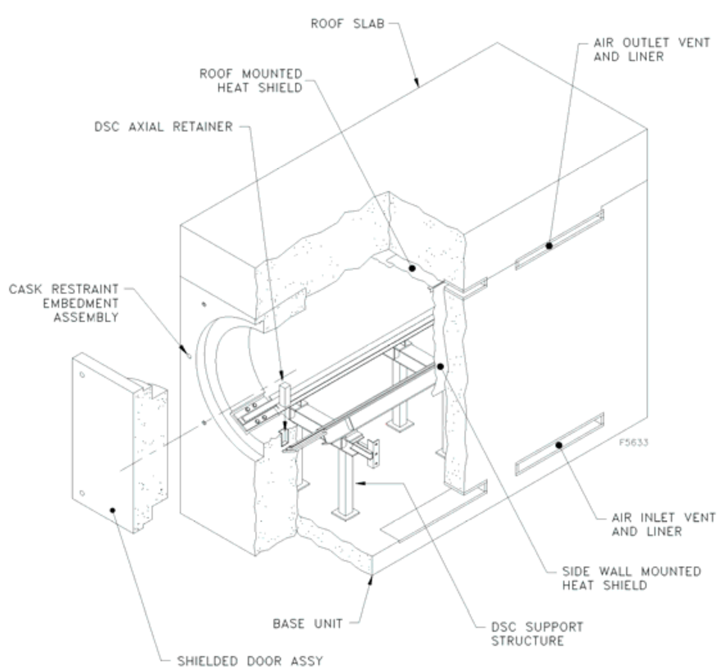

Figure 2.2: Design of a Horizontal Rectangular Module

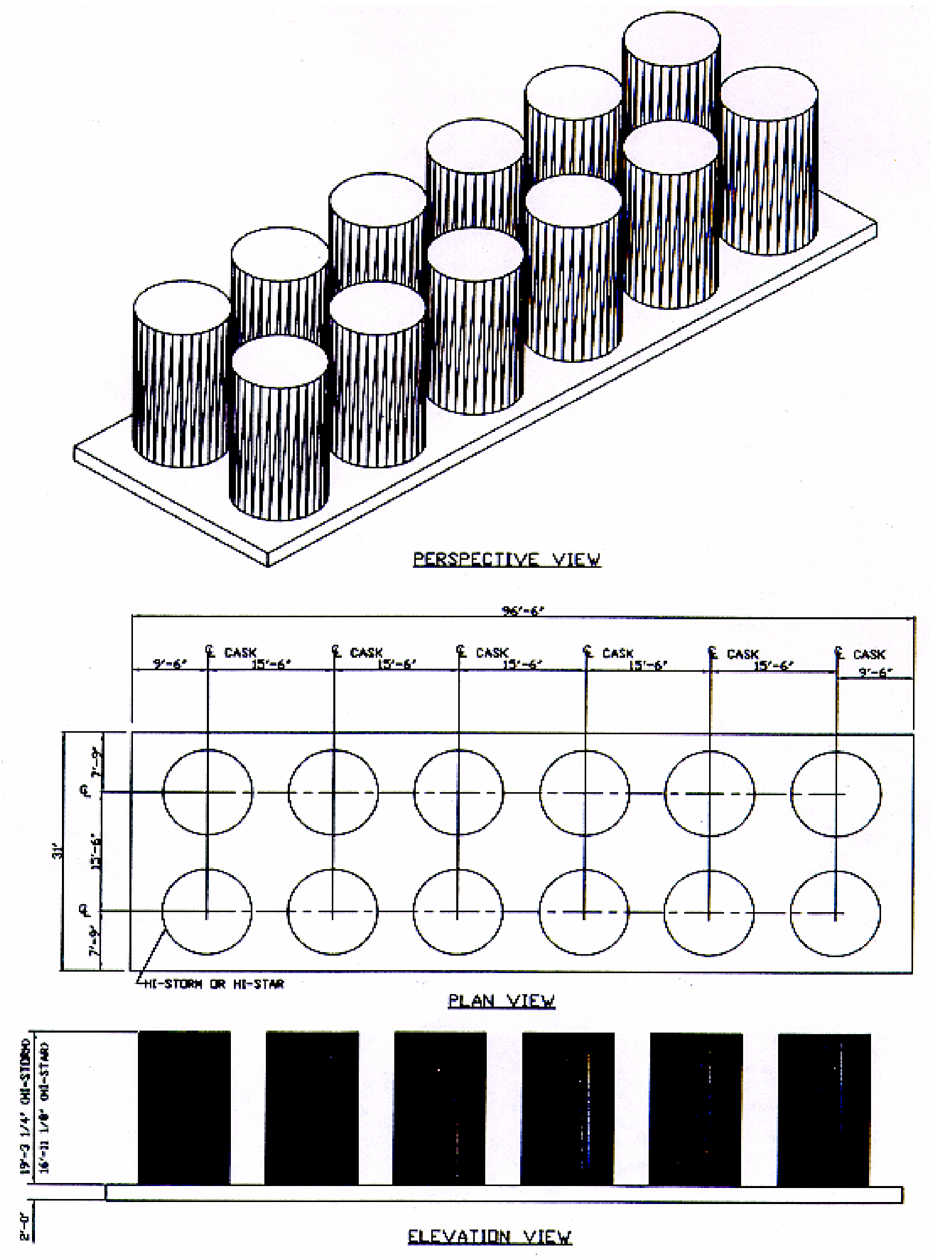

Figure 2.3: Typical HI-STORM 100 Cask Array on an ISFSI Pad at Hatch Nuclear Power Station
Note: 1ft = 30.48 cm

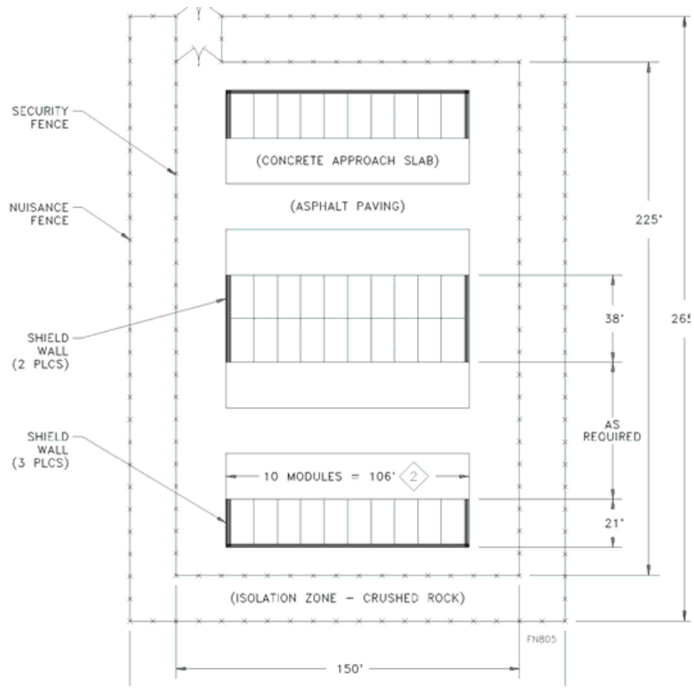

Figure 2.4: Typical ISFSI Layout of Horizontal Rectangular Modules

3. Coupled Finite Element Models

Because of the highly nonlinear nature of the cask response after the onset of sliding or uplift from the pad, it is difficult to apply appropriate methods to characterize the cask response. Realistically modeling the cask response is essential to determine the point at which the cask becomes unstable or collides with a neighboring cask. In the present work, nonlinear finite element analysis has been employed to characterize the full range of cask response. The details of the modeling approach used in this study will be described in this chapter.

3.1 Description of Analysis Approach

3.1.1 Coupled Modeling Methodology

The philosophy of the analysis effort has been to model the full nonlinear behavior of the freestanding cask system as realistically as possible. To that end, the freestanding cask, pad, and foundation are modeled as independent bodies, each capable of experiencing large independent movements relative to one another. Contact constraints are used to model realistically the interactions between these bodies.

The ABAQUS [2] finite element analysis program, Version 6.4, was used to perform these analyses. There are two major components of the ABAQUS program: ABAQUS/Standard, which uses an implicit solver, and ABAQUS/Explicit, which uses an explicit time integration approach. In this work, ABAQUS/Standard was used to apply the gravity load quasi-stacially. Once the gravity load was applied, the analysis was re-started using the final state of the gravity load analysis, and ABAQUS/Explicit was used to analyze the effects of the seismic ground motion while retaining the gravity load. The explicit time domain analysis approach was employed in this work to handle the high degree of nonlinearity present in this problem. Explicit time stepping algorithms are typically used for modeling highly dynamic events of short duration. Very small time steps are used, and the accelerations at the previous time step are used to advance the solution to the current time step.

A solution for the contact constraints, which are an integral part of the problem at hand, can be extremely difficult using implicit methods. The explicit time stepping method was selected for this work because there was no need for an iterative solution of nonlinear equations, as is the case in the implicit methods typically used for analysis of structures under seismic events. Initial attempts were made to use an implicit procedure to perform the nonlinear analysis of the cask response due to earthquake loading, but obtaining a converged solution for this problem became extremely difficult once the cask began to move relative to the pad.

In the explicit method, the size of the time step is controlled by a stability limit, which is a function of the shortest amount of time required for a wave to traverse any of the elements in the model. This means that the time step is typically governed by the size of the smallest element in the model. As the size of the smallest element decreases, the critical time step also decreases, and the time required for the computation increases. For this reason, great care was taken to keep the smallest element as large as possible while still retaining accuracy of the model.

Figure 3.1 shows a finite element model representative of the physical configuration under investigation in this work. In this model, a cask rests on a concrete pad at the top center of a large foundation. Details of the models differ for the cylindrical casks and the rectangular modules selected for parametric analyses, but these models have much in common as discussed in the following subsections.

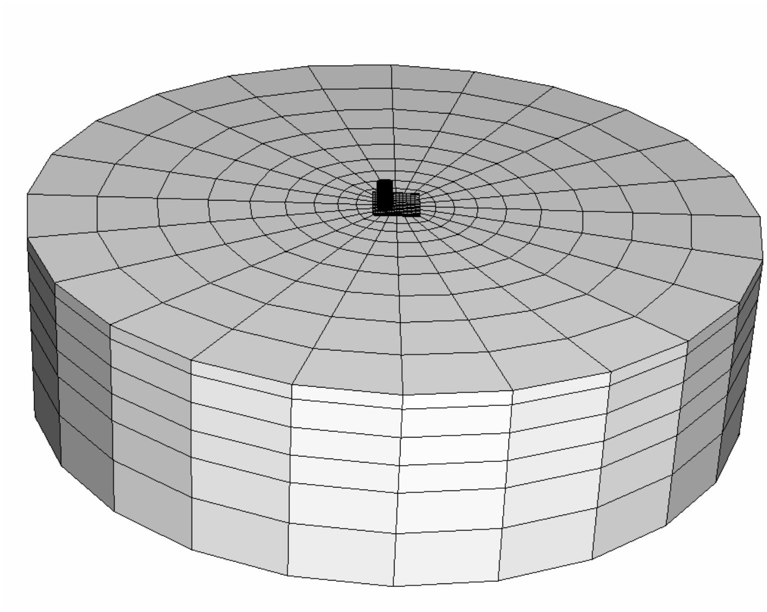

Figure 3.1: Typical Finite Element Model of Cask, Pad, and Foundation

3.1.1.1 Cask Submodel

In the case of the rectangular module model, the module was modeled using standard eight-noded reduced integration solid elements. However, the cylindrical cask was modeled as a rigid body. The rationale for these modeling approaches will be elaborated in the following sections.

3.1.1.2 Pad Submodel

Both types of cask designs rest on rectangular concrete pads. Although the dimensions of the pads used in the analysis models differ, a similar approach was used to model the pad in both cases. In explicit dynamic finite element analysis programs, the element library typically consists primarily of reduced integration elements. This is due to the fact that most of the computation time is spent in the element subroutines because there is no iterative solver. By using reduced integration elements with an hourglass control algorithm, the analysis time can be reduced significantly compared to the time required for fully integrated elements. Consequently, a minimum of approximately 4 or 5 layers of elements is required through the thickness of a body to avoid hourglassing problems in the computation.

The concrete pad is a relatively slender structure, with lateral dimensions much larger than the thickness dimension, which is 0.6–0.9 m (2–3 ft). If four layers of solid elements were to be used to model the pad, the dimension of the elements in the thickness of the pad would be sufficiently small to control the critical time step and increase the analysis time. In addition, a large number of elements would be required in the lateral dimension of the pad to maintain reasonable element aspect ratios to ensure the quality of analysis results. To circumvent these problems, the concrete pads are modeled using continuum shell elements. These special-purpose elements, available for the first time in ABAQUS Version 6.4, behave like shell elements in bending modes but have eight nodes with the appearance of conventional brick elements. Since the through-thickness dimension is modeled, these elements can capture the deformation through the shell thickness, unlike conventional shell elements. In the pad models, a single layer of continuum shell elements was used to model the pad, allowing the model to reasonably capture the physics of the problem with a minimum of computation time.

3.1.1.3 Foundation Submodel

The foundation was modeled as a cylinder comprised of horizontal layers of elements. Different sets of material properties were assigned to the foundation models for soft soil, stiff soil, and rock. Each of these three foundation types has material properties that vary with depth. The material properties of the elements in a given layer are uniform, and each layer in all of these models has material properties that reflect the properties of the soil at that depth. The seismic ground motion was applied at the foundation base.

In this study the top of the soil foundation was modeled as a flat surface with a concrete pad resting on its top surface. In many cask system designs, the concrete pad is embedded in soil, so that the top of the pad is level with the top of the surrounding soil. This embedment provides confinement, restricting lateral movement of the slab relative to the soil. This embedment was not explicitly modeled in the current work, but its lateral movement-resisting effect was approximated by increasing the coefficient of friction between the pad and the soil surface.

One of the challenging aspects of modeling the foundation is applying appropriate boundary conditions. In an idealized, infinitely wide stratified soil mass subjected to earthquake motions applied at the base, the displacements at any two points having the same vertical coordinate but differing horizontal coordinates should be equal at every time step. Because of this, the behavior of such a semi-infinite soil mass can be idealized as a one-dimensional soil column. If a structure is placed at the surface of this semi-infinite soil mass, there will be disturbances in the uniform displacement field in the region of the soil column near the structure due to the interaction between the soil mass and the structure. The effects of these local disturbances decrease as the distance from the structure increases because the waves radiating from the structure are damped out.

Ideally, the boundary conditions chosen for the finite element foundation model should allow for the foundation to behave globally as a one-dimensional soil column but allow for local soil-structure interaction effects in the region of the cask and the pad. As mentioned above, the ground motion is applied at the foundation base to allow for soil-structure interaction. A ground motion time history is initially specified for the surface. A deconvolution procedure, explained in detail in Section 3.1.5, is used to compute a time history of ground motion that, when applied to the foundation base, results in motion at the surface that approximates the initial specified surface ground motion. A fundamental assumption in the deconvolution procedure is that the foundation behaves as a semi-infinite layered medium and thus can be approximated as a one-dimensional soil column.

To approximate a semi-infinite soil mass while still accommodating local disturbances in the displacement field due to soil-structure interaction, the foundation was modeled as a large, layered cylinder. Multi-point constraints (MPC) were applied to tie together all of the nodes around the outside edge of a layer, as shown in Figure 3.2. One node on each layer was designated as a master node, and all of the other nodes on the outside boundary of the foundation on that layer were designated as slaves and constrained to have the same displacement as the master node.

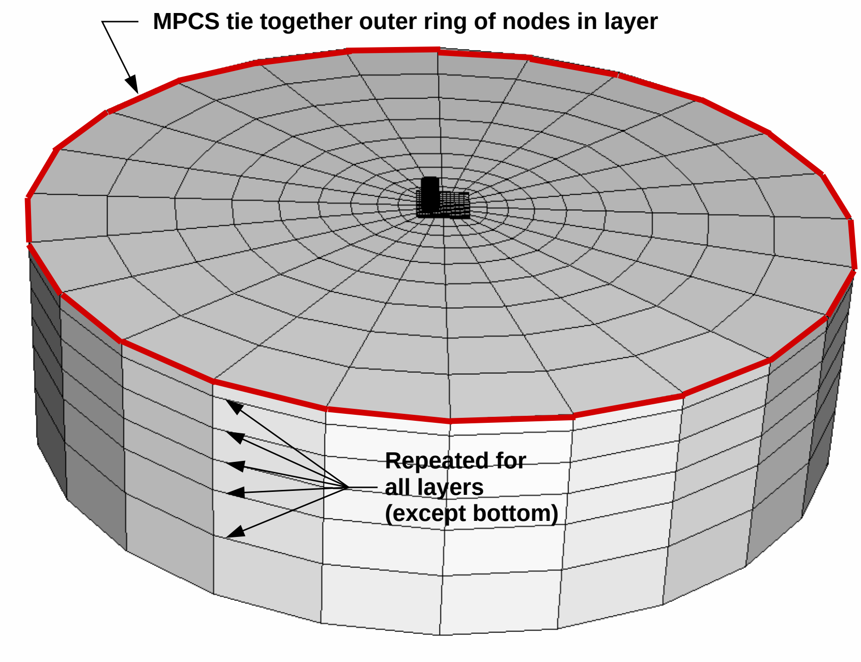

Figure 3.2: Multi-Point Constraints in Soil Foundation Layers

This approach allows for local disturbances in the region surrounding the cask and pad but forces the foundation to behave globally as a soil column. Shear deformations of the layers are allowed, but the MPCs prevent the column from deforming in a bending mode or expanding or contracting laterally. If the structure is removed and the foundation submodel is analyzed under an earthquake loading, all of the nodes in each layer have the same displacement at every point in time.

One issue often encountered in modeling semi-infinite media such as foundations is that waves can reflect from the boundary and cause undesirable effects in the region of interest. Infinite medium finite elements, which can be inserted at the boundary of the finite portion of the modeled medium, have been developed expressly for this purpose and are available in many general-purpose finite element analysis codes such as ABAQUS. These elements are designed to create "quiet" boundaries and not reflect waves back into the medium.

As part of this work, attempts were made to use such infinite elements at the boundaries, but it was found that when such boundaries were used, the ground motion computed at the surface had significantly different spectral characteristics from the specified surface ground motion. This is due to the fact that the infinite elements do not enforce the soil column constraints, so the column is able to deform in bending modes and expand and contract laterally.

To enforce soil column constraints while minimizing the effects of reflected waves, the approach taken in this work was to make the horizontal dimension of the soil column much larger than the dimensions of the structure to allow for waves radiating from the structure to be significantly damped out before they reflect back from the boundaries and reach the structure. A series of analyses were performed using varying dimensions of the soil column to determine the sensitivity of the response to those dimensions. These analyses indicated that the selected dimensions of the soil column are sufficiently large to not unduly affect the analysis results. The cylindrical shape was chosen for the foundation so that the horizontal distance from the pad would be approximately the same in any direction. This shape also eliminates any effects that could be potentially caused by corners if a rectangular shape had been used.

It is important to remember that in addition to being reflected from the vertical edges that bound the foundation submodel in the horizontal direction, waves can be reflected from the base of the model, where the input motion is being applied. Since the horizontal dimensions of the foundation model are larger than the vertical dimension, the reflected waves are likely to come from the base rather than from the sides. Because of this, little benefit would be realized by increasing the lateral dimensions without also increasing the vertical dimension of the foundation submodel.

3.1.2 Nonlinear Frictional Contact at Interfaces

Surface-based contact algorithms were used to prevent interpenetration between the cask and the concrete pad, and the concrete pad and the foundation. One of the most critical aspects of this analysis was correctly modeling these contact constraints. Using contact constraints allowed for a high degree of realism in modeling the cask motion. After the gravity load was applied, the cask and the pad, and the pad and the foundation are in full contact with each other. Until the point when the seismic ground motion is sufficiently high to cause uplift or sliding of these bodies relative to each other, they essentially behave as if they were bonded due to the presence of the gravity load and the friction at the contact interfaces.

Once uplift or sliding occurs, the cask, pad, and foundation move independently. The contact constraints govern the coupling between these bodies as they move relative to each other. The cask is free to lift up, rotate, and slide relative to the pad. Due to the fact that the gravity load is generally greater than the vertical acceleration caused by the ground motion, at least one point on the edge of cask base is typically in contact with the pad at any given time in the analysis. The contact constraints allow for the cask to move naturally, as governed by the motion applied at the base, and prevent penetration of the cask into the pad.

General-purpose finite element analysis codes such as ABAQUS typically offer the user a wide array of options in defining contact interactions. In ABAQUS/Explicit, for modeling surface-based contact, the user can choose between “general contact” and “contact pair” algorithms. General contact is a fairly new feature and allows for simple definition of contact interactions on a large number of surfaces with a minimum of user input. While the general contact algorithm permits some types of modeling that were not previously possible with the contact pair algorithm, there are still some options available in the contact pair algorithm that are not yet available with general contact. Because the cask model involves only two contact surfaces and maximum flexibility was desired with respect to contact options, the contact pair algorithm was used in this work.

ABAQUS employs a master/slave concept for contact interactions. In its simplest form, one of the two surfaces comprising a contact pair is designated as a master surface, and the other is designated as a slave surface. The contact algorithm checks for interpenetration of these two surfaces and adjusts nodal displacements to ensure that interpenetration does not occur. Figure 3.3 demonstrates the behavior of the master and slave surfaces. The surface designated as the master surface is comprised of element edges in two-dimensional analyses, or element faces in three-dimensional analyses. The slave surface is comprised of the nodes connected to the element faces that make up the surface. The slave nodes are constrained not to penetrate the master edges or faces. As shown in Figure 3.3, the nodes on the master surface are able to penetrate the edges or faces that make up the slave surface.

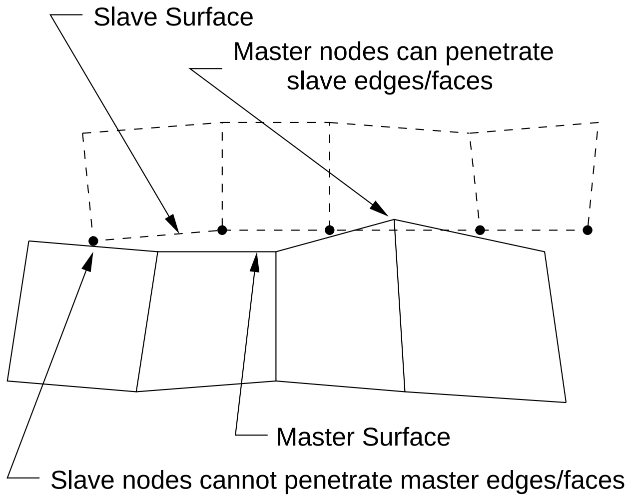

Figure 3.3: Master/Slave Contact Concepts

By default, ABAQUS/Explicit uses a balanced master/slave approach. This approach takes the average of the solutions obtained by setting one surface as a master and the other as a slave, and then reversing them. In this work, it is advantageous to use pure master/slave contact for both the cask/pad and the pad/foundation interface. Figure 3.4 shows an idealized diagram of the finite element meshes of the various submodels and the master/slave assignments used in this work.

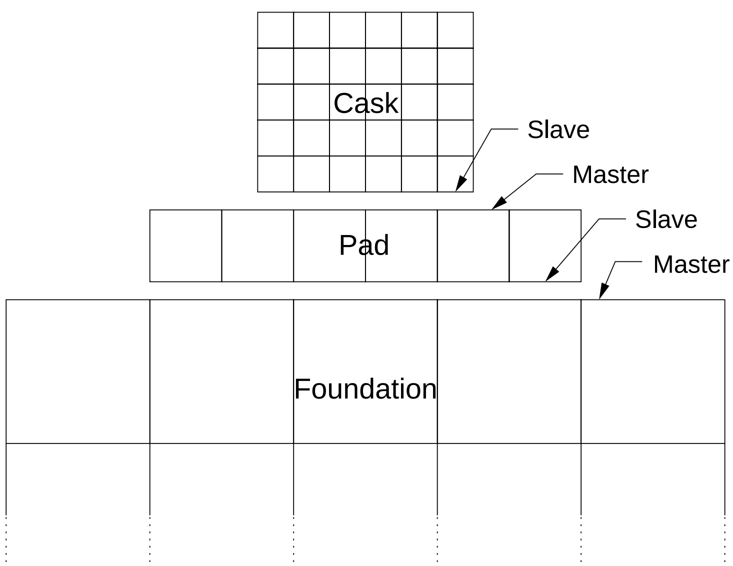

Figure 3.4: Idealized Mesh with Master/Slave Surface Assignments

There are three primary reasons for choosing this master/slave option. The first is that it is important for the corner of the cask not to penetrate the pad, and for the corner of the pad not to penetrate the foundation. Since the nodes on slave surfaces cannot penetrate master surfaces, the nodes at the corners of the cask and pad cannot penetrate the element faces on the top surfaces of the pad and foundation, respectively. The second reason is that if the elements adjacent to a slave surface have significantly more mass than the elements adjacent to its master counterpart, contact chatter can result. This high frequency noise can potentially resonate within the bodies and eventually result in an unrealistic response. In the models used in this work, the elements in the foundation are larger than those in the pad, and the elements in the pad are larger than those in the cask. Pure master/slave contact in the chosen configuration results in minimal contact chatter. Finally, in the case of the cylindrical cask, the cask is modeled as a rigid body. In ABAQUS/Explicit, surfaces attached to rigid bodies must be designated as slave surfaces.

There are three types of sliding formulations in the ABAQUS/Explicit code: finite, small, and infinitesimal. The finite sliding formulation is the most general and allows for large changes in the position of the contacting surfaces in relation to each other during the computation. This allows for pairs of element faces and nodes that come into contact to change as the analysis proceeds. In the small and infinitesimal sliding formulations, assumptions are made that the nodes and element faces that are initially paired up will remain that way throughout the computation. This saves the computational cost of performing the search for paired nodes and element faces at every step if the relative movement of the surfaces is known to be small prior to the analysis. Since the freestanding cask can clearly experience large motions relative to the pad, the finite sliding formulation is used for the cask/pad interface. The pad experiences small motions relative to the top surface of the foundation in the cases studied here. The small sliding formulation provides an adequate approximation at that interface, but the savings in computational cost obtained by using that formulation have been shown to be very minimal in this case. Therefore, the finite sliding formulation was also used for the pad/foundation interface in the models used in this study.

In addition to the options mentioned above, the ABAQUS/Explicit user must choose between the kinematic and penalty method of contact constraint enforcement. The kinematic constraint algorithm uses a predictor/corrector approach to enforce contact constraints. The deformed configuration is initially computed without regard to contact constraints. If any of the contact constraints are violated, resisting forces are computed to oppose the penetration so that if they were applied during the increment, the contact constraint would be exactly satisfied. These forces are then distributed to the nodes connected to the faces comprising the master surface, and adjusted accelerations are computed so that the contact constraint is satisfied at that loading increment.

The penalty method of satisfying contact constraints applies equal and opposite forces to the two contacting surfaces that are linear functions of the penetration distance. This is conceptually similar to introducing stiff springs between the two surfaces. This method allows for the solution of a wider variety of problem types than can be solved using kinematic contact. To minimize errors due to penetration, it is important that the penalty stiffness be set as high as possible. Setting this stiffness high comes at a cost, however, because in the explicit time integration method, the critical time step is controlled by the stiffest element. The contact constraint essentially behaves as an element, so it can potentially control the time step. In ABAQUS/Explicit, the penalty stiffness is automatically computed to be as stiff as possible while having a minimal effect on the critical time step. The user has the option of specifying a multiplier that is applied to this automatically computed stiffness.

While the kinematic contact formulation allows for shorter execution times, it was found that the models are more prone to experience high frequency chatter at the interfaces with this option. This can result in an unreasonably large cask response to a seismic event. For this reason, the penalty contact formulation was used in the present work. A multiplier of 3 was applied to the automatically-computed penalty stiffness to decrease the potential negative effects of contact penetration while still minimally affecting the critical time step.

Finally, the constitutive behavior of the interacting surfaces must be defined. A simple Coulomb friction model is used in this work. If the shear stress on the interface is less than the product of the normal compressive stress and the friction coefficient, the surfaces are not allowed to slide relative to each other. Once the shear stress exceeds this limit, the surfaces can slide. A single coefficient of friction was used for both static and kinetic friction.

3.1.3 Representation of Damping

The method used to represent structural damping is an important consideration in the seismic modeling of the cask system. Since the foundation is assumed to behave as a linearly elastic material, there are no inherent energy dissipation mechanisms. Rayleigh damping is imposed on the foundation material to approximate the natural energy dissipation mechanisms. In Rayleigh damping, the damping matrix, $\boldsymbol{C}$, is formed by summation of the mass matrix, $\boldsymbol{M}$, and the stiffness matrix, $\boldsymbol{K}$:

$$\boldsymbol{C} = \alpha\, \boldsymbol{M} + \beta\, \boldsymbol{K} \tag{3.1}$$

The factors α and β are used to control the amounts of mass-proportional and stiffness-proportional contributions to the damping matrix. The mass-proportional damping has a greater effect on the lower frequency modes of a structure, while the stiffness-proportional damping has its greatest influence on higher frequency modes. Typically, the values of α and β are calibrated so that the desired level of damping is achieved for high and low frequency modes chosen by the analyst.

The application of an explicit time integration method presents some special challenges regarding damping. Contrary to intuition, introducing damping decreases the critical time step, making the analysis take longer to complete. In the presence of damping, the critical time step, Δt_{crit}, is computed as:

$$\Delta t_{crit} = \frac{2}{\omega_{\max}}\left(\sqrt{1+\xi_{\max}^2} - \xi_{\max}\right) \tag{3.2}$$

where $\omega_{\max}$ is the frequency of the highest frequency mode of the structure and $\xi_{\max}$ is the fraction of critical damping acting on that mode. It can be seen that an increase in the damping on the highest frequency mode can dramatically decrease the stable time step. Since mass-proportional damping has its greatest effect on low frequency modes, introducing this type of damping has little effect on the critical time step, but introducing even a small amount of stiffness-proportional damping can significantly decrease the critical time step. It should be noted that the ABAQUS/Explicit automatically introduces a small amount of bulk viscosity to provide damping against high-frequency vibrations.

Only mass-proportional damping was used in the parametric analyses because of the issues discussed above. The mass-proportional damping was applied to the foundation but not to the cask or the pad. Some analysis cases were executed using the stiffness-proportional damping, and analysis results indicate that the cask response was affected very little by the stiffness-proportional damping, while the analysis time increased significantly. The mass-proportional damping has an effect analogous to that of air friction. If such damping were applied to the cask or pad, which are independent bodies, it would limit their absolute motion. If high enough values of mass-proportional damping were applied to these bodies, they would remain essentially stationary as the foundation moves beneath them.

The target percentages of critical damping for the various layers of the foundation were computed to generate values compatible with the strains that occur with an earthquake conforming to the NUREG/CR-0098 spectral curve shape with a peak ground acceleration of 0.25 g, as described in Appendix I. These damping ratios are shown graphically for the soil profiles used in Figure 3.5. For each of the three foundation types, the fundamental frequency of an idealized one-dimensional soil column is computed, and the mass-proportional damping coefficient, α, is computed for each of the layers to result in the target percentage of critical damping for that layer.

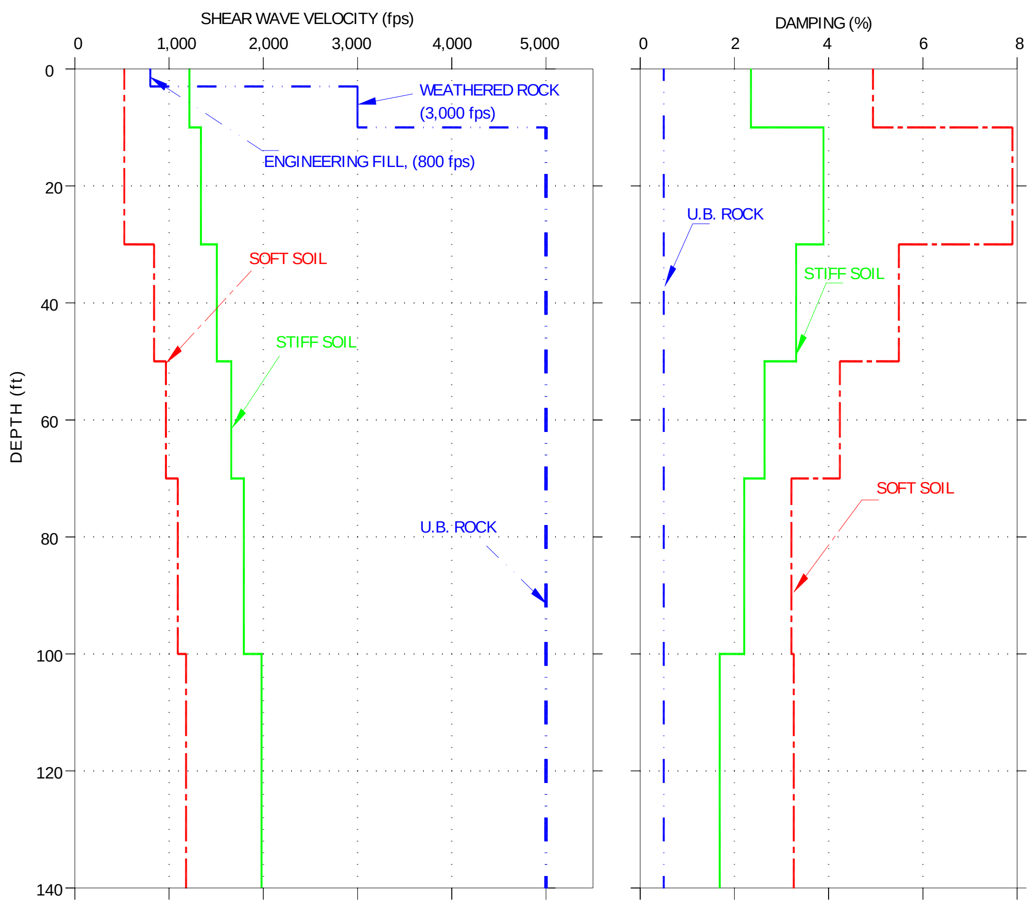

Figure 3.5: Soil Profiles Used in Parametric Deconvolution Site Response Analyses

3.1.4 Treatment of Seismic Ground Motions

The strategy for developing input ground motions for the coupled model has been geared toward supporting the NRC staff in the safety review of cask design licensing applications, which may cover a wide range in geographical regions, including the seismically active Western United States (WUS) and the less active Central and Eastern United States (CEUS).

In addition to varying levels of Peak Ground Acceleration (PGA) shaking levels, the ground motion characteristics from cask design licensing applications may contribute to a wide range of response spectral shapes to cover different seismological conditions between the WUS and the CEUS. Recent seismological studies conducted for the CEUS suggest a much lower shaking level for long period ground motions as compared to strong ground motion observed in historical data recorded in the WUS.

Differences in soil conditions, including soil versus rock site conditions, would also contribute to variations in ground motion characteristics and would especially account for differences in terms of spectral shapes. As a result of the wide range of variations, there is a need to conduct dynamic response analyses for a large number of cases of input motion conditions including varying PGA levels scaling to different response spectral shapes.

This project emphasized documenting in the project library a sufficiently wide range of cask response results, which would in turn allow cask design licensing applicants to compare the ground shaking intensity to the range of input motion characteristics based on their response spectra. The resultant response solutions from the appropriate input motion can then be used for determining the response level of the specific design of a dry cask system.

In deciding the scope of the parametric study, three spectral shapes were selected: (1) NUREG/CR-0098 spectral shape [6], (2) Regulatory Guide 1.60 spectral shape [7] and (3) CEUS generic site spectral shape [8]. For each selected spectral shape, five sets of spectrum-compatible acceleration time histories were developed for supporting the parametric study. Further discussions on background information on the choice of the three spectral shapes and the number of sets of input ground motions for various PGA levels and spectral shapes are discussed in Section 4.1.

As previously discussed, the ground motions were input at the foundation base of the coupled model. However, cross-comparison of input motions between the project library with submittals from specific applications would be made in terms of free-field ground-surface (outcrop) motions, which would be different from the expected shaking intensity at the base of a foundation column. To address this issue, the first step was to develop the required time histories of ground motion for the conventional ground-surface outcrop condition to facilitate cross comparison to design ground motion criteria for site specific applications. The second step was to perform deconvolution analyses to generate input ground motions that would be appropriate as prescribed input ground motions to the foundation base of the coupled model. Additional discussions on the deconvolution procedures are presented in the following section.

3.1.5 Deconvolution Procedure

Coupled response models consisting of the cask, pad, and foundation were developed in this study in order to incorporate soil-structure interaction effects. The presence of a foundation in the coupled response model requires the application of seismic motions, which are traditionally recorded and defined at the ground surface, at the foundation base. A deconvolution procedure was thus developed to generate input seismic motions based on the target surface ground motions in such a way that when the seismic motions are applied at the base of the foundation, the resulting motion at the top of the foundation is approximately the same as the original desired surface motions. The ground motions at the surface are different from the target motions in the immediate vicinity of the structure due to the soil-structure interaction effects, but the surface motions (measured at a point in the model on the surface of the foundation sufficiently far from the structure, or at the surface of a model of the foundation without the structure present) will be approximately equivalent to the original prescribed surface motions. Idriss and Seed [16] and Schnabel et al. [17] provide detailed discussions on the deconvolution procedure.

Concepts in the deconvolution analysis were originally developed as an extension of the classical site response analysis. The underlying principle in site response has been based on the vertically propagating body wave, where horizontal and vertical component ground motions are governed by vertically propagating shear and compression waves, respectively. Typically, the objective in conventional site response analyses was to account for how localized soil properties would modify ground-motion shaking levels as the earthquake propagates from a deep seismogenic zone (typically at tens of kilometers) up to the ground surface where most structures are located. Site response analysis results are generally used in conjunction with other seismological information (e.g., earthquake event magnitude and distance from seismic source to project site) for defining the appropriate ground-shaking level for design purposes.

Site response analyses are commonly conducted by using a widely distributed computer program, SHAKE91 [13], which models a soil column by way of a low-strain soil modulus profile in conjunction with a set of strain-dependent stiffness modification and damping-ratio functions to develop a set of strain-compatible soil properties (i.e., soil modulus and damping ratio profiles). After developing the appropriate equivalent linear soil stiffness and damping, transfer functions are calculated and then applied to the expected bedrock motion at a depth to derive the ground-surface outcrop motion for design analysis of near surface structures. The concept of deconvolution is essentially making an inverse of the transfer functions and then applying them to a set of ground-surface outcrop motions to develop any ‘within’ motion representing the ground motion characteristics at a given depth. In this parametric study, the deconvolution analyses were performed using the SHAKE91 program.

In the context of this project, the deconvolution site response analysis was conducted so that the inherent site response solution implied by the dry cask model would reproduce the intended target benchmark free-field outcrop ground-shaking level. To achieve this objective, it is very important that the soil properties used in the deconvolution analysis be consistent with those used in the coupled-cask analysis model. In support of the parametric analyses, deconvolution solutions for three sets of soil properties have been obtained, including a so-called benchmark stiff as well as a soft-soil profile and an upper-bound rock profile as summarized in Figure 3.5. The top 0.9 m (3 ft) of the rock profile reflects the general practice of placing a thin layer of engineering fill followed by 2.1 m (7 ft) of a softer weathered rock, a condition that is expected to be prevalent at most rock sites. Additional details and background information leading to the selection of the adopted soil properties are included in Appendix I.

The equivalence of the original target surface motion and the motion obtained at the surface of a finite element model of the soil column was initially verified using a two-dimensional finite element model of the soil column using the DYNAFLOW [18] finite element analysis program. Once the full three-dimensional model of the cask, pad, and soil had been developed, the cask and pad were removed from the soil column model, and the response at the surface of that finite element model was calculated, as described in Section 5.1.3.

In summary, deconvolution analyses have been performed using the referenced ground-surface spectrum-compatible motions as input for deducing the appropriate input motion at the foundation base of the coupled models. The same set of soil parameters (i.e., soil modulus and damping) are used in both the deconvolution analyses and the coupled cask responses analyses to maintain the compatibility in soil properties between the deconvolution and the coupled-model response solutions. Deconvolution analyses have been conducted for three sets of soil stiffness properties that can then be used to match soil properties in future licensing applications.

The soil models utilized in the coupled response model for this study are implicitly based on equivalent linear elasto-dynamic modeling approaches. It is not the intention of this study to address permanent nonlinear near-field soil yielding and deformation shear failure or liquefaction effects. The profiles presented in Figure 3.5 were strain compatible to shaking corresponding to spectrum-compatible time histories with a PGA of 0.25 g scaling to the NUREG/CR-0098 target spectral shape. The same profiles were used for input motions conforming to other spectral shapes and to other PGA values at 0.6 g, 1.0 g and 1.25 g. The decision was to minimize confusion for comparing dry cask response at different inertial input levels. Furthermore, the implication of the strain-compatible soil profile properties is relatively minor because of our approach to calibrate and to compare shaking at the ground surface. Also, some of the cask response solutions at the higher level of ground shaking (e.g., at 1.0 g and 1.25 g) are merely intended to approximate potential cask responses qualitatively at extreme levels of ground shaking. These high ground-motion levels would be very unlikely be encountered in future licensing situations.

One of the major contributions in this project relates to the advancement of the state-of-the-art soil-structure interaction analysis procedure to beyond the traditional frequency domain elasto-dynamic approaches due to the importance of the base contact separation issues on the cask response. The subject of site response and wave scattering has traditionally been treated by frequency domain computer codes such as SHAKE [17] or SASSI [12]. For past 20 years, these programs have been used in the nuclear power plant industry for seismic designs of containment systems, which are typically founded on competent soil conditions. In earlier days, such approaches, which often permit substructuring to economize computer resources, were necessary. Because of the advancement of computer technologies, time-domain structural engineers prefer modeling the total soil-foundation-superstructure system. It is highly desirable that the wave propagation and scattering analyses be conducted in time domain, or in a numerical platform that is commonly used for global structural response analyses. This will allow both groups of specialists (geotechnical professionals who are familiar with wave propagation analyses and structural engineers performing the global structural model) to work simultaneously on the same computer platform to contribute both their expertise to the total problem. In many major seismic response projects (e.g., in highway bridges) such a time-domain total-system approach is preferred because it allows the structural engineers to capture various nonlinear response phenomena. Another major benefit is that it minimizes the amount of work for data transfer and the potential for error arising from solutions from separate numerical platforms.

In order to advance the time-domain approach for solving wave propagation and wave scattering problems, these new approaches need to be verified to the classical proven approaches (e.g., solutions from SHAKE and SASSI). Appendix II presents some of these verifications and various sensitivity analyses for developing the appropriate input motions to a finite-domain finite-element model, and for minimizing wave reflection and refraction at the model's side boundaries. Numerical integration schemes and implementation of Rayleigh damping parameters are discussed. Careful examination of a wave traveling through the bottom boundary would allow proper modeling of the half-space below the region of interest.

3.2 Details of Coupled Models

3.2.1 Vertical Cylindrical Cask

In typical vertical cylindrical cask applications, an array of casks rests on a single concrete pad. The casks are typically arranged in two rows, as illustrated in Figure 2.3. For the parametric analyses performed in this study, the analysis model involves a single cask resting on one quadrant of a pad that can accommodate a 2x2 array of casks. Figure 3.6 shows views of the entire finite element model of the cylindrical cask, pad, and foundation.

Modeling a single cask instead of the whole array of casks simplifies the analysis procedure considerably and reduces the time required to run the analyses. To assess the validity of this simplified approach, a model very similar to that shown here was developed with four freestanding casks on a pad. In the cases that were studied with the four-cask model, the four casks exhibited responses that were very similar to those of the single cask under the same conditions. In those cases, the single cask had a higher response. Based on those analyses, it was determined that the single cask model provides a reasonable approximation of the response of a cask in a larger array.

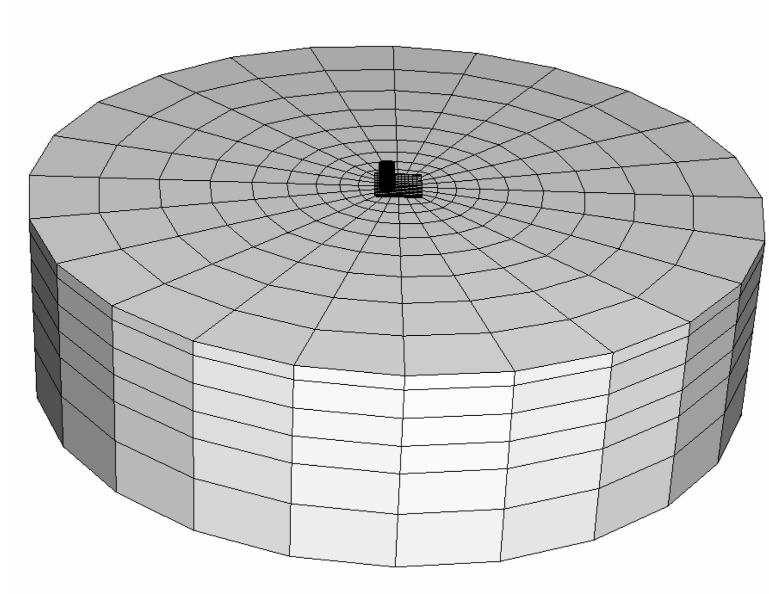

(a) Overall Model

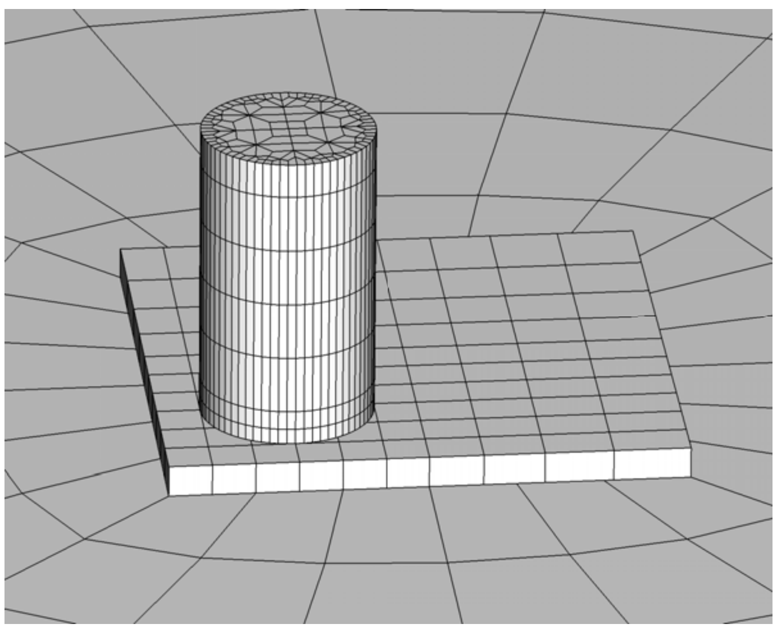

(b) Detailed View of Region of Model with Cask and Pad

Figure 3.6: Finite Element Model of Cylindrical Cask, Pad, and Foundation

3.2.1.1 Cask Submodel

Modeling the cylindrical cask in the framework of the finite element method with explicit time integration presents some challenges because of the cask geometry. In an upright cylindrical cask, the edge of the cask base contacting the pad is curved. When the cask begins to roll along the edge of its base, the discretization of this edge into a series of nodes connected by straight lines can potentially cause errors. As the number of elements around the edge of the base is increased, these errors decrease. An undesirable side effect of this modeling scheme is that to obtain a reasonable level of refinement along this curve, the edge lengths of the elements along the curve become the shortest of all elements in the model, and these elements control the size of the critical time step, and hence, the analysis time.

Figure 3.7 shows a top view of the finite element mesh for the cylindrical cask. A surface mesh was initially generated on the cask base. This surface mesh was then swept up through the cask to generate a solid mesh comprised of seven layers of three-dimensional, eight-noded hexahedral elements. The cross section of the cylinder is assumed constant through its height, so slices of the mesh taken perpendicular to the vertical axis of the cask at different heights are always the same. In the picture of the cask top, it can be seen that there are 64 elements around the edge of the cask. The mesh is more refined around the edge than in the middle to allow for fewer elements to be used where a high degree of refinement is not needed.

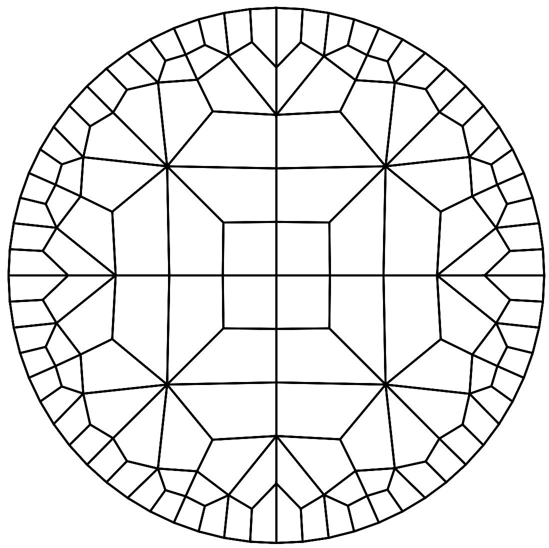

Figure 3.7: Top View of Cylindrical Cask Mesh

3.2.1.1.1 Structural Features

The cylindrical cask system usually consists of a multi-purpose canister and an overpack. The same overpack can be used with a number of different canisters, which have different designs to accommodate various types of spent fuel. The overall properties of the loaded overpack vary depending on the type of multi-purpose canister. For this study, it was assumed that the cylindrical cask contains a fully loaded multi-purpose canister, which is used for the storage of spent fuel from a Boiling Water Reactor (BWR). This cask design was chosen because the overall cask system is slightly heavier and has a slightly higher center of gravity than other alternatives. Therefore, the chosen cask design should result in the highest response of the available designs, but the results should be applicable to all designs because the differences are minor.

3.2.1.1.2 Material Properties

As mentioned above, the cask mesh is composed of seven layers of solid elements. Material properties were assigned to these layers to approximate the overall mass properties of the loaded cylindrical cask. The internals of the cask are complex but have little effect on the seismic response of the cask. The mass and stiffness properties of the cask internals were approximated and averaged out in the horizontal layers. The densities of the layers were iteratively adjusted to obtain a reasonable approximation of the overall mass, center of gravity height, and rotational moments of inertia of the cask. Table 3.1 shows the material properties for this cask design. The top and bottom element layers were assigned unique material properties, while the middle five layers were all assigned the same properties.

Table 3.1: Cylindrical Cask Finite Element Model Material Properties by Layer

Layer	Layer Thickness	Elastic Modulus	Poisson's Ratio	Density
1	0.203 m (8.0 in)	27.8 GPa (4031 ksi)	0.2	3379 kg/m^3 (211 lb/ft^3)
2-6	4.994 m (196.6 in)	27.8 GPa (4031 ksi)	0.2	2984 kg/m^3 (186 lb/ft^3)
7	0.676 m (26.6 in)	27.8 GPa (4031 ksi)	0.2	3850 kg/m^3 (240 lb/ft^3)

Table 3.2 shows a summary of the mass properties of the cask submodel using the finite element mesh with the material properties listed in Table 3.1. For the purposes of the moment of inertia calculations, the *x* and *y* axes are oriented in the horizontal plane, and the *z* axis points in the vertical direction.

Table 3.2: Summary of Cylindrical Cask Finite Element Model Properties

Height of Center of Gravity	3.002 m (118.2 in)
Base Radius	1.683 m (66.25 in)
Overall Height	5.874 m (231.25 in)
Weight	161948 kg (357033 lb)
Moment of Inertia I_{xx}, I_{yy}	6.36x10^5 kg-m^2 (2.17x10^9 lb-in^2)
Moment of Inertia I_{zz}	2.36x10^5 kg-m^2 (8.08x10^8 lb-in^2)

3.2.1.1.3 Rigid Cask Model

As mentioned in Section 3.2.1.1, modeling an upright cylindrical cask presents challenges because the elements around the cask boundary control the critical time step, resulting in long run times for the analysis. With the original cask model used in this study, the long run times dictated by these elements prohibited completing the large number of parametric analyses in a practically reasonable schedule. To overcome this problem, the cask was treated as an element-based rigid body. The ABAQUS code allows groups of elements to be treated as rigid bodies rather than elastic bodies with a very minor change to the input file. In this setting, the mass properties of the elastic material are used, but the material is no longer able to deform. Since the rigid body behavior of the cask is much more important than its deformation, this provides a reasonable approximation of the cask response.

When the cylindrical cask is treated as a rigid body, the cask elements no longer govern the critical time step. The thickness of the concrete pad becomes the controlling factor for the critical time step. The analysis time is reduced by approximately a factor of four by simulating the cask as a rigid body.

It is important to mention that initial analysis runs performed using the rigid cask model sometimes produced a higher than expected cask response, especially when a very stiff soil profile was used. The cause of this problem was that the default critical time step chosen by the ABAQUS code was too large for this particular model. The user has the ability either to control the analysis time step directly or to specify a multiplier to scale the automatically chosen value. It was found that using a multiplier to force the program to use a time step 50% the size of the automatically chosen value results in a stable solution. A convergence study indicated that further reducing the time step did not significantly change the results.

3.2.1.2 Concrete Pad Submodel

As mentioned above, the square reinforced concrete pad beneath the cylindrical cask is large enough to accommodate a 2x2 array of casks. The pad is 0.610 m (2.0 ft) thick and 10.06 m (33 ft) wide. The cask is positioned at the center of one quadrant of the pad. Figure 3.8 shows a detailed view of the mesh for the pad with the highlighted quadrant where the cask is positioned. In this figure, the element edges of the cask base are shown with light lines to differentiate them from the pad elements, the edges of which are shown with dark lines. With these pad dimensions and positioning of the cask on the pad, the closest distance from the edge of the cask in its initial position to an edge of the pad is 0.8319 m (32.75 in). In earlier revisions of the model, the dimensions of the pad were smaller, but cases were encountered where the cask partially slid off the pad during the course of the analysis. The larger dimensions were chosen to ensure that the cask would remain on the pad except for the cases when it tips over. The dimensions of a pad in an actual application would be governed by the expected amount of sliding.

In Figure 3.8, the pad is modeled with a single layer of continuum shell elements. In the quadrant where the cask is located, these elements have lateral dimensions of 0.838 m (33 in). The mesh is coarsened slightly in the other three quadrants of the pad to reduce the model size. The reinforced concrete pad material is assumed to be linearly elastic, with an elastic modulus of 24.9 GPa (3605 ksi), and Poisson's ratio equal to 0.2. The density of the pad material is 2792 kg/m^3 (174 lb/ft^3).

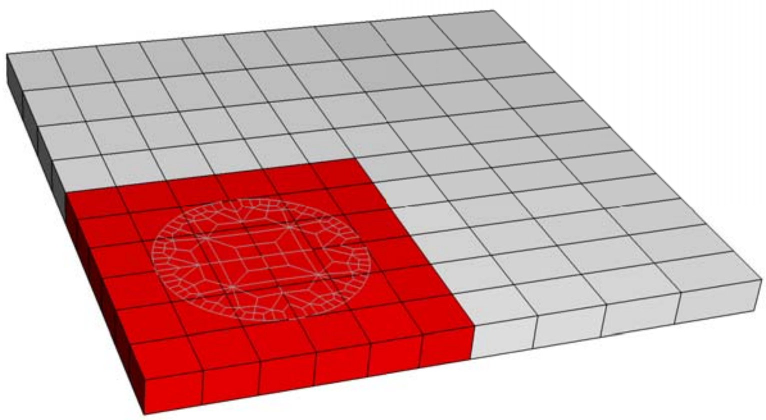

Figure 3.8: Detailed View of Pad for Cylindrical Cask

3.2.2 Rectangular Module

As illustrated in Figure 2.4, the rectangular modules are arranged in either a single row or pairs of rows. The side and rear walls of the rectangular modules are not thick enough to offer adequate shielding by themselves. There is not an issue if modules are placed side-by-side or back-to-back, but additional shielding walls must be placed at the ends of rows or along the backs of the modules if a single row configuration is used. There are 0.152-m (6-in) gaps between the sides of adjacent casks in rows and between the first or last cask in a row and the shield wall.

Because of these shielding considerations, a single rectangular module would never stand in isolation. For performing the parametric analyses, however, a relatively simple, bounding configuration was needed. A single module is more likely to tip over than a row of module, and would behave in approximately the same way as a row of modules in sliding. Therefore, for the parametric analyses, a single module was modeled with an attachment of the shield wall section.

Figure 3.9(a) shows a view of the overall model of the rectangular module with the pad and the foundation. A detailed view of the region around the module and pad is shown in Figure 3.9(b).

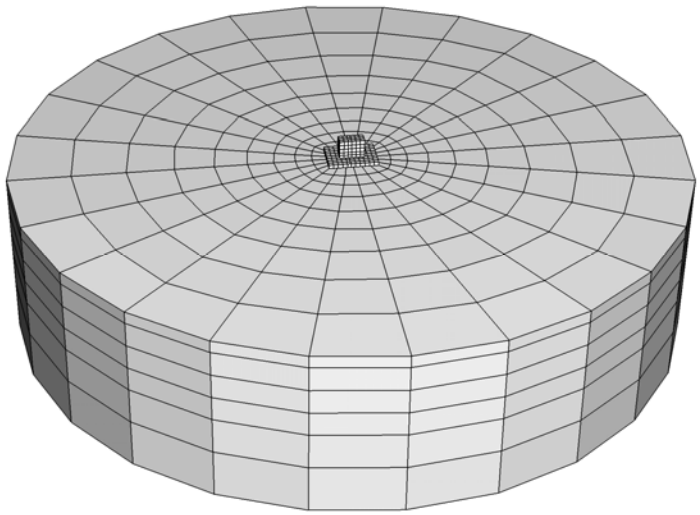

(a) Overall Model

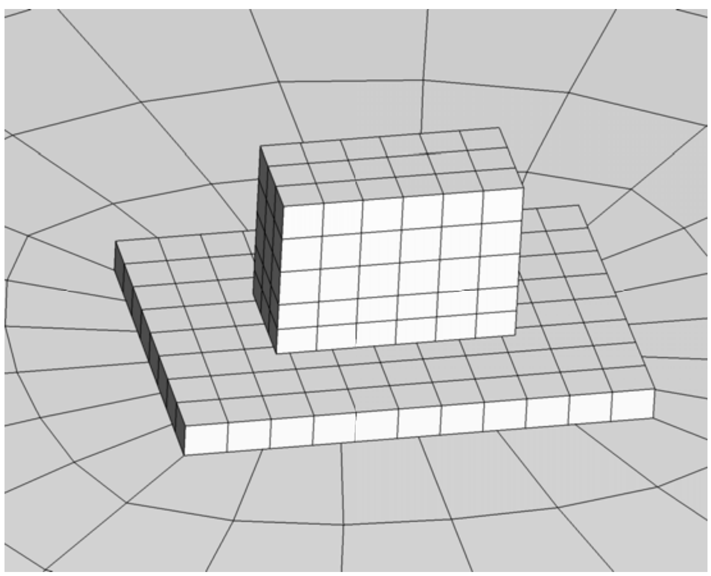

(b) Detailed View of Region of Model with Module and Pad

Figure 3.9: Finite Element Model of Rectangular Module, Pad, and Foundation

3.2.2.1 Module Submodel

3.2.2.1.1 Structural Features

Similar to the cylindrical cask system, the rectangular module system is comprised of a sealed canister containing spent fuel rods. The canister is inserted into a shielding overpack. As can be seen in the cut-away view of the module shown in Figure 2.2, the cylindrical cask is slid horizontally into a rectangular overpack. The rectangular module system can also accommodate a number of different types of canisters, which are used for different purposes. There are two different lengths of the rectangular modules. One type of module is 0.254 m (10 in) deeper than the other to accommodate longer canisters. For the analysis here, the shorter type of module is considered because it is more likely to be susceptible to tipping. The length difference has a negligible influence on the results because the cask is far more susceptible to tipping with the shorter dimension. The analysis results indicate only negligible rotations in the long dimension.

For the parametric analyses, the module is assumed to be loaded with the canister that contains spent fuel from Pressurized Water Reactor (PWR) plants. This is the heaviest of the canisters that can fit in the shorter module used in these analyses.

3.2.2.1.2 Material Properties

Similar to the cylindrical cask system, the rectangular module system is modeled with horizontal layers of solid elements whose densities are iteratively adjusted to achieve a reasonable approximation of the overall mass properties of the module. Since the overall shape of the module is a right rectangular prism, the mesh is much simpler than that for the cylindrical cask. The model used in the parametric analyses is fairly coarse. A more refined model of the module and pad was investigated, but a comparison of the results with this coarse model showed that the two models produced nearly identical displacement histories. The shortest edge length of the module elements is roughly equivalent to the pad thickness, so the module elements do not cause a decrease in the critical time step, as was the case for the elastic cylindrical cask. Thus, there was no need to use a rigid approximation of the rectangular module to save analysis time.

The rectangular module system is modeled with five layers of hexahedral continuum elements. Table 3.3 shows the properties assigned to these layers of elements. In the rectangular module design, the lower part of the module is essentially hollow and contains a steel support frame for the canister. The module is approximated as a solid block in the model. The elastic modulus and density of the lower layers are reduced to account for this hollow area at the module base.

Table 3.3: Rectangular Module Finite Element Model Material Properties by Layer

Layer	Layer Thickness	Elastic Modulus	Poisson's Ratio	Density
1	0.762 m (30 in)	18.1 GPa (2620 ksi)	0.2	1412 kg/m^3 (88.1 lb/ft^3)
2	0.762 m (30 in)	11.4 GPa (1653 ksi)	0.2	749 kg/m^3 (46.7 lb/ft^3)
3-4	2.032 m (80 in)	27.8 GPa (4031 ksi)	0.2	2620 kg/m^3 (164 lb/ft^3)
5	1.016 m (40 in)	27.8 GPa (4031 ksi)	0.2	2016 kg/m^3 (126 lb/ft^3)

Table 3.4 shows a summary of the mass properties of the finite element model of the rectangular module. As was done with the cylindrical cask, the densities of the material layers in the module were adjusted iteratively to obtain reasonable approximations of the overall mass, center of gravity height, and rotational moments of inertia. For the reported moments of inertia, the x axis points in the horizontal direction normal to the long side of the module, the y axis points in the horizontal direction normal to the short side of the module, and the z axis points in the vertical direction.

Table 3.4: Summary of Critical Rectangular Module Finite Element Model Properties

Height of Center of Gravity	2.54 m (100 in)
Width	2.95 m (116 in)
Depth (with Shield Wall)	6.40 m (252 in)
Overall Height	4.57 m (180 in)
Weight	170,098 kg (375001 lb)
Moment of Inertia I_{xx}	8.85x10^5 kg-m^2 (3.02x10^9 lb-in^2)
Moment of Inertia I_{yy}	4.22x10^5 kg-m^2 (1.44x10^9 lb-in^2)
Moment of Inertia I_{zz}	7.63x10^5 kg-m^2 (2.61x10^9 lb-in^2)

3.2.2.2 Concrete Pad Submodel

The concrete pad beneath the rectangular module is modeled in a manner similar to the pad for the cylindrical cask. The pad is 0.914 m (3 ft) thick and has lateral dimensions of 9.04 m (29.7 ft) x 12.5 m (41 ft). The module is placed at the center of the pad, and there is 3.048 m (10 ft) between the module and the edge of the pad in both lateral directions. The pad is modeled with a single layer of continuum shell elements. These elements are 0.914 m (36 in) thick and have lateral dimensions of 1.13 m (44.5 in) x 1.14 m (44.7 in). As with the pad beneath the cylindrical cask model, the material for this pad is assumed to be linearly elastic, with an elastic modulus of 24.9 GPa (3605 ksi), Poisson's ratio of 0.2, and density of 2792 kg/m^3 (174 lb/ft^3).

3.2.3 Foundation Submodel

3.2.3.1 Structural Features

Basic descriptions of the modeling technique for the foundation have been provided in previous sections. The foundation submodel meshes for the cylindrical cask and rectangular module models differ slightly because they are configured so that element edges are aligned with the edges of the pads, which have different dimensions. However, the outside dimensions and overall configurations of the meshes are the same. The outside diameter of all of the cylindrical foundation submodels is 167.5 m (549.6 ft), and they all have an overall depth of 42.7 m (140 ft). The largest diagonal dimension of the two types of concrete pads used in this project is 14.2 m (46.7 ft) for the cylindrical cask pad. The foundation is 11.8 times wider than this dimension. This configuration exceeds the recommendation of the US Army Corps of Engineers [19] that the foundation be at least 7 times wider than the dimension of the structure.

Figure 3.10 shows the foundation submodel used in the cylindrical cask analyses with the soft and stiff soil profiles. As can be seen in the figure, the mesh in the center of the top surface is rectangular and coincides with the shape of the pad. There are six elements across the region directly beneath the pad in both directions. For the cylindrical cask model, the pad is square, but for the rectangular module model, one dimension of the rectangular pad is greater than the other. Rings of elements encircle this rectangular zone. These rings become more circular in shape as the distance from the center increases. The surface mesh is swept through the depth of the foundation, so that horizontal cross sections of the mesh appear identical no matter where they are taken in the foundation depth.

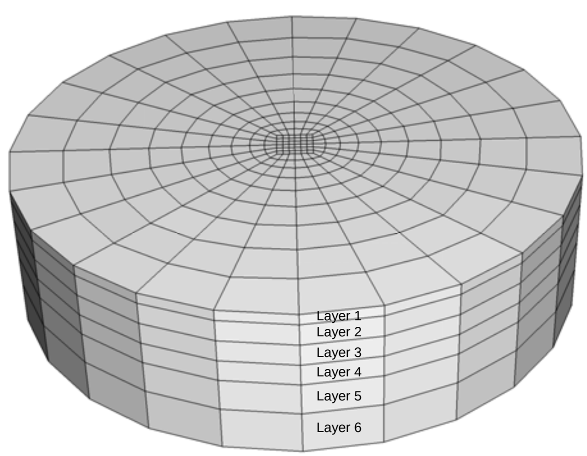

Figure 3.10: Representative Soil Foundation Submodel for Cylindrical Cask Analyses

The soil foundations with a depth of 42.7 m (140 ft) are comprised of six layers, each having unique material properties. The layers of elements in the soil foundation meshes coincide with these soil layers. The top layer is 3.05 m (10 ft) thick and the next three layers down are each 6.10 m (20 ft) thick. After that, the 5th layer is 9.14 m (30 ft) thick, and the bottom layer is 12.2 m (40 ft) thick. These six layers are labeled in Figure 3.10. The 42.7-m (240-ft) depth was chosen to reach a level below which the soil stiffness increases monotonically with depth. In addition, it was also based on satisfying the guidelines in American Society of Civil Engineers (ASCE) Standard [20].

As shown in Figure 3.11, the rock foundation submodels are essentially the same as those for the soil foundations. The overall dimensions of the foundations are the same, and the surface meshes that are swept through the layers of the foundation are the same as those that are used for the soil foundations. The only difference is that two different layers replace the top layer of the soil foundation. The uppermost of these layers is 0.914 m (3 ft) thick and is used to represent a thin layer of engineered fill material placed on top of the underlying rock material. Below this layer is a 2.13 m (7 ft) thick layer that represents weathered rock. Below this point, the mesh for the foundation is identical to that used in the soil foundation models. The layers below this point represent rock, and the material properties of the rock are constant through the rest of the depth.

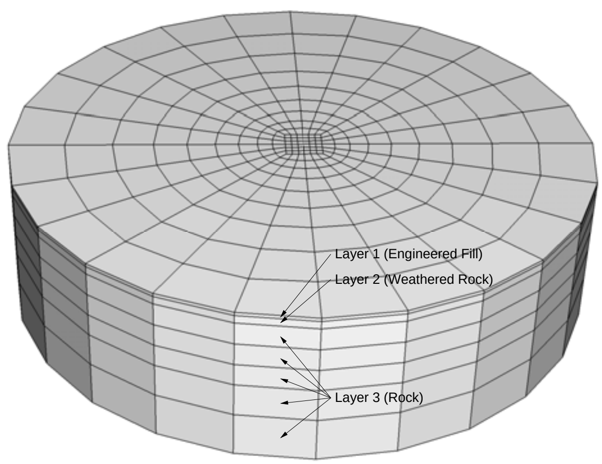

Figure 3.11: Representative Rock Foundation Submodel for Cylindrical Cask Analyses

3.2.3.2 Material Properties

The layered finite element meshes for the foundations have been described in the previous section. Three different foundation types have been used in this study. Soil profiles are very site-specific, and it is not possible to pick a generic soil profile that characterizes every site in the United States. The intent of this parametric study is to pick three soil profiles that bound the characteristics of a wide range of possible sites to investigate the sensitivity of the cask response to the selected soil profile. The three selected profiles represent a soft soil site, a stiff soil site, and a rock site.

It would be informative to calculate the equivalent shear velocity for the 42.7-m (140-ft) depth soil column model used in the cask response model to account for the variation of thickness and shear wave velocity of each of the six layers. Based on the ratio of the soil column height (i.e., 140 ft) to the time delay in a vertically propagating shear wave transmitting over the soil column for the soft soil, stiff soil and the rock profiles, the equivalent shear velocity for the 42.7-m (140-ft) depth soil column are 271, 500, and 1330 m/s (888, 1639 and 4364 ft/s), respectively.

3.2.3.2.1 Soft Soil Foundation
The material properties of the six layers in the soft soil profile are listed in Table 3.5. The elastic modulus, Poisson's ratio, density, and mass-proportional damping coefficient are material parameters, while the shear wave velocity is a function of the elastic properties and density.

Table 3.5: Soft Soil Foundation Material Properties

Layer	Layer Thickness	Elastic Modulus	Poisson's Ratio	Density	Shear Wave Velocity	Damping (α)
1	3.05 m (10 ft)	133 MPa (19.3 ksi)	0.3	2002 kg/m^3 (125 lb/ft^3)	160 m/s (524 ft/s)	1.19
2	6.10 m (20 ft)	181 MPa (26.2 ksi)	0.3	2002 kg/m^3 (125 lb/ft^3)	186 m/s (612 ft/s)	1.91
3	6.10 m (20 ft)	341 MPa (49.5 ksi)	0.3	2002 kg/m^3 (125 lb/ft^3)	256 m/s (840 ft/s)	1.33
4	6.10 m (20 ft)	451 MPa (65.4 ksi)	0.3	2002 kg/m^3 (125 lb/ft^3)	294 m/s (966 ft/s)	1.02
5	9.14 m (30 ft)	577 MPa (83.6 ksi)	0.3	2002 kg/m^3 (125 lb/ft^3)	333 m/s (1092 ft/s)	0.78
6	12.2 m (40 ft)	673 MPa (97.7 ksi)	0.3	2002 kg/m^3 (125 lb/ft^3)	360 m/s (1180 ft/s)	0.79

3.2.3.2.2 Stiff Soil Foundation
The properties of the six layers of the stiff profile are outlined in Table 3.6. As mentioned previously, the finite element models used for the soft and stiff soil profiles are the same except for the foundation material properties.

Table 3.6: Stiff Soil Foundation Material Properties

Layer	Layer Thickness	Elastic Modulus	Poisson's Ratio	Density	Shear Wave Velocity	Damping (α)
1	3.05 m (10 ft)	715 MPa (104 ksi)	0.3	2002 kg/m^3 (125 lb/ft^3)	371 m/s (1216 ft/s)	0.95
2	6.10 m (20 ft)	865 MPa (125 ksi)	0.3	2002 kg/m^3 (125 lb/ft^3)	408 m/s (1338 ft/s)	1.58
3	6.10 m (20 ft)	1096 MPa (159 ksi)	0.3	2002 kg/m^3 (125 lb/ft^3)	458 m/s (1506 ft/s)	1.34
4	6.10 m (20 ft)	1331 MPa (193 ksi)	0.3	2002 kg/m^3 (125 lb/ft^3)	506 m/s (1660 ft/s)	1.07
5	9.14 m (30 ft)	1552 MPa (225 ksi)	0.3	2002 kg/m^3 (125 lb/ft^3)	546 m/s (1792 ft/s)	0.90
6	12.2 m (40 ft)	1896 MPa (275 ksi)	0.3	2002 kg/m^3 (125 lb/ft^3)	604 m/s (1981 ft/s)	0.69

3.2.3.2.3 Rock Foundation
Table 3.7 lists the material properties of the rock foundation. Unlike the soil foundation models, the layers of finite elements do not necessarily have different material properties. The top two layers have unique material properties, but the properties are the same for all finite element layers below that point. The layer numbers in this table refer to layers of material rather than layers of finite elements.

Table 3.7: Rock Foundation Material Properties

Layer	Layer Thickness	Elastic Modulus	Poisson's Ratio	Density	Shear Wave Velocity	Damping (α)
1	0.91 m (3 ft)	309 MPa (44.8 ksi)	0.3	2002 kg/m^3 (125 lb/ft^3)	244 m/s (800 ft/s)	0.57
2	2.13 m (7 ft)	4349 MPa (630 ksi)	0.3	2002 kg/m^3 (125 lb/ft^3)	914 m/s (3000 ft/s)	0.57
3	39.6 m (130 ft)	12082 MPa (1752 ksi)	0.3	2002 kg/m^3 (125 lb/ft^3)	1523 m/s (5000 ft/s)	0.57

3.2.4 Properties of Interfaces Between Submodels

Contact interactions are defined at the interfaces between the cask and pad submodels, and between the pad and foundation submodels. A detailed overview of the various options available for modeling contact has been given in Section 3.1.2. When sufficiently high ground motions are applied to the base of the cask model, the cask can potentially experience very large motions relative to the pad. In contrast, the relative movements between the pad and foundation are generally quite small.

As mentioned previously, a single coefficient of friction is used for both static and kinetic friction. The intent in modeling the interfacial friction between the cask and pad is to use a reasonable estimate of the friction coefficient to simulate the cask behavior as accurately as possible for a variety of situations. In the parametric analyses, this friction coefficient is varied to represent a best estimate case, as well as lower and upper bound cases. The actual values used in the parametric analyses for the cask/pad friction coefficient, as well as the basis for the selection of these values are outlined in the next chapter.

During the analysis frictional contact surfaces were included between the pad and soil foundation primarily to allow for the pad to lift up slightly from the soil foundation. If the pad were directly bonded to the soil, the resulting system would be overly stiff. In many installations, the pad is embedded in the soil, so the soil on the sides of the pad provides a restraining effect against sliding. It would be possible to model explicitly this effect with additional contact surfaces around the sides of the pad, but the benefits of doing this would not justify the additional complexity required in the model.

To approximate this restraining effect while allowing for pad uplift, a relatively high coefficient of friction, 1.0, is used between the pad and the soil. The lateral displacements of the pad relative to the foundation observed in the analyses with this coefficient of friction are very small, and the desired ability for the pad to lift up from the foundation is maintained. It is important to realize that the relative sliding between the pad and foundation is likely to decrease the response of the pad because sliding would result in decreased seismic input being transferred to the pad. Therefore, using a higher coefficient of friction at this interface results in more conservative results than would be obtained with a lower coefficient of friction. In summary, the adopted modeling approach provides conservative results that are for pads that are embedded in the surrounding foundation material, as well as those that rest on top of the foundation.

4. Scope of Parametric Analyses

This research effort involved investigating the seismic response of dry cask storage systems using coupled three-dimensional finite element models of cask/pad/foundation. The objective of performing seismic analyses with these coupled models is to capture the nonlinear dynamic behavior of these storage systems including the nonlinear frictional contact algorithm at the cask/pad interface and the soil-structure interaction effects. A comprehensive series of parametric analyses was conducted to investigate the sensitivity of cask responses to a selected set of input parameters. The scope of parametric analyses, as shown in Table 4.1, is by no means exhaustive, but it does cover a broad and practical range of important parameters, with the intention of demonstrating the relative influence on the trend of variation of cask responses. These input parameters will be described in detail in this chapter.

Table 4.1: Scope of Parametric Analyses

Input Parameter	Description	Details
Coupled finite element models	2 Cask designs	Vertical cylindrical cask and horizontal rectangular module
	3 Foundation types	Soft soil, stiff soil, and rock
	3 Coefficients of friction at cask/pad interface	0.20, 0.55, and 0.80
Seismic ground motions	3 Spectral shapes	NUREG/CR-0098 Regulatory Guide 1.60 NUREG/CR-6728
	5 Selected earthquake records	NUREG/CR-0098 and Regulatory Guide 1.60: 1) 1978 Iran Tabas 2) 1999 Taiwan Chi-Chi 3) 1992 Landers 4) 1994 Northridge 5) 1979 Imperial Valley
		NUREG/CR-6728: A) 1985 Nahanni B) 1988 Saguenay C) 1979 Imperial Valley D) 1989 Loma Prieta E) 1994 Northridge
	4 PGA (Peak Ground Acceleration) levels	0.25, 0.60, 1.00, and 1.25 g

4.1 Seismic Loading – Time Histories of Accelerations

Current trend in the seismic design analysis recognizes that the earthquake ground motion should be regarded as stochastic processes, and thus the seismic response of a dry cask using one time history might not always lead to a predictable response. It is increasingly obvious that a suite of earthquake inputs should be examined in order to obtain statistically stable mean and standard variation in the response to form the basis for design decision. This would require multiple runs using several earthquake records. Furthermore, as discussed in Section 3.1.1, a sufficiently wide range in parametric variations in ground shaking characteristics would be needed for covering a wide variation in seismological and soil conditions.

In the parametric analyses of dry casks, the investigation scope includes formulating the ground motion characteristics having the target design response spectra in accordance with three spectral shapes: the NUREG/CR-0098, the Regulatory Guide 1.60, and the NUREG/CR-6728. These three spectral shapes were chosen because of their potential use by cask design applicants. Furthermore, the three postulated spectral shapes would provide for a sufficiently wide range of coverage with respect to the variations in the seismological conditions including WUS (western United States) and CEUS (central and eastern United States) as well as the variation in ground motion characteristics due to different soil conditions.

Historically, due to the absence of strong motion data from actual recordings from the CEUS sites, seismic design practice in CEUS ground motion criteria has generally been developed by using smaller Peak Ground Acceleration (PGA) values applied to empirical WUS spectral shapes (e.g., the earlier discussed NUREG-0098 and the Regulatory Guide 1.60 methods) for developing the target design spectrum for CEUS conditions. Recent seismological studies confirmed by limited available CEUS strong motion recordings led to the current thinking that the historical practice on the use of WUS spectral shapes would still lead to unrealistic target shaking characteristics for the CEUS sites. Studies such as the NUREG/CR-6728 conclude that the differences in CEUS seismological conditions would not only result in lower shaking levels (i.e., lower PGA), but would also result in much lower long-period contents for the CEUS sites. The NUREG/CR-6728 studies have been adopted by the NRC for implementing more current seismological studies for CEUS design conditions that would be fundamentally different from historical WUS practice. Figure 4.1 presents the WUS and CEUS geographical boundary following the USGS seismic-hazard mapping program. The boundary basically follows the US Rocky Mountains passing through Montana, Wyoming, Utah, Arizona, then bending east through Southern Colorado, New Mexico and western Texas.

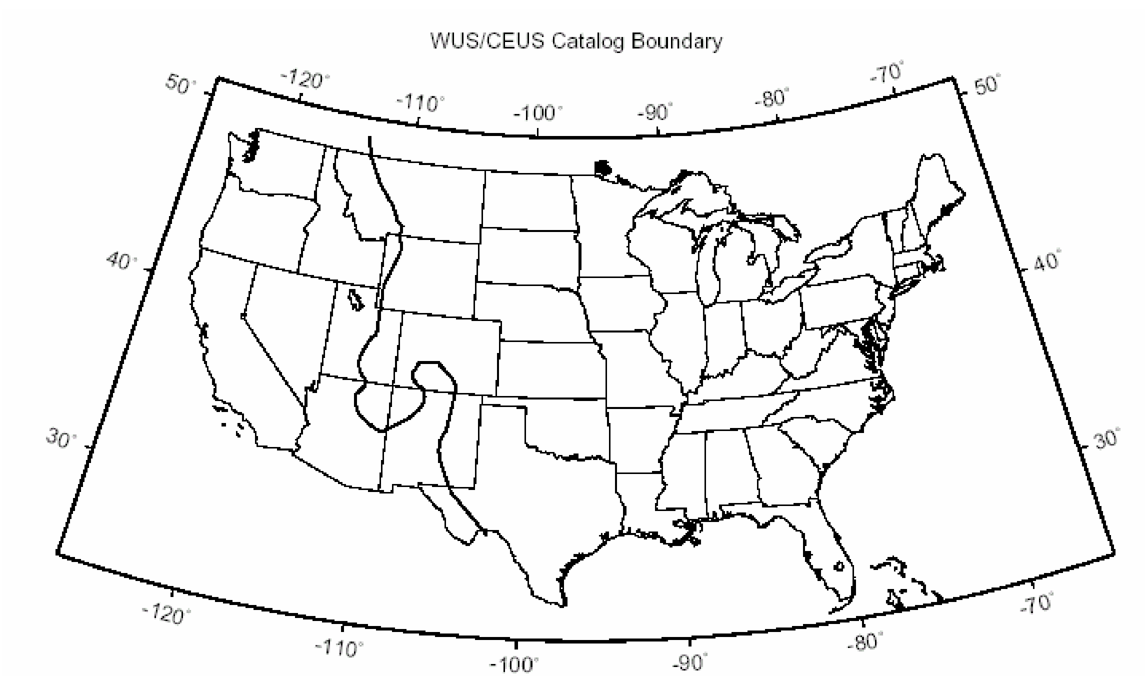

Figure 4.1: Boundary between Western US (WUS) and Central and Eastern US (CEUS)

Table 4.2 shows the tabulation of the spectral acceleration curve shapes, after normalizing by the horizontal motion for PGA Values. The NUREG/CR-6728 procedure has been used initially for developing the CEUS rock site spectral shapes. However, the report did not present a procedure suitable for developing generic soil site spectral shapes. The report assumed that site specific response analyses would be conducted for soil sites, which cannot be used for the current generic site study. Some generic randomized site response analyses were performed in order to rationalize a generic soil site spectral shape for the CEUS sites. Because of the relatively competent site soil conditions expected for typical nuclear power plant sites along with the relatively low level of shaking expected for typical CEUS conditions, differences of ground shaking between rock and soil sites in CEUS is not anticipated to be a very big factor. Ultimately, the generic CEUS soil site spectrum based on the randomized site response analyses was adopted to complement the procedure for the two WUS (i.e., NUREG/CR-0098 and the Regulatory Guide 1.60 spectral shapes) spectral shapes in the parametric response study. The NUREG/CR-6728 CEUS spectral shape would provide reasonable representations for both soil and rock sites for CEUS ground motion conditions.

Figure 4.2 presents a plot to compare the three spectral acceleration curve shapes for (a) the horizontal and (b) the vertical motions in terms of log-log plots of normalized spectral acceleration versus frequency. Corresponding comparisons of horizontal and vertical shaking, in terms of linear plots of normalized spectral displacement and acceleration versus period, are showed in Figures 4.3 and 4.4, respectively.

From these presented figures, it can be observed that the shaking demand for the three spectral shapes, especially at increasingly longer periods, decreases progressively and systematically from the Regulatory Guide 1.60 to the NUREG/CR-0098 and then to the lowest shaking NUREG/CR-6728 CEUS spectral shape. It should be noted that even though the three cited procedures were used for formulating the spectral shapes in developing the period-dependent demand of target ground motion, they are not intended to establish the demand level for project specific designs. There should be a wider degree of latitude in utilizing the response solutions from the project library so long as the cross comparison of reference ground surface design response spectra between project specific cases are made to the parametric library. For example, the reference surface spectra using the NUREG/CR-6728 CEUS spectral shape might be found to compare favorably to the ground motion shaking characteristics established for WUS rock sites in some site-specific projects. In such cases, even though the reference surface spectra are developed in accordance with the NUREG/CR-6728 CEUS spectral procedure for CEUS seismological conditions, they can also be used for WUS rock sites.

It should be observed that for a specific PGA, the variation in spectral demands among the three spectral shapes at longer periods ranges from about 3 times at about 1-second period, to as much as 10 folds at periods longer than 4 seconds. This sufficiently wide range may be adequate to cover the potential ranges in ground motion demanded from various cask design applicants, including variations in seismological and soil conditions. It should also be recognized that the three adopted spectral shapes are nicely separated to allow a reasonable interpolation of response solutions for different cask design applicants. The following sections provide background details regarding each of the three adopted spectral shape procedures.

Table 4.2: Tabulation of Spectral Shapes

PERIOD (SECOND)	Frequency (Hz)	SA/PGA							
		REG. GUIDE 1.60, HOR.	REG. GUIDE 1.60, VERT.	NUREG/CR-0098, HOR.	NUREG/CR-0098, VERT.	CEUS, HOR. ROCK	CEUS, VERT. ROCK	CEUS, HOR. SOIL	CEUS, VERT. SOIL
0.01	100.00	1.0000	1.0000	1.0000	0.6500	1.0000	1.0000	1.0000	1.0000
0.03	33.33	0.9998	0.9998	1.0000	0.6500	2.2391	2.1719	1.6532	2.3565
0.04	25.00	1.2321	1.2321	1.1554	0.7510	2.2375	1.9690	2.1180	2.1363
0.05	20.00	1.4572	1.4572	1.2976	0.8434	2.1911	1.8076	2.5692	1.9613
0.06	16.67	1.6714	1.6714	1.4267	0.9273	2.1285	1.7050	2.5719	1.8500
0.07	14.29	1.8769	1.8769	1.5458	1.0047	2.0593	1.6233	2.5785	1.7613
0.08	12.50	2.0752	2.0752	1.6569	1.0770	1.9883	1.5420	2.5814	1.6731
0.09	11.11	2.2674	2.2674	1.7616	1.1450	1.9184	1.4633	2.5656	1.5877
0.10	10.00	2.4544	2.4544	1.8608	1.2095	1.8509	1.3882	2.5692	1.5062
0.11	9.09	2.6368	2.6368	1.9554	1.2710	1.7866	1.3400	2.5722	1.4539
0.12	8.33	2.6861	2.6776	2.0459	1.3298	1.7257	1.2943	2.5746	1.4043
0.13	7.69	2.7172	2.6996	2.1329	1.3864	1.6683	1.2512	2.5767	1.3576
0.14	7.14	2.7462	2.7201	2.1622	1.4054	1.6141	1.2106	2.5785	1.3135
0.15	6.67	2.7735	2.7393	2.1623	1.4055	1.5630	1.1723	2.5801	1.2719
0.16	6.25	2.7993	2.7574	2.1623	1.4055	1.5147	1.1361	2.5713	1.2326
0.17	5.88	2.8237	2.7746	2.1624	1.4056	1.4691	1.1018	2.5730	1.1955
0.18	5.56	2.8470	2.7908	2.1624	1.4056	1.4258	1.0694	2.5746	1.1603
0.19	5.26	2.8691	2.8063	2.1625	1.4056	1.3847	1.0385	2.5761	1.1268
0.20	5.00	2.8903	2.8210	2.1625	1.4057	1.3456	1.0092	2.5774	1.0950
0.21	4.76	2.9106	2.8351	2.1626	1.4057	1.3083	0.9812	2.5785	1.0647
0.22	4.55	2.9301	2.8486	2.1626	1.4057	1.2727	0.9546	2.4983	1.0357
0.23	4.35	2.9488	2.8616	2.1627	1.4057	1.2387	0.9290	2.3896	1.0080
0.24	4.17	2.9669	2.8740	2.1627	1.4058	1.2061	0.9046	2.2901	0.9815
0.25	4.00	2.9843	2.8860	2.1628	1.4058	1.1749	0.8812	2.1985	0.9561
0.26	3.85	3.0011	2.8976	2.1628	1.4058	1.1449	0.8587	2.1139	0.9317
0.27	3.70	3.0174	2.9088	2.1628	1.4058	1.1161	0.8371	2.0356	0.9082
0.28	3.57	3.0332	2.9196	2.1629	1.4059	1.0884	0.8163	1.9629	0.8857
0.29	3.45	3.0485	2.9301	2.1629	1.4059	1.0617	0.7963	1.8952	0.8640
0.30	3.33	3.0634	2.9403	2.1629	1.4059	1.0360	0.7770	1.8321	0.8430
0.31	3.23	3.0778	2.9501	2.1630	1.4059	1.0112	0.7584	1.7730	0.8229
0.32	3.13	3.0918	2.9597	2.1630	1.4059	0.9873	0.7405	1.7176	0.8034
0.33	3.03	3.1055	2.9690	2.1630	1.4060	0.9642	0.7231	1.6655	0.7846
0.34	2.94	3.1188	2.9781	2.1630	1.4060	0.9419	0.7064	1.6165	0.7664
0.35	2.86	3.1318	2.9869	2.1631	1.4060	0.9203	0.6902	1.5703	0.7489
0.36	2.78	3.1445	2.9955	2.1631	1.4060	0.8994	0.6745	1.5267	0.7319
0.37	2.70	3.1569	3.0039	2.1631	1.4060	0.8792	0.6594	1.4855	0.7154
0.38	2.63	3.1690	3.0121	2.1631	1.4060	0.8596	0.6447	1.4464	0.6995
0.39	2.56	3.1808	3.0201	2.1632	1.4061	0.8406	0.6305	1.4093	0.6841
0.40	2.50	3.1924	3.0279	2.1632	1.4061	0.8222	0.6167	1.3740	0.6691
0.41	2.44	3.1267	2.9547	2.1632	1.4061	0.8044	0.6033	1.3405	0.6546
0.42	2.38	3.0638	2.8849	2.1632	1.4061	0.7871	0.5903	1.3086	0.6405
0.43	2.33	3.0037	2.8183	2.1633	1.4061	0.7703	0.5778	1.2782	0.6269
0.44	2.27	2.9461	2.7547	2.1633	1.4061	0.7541	0.5655	1.2491	0.6136
0.45	2.22	2.8909	2.6940	2.1465	1.3952	0.7382	0.5537	1.2214	0.6007
0.46	2.17	2.8378	2.6359	2.0998	1.3649	0.7229	0.5421	1.1948	0.5882
0.47	2.13	2.7869	2.5802	2.0551	1.3358	0.7079	0.5310	1.1694	0.5761
0.48	2.08	2.7379	2.5269	2.0123	1.3080	0.6934	0.5201	1.1450	0.5643
0.49	2.04	2.6907	2.4757	1.9712	1.2813	0.6793	0.5095	1.1217	0.5528
0.50	2.00	2.6453	2.4266	1.9318	1.2557	0.6656	0.4992	1.0992	0.5417
0.51	1.96	2.6016	2.3794	1.8939	1.2311	0.6523	0.4892	1.0777	0.5308
0.52	1.92	2.5594	2.3340	1.8575	1.2074	0.6393	0.4795	1.0570	0.5203
0.53	1.89	2.5186	2.2903	1.8225	1.1846	0.6267	0.4700	1.0370	0.5100
0.54	1.85	2.4793	2.2482	1.7887	1.1627	0.6144	0.4608	1.0178	0.5000
0.55	1.82	2.4413	2.2077	1.7562	1.1415	0.6025	0.4519	0.9993	0.4903
0.56	1.79	2.4045	2.1686	1.7248	1.1211	0.5909	0.4431	0.9815	0.4808
0.57	1.75	2.3689	2.1308	1.6946	1.1015	0.5795	0.4347	0.9642	0.4716
0.58	1.72	2.3345	2.0944	1.6654	1.0825	0.5685	0.4264	0.9476	0.4626
0.60	1.67	2.2687	2.0251	1.6098	1.0464	0.5474	0.4105	0.9160	0.4454
0.62	1.61	2.2069	1.9603	1.5579	1.0126	0.5273	0.3955	0.8865	0.4291
0.64	1.56	2.1487	1.8995	1.5092	0.9810	0.5082	0.3812	0.8588	0.4136
0.66	1.52	2.0937	1.8424	1.4635	0.9513	0.4901	0.3676	0.8328	0.3989
0.68	1.47	2.0417	1.7886	1.4204	0.9233	0.4730	0.3547	0.8083	0.3849
0.70	1.43	1.9925	1.7379	1.3799	0.8969	0.4566	0.3425	0.7852	0.3716
0.72	1.39	1.9458	1.6900	1.3415	0.8720	0.4411	0.3308	0.7634	0.3590
0.74	1.35	1.9014	1.6447	1.3053	0.8484	0.4264	0.3198	0.7427	0.3470
0.76	1.32	1.8591	1.6017	1.2709	0.8261	0.4123	0.3092	0.7232	0.3355
0.78	1.28	1.8189	1.5610	1.2383	0.8049	0.3989	0.2992	0.7046	0.3246
0.80	1.25	1.7805	1.5223	1.2074	0.7848	0.3862	0.2897	0.6870	0.3143

Table 4.2. Tabulation of Spectral Shapes (cont'd)

PERIOD (SECOND)	Frequency (Hz)	SA/PGA							
		REG. GUIDE 1.60, HOR.	REG. GUIDE 1.60, VERT.	NUREG/CR-0098, HOR.	NUREG/CR-0098, VERT.	CEUS, HOR. ROCK	CEUS, VERT. ROCK	CEUS, HOR. SOIL	CEUS, VERT. SOIL
0.82	1.22	1.7439	1.4854	1.1779	0.7657	0.3741	0.2805	0.6703	0.3044
0.84	1.19	1.7088	1.4503	1.1499	0.7474	0.3625	0.2719	0.6543	0.2950
0.86	1.16	1.6753	1.4169	1.1231	0.7300	0.3514	0.2636	0.6391	0.2860
0.88	1.14	1.6432	1.3849	1.0976	0.7135	0.3409	0.2557	0.6246	0.2774
0.90	1.11	1.6123	1.3544	1.0732	0.6976	0.3308	0.2481	0.6107	0.2692
0.92	1.09	1.5828	1.3252	1.0499	0.6824	0.3212	0.2409	0.5974	0.2614
0.94	1.06	1.5543	1.2972	1.0276	0.6679	0.3120	0.2340	0.5847	0.2539
0.96	1.04	1.5270	1.2704	1.0061	0.6540	0.3032	0.2274	0.5725	0.2467
0.98	1.02	1.5007	1.2447	0.9856	0.6407	0.2948	0.2211	0.5608	0.2399
1.00	1.00	1.4754	1.2200	0.9659	0.6278	0.2867	0.2150	0.5496	0.2333
1.05	0.95	1.4160	1.1623	0.9199	0.5979	0.2679	0.2010	0.5235	0.2180
1.10	0.91	1.3616	1.1099	0.8781	0.5708	0.2510	0.1883	0.4908	0.2043
1.15	0.87	1.3116	1.0620	0.8399	0.5459	0.2357	0.1768	0.4497	0.1918
1.20	0.83	1.2654	1.0181	0.8049	0.5232	0.2218	0.1664	0.4133	0.1805
1.25	0.80	1.2226	0.9777	0.7727	0.5023	0.2092	0.1569	0.3812	0.1702
1.30	0.77	1.1829	0.9404	0.7430	0.4830	0.1976	0.1482	0.3515	0.1608
1.35	0.74	1.1458	0.9058	0.7155	0.4651	0.1871	0.1403	0.3264	0.1522
1.40	0.71	1.1113	0.8737	0.6899	0.4485	0.1773	0.1330	0.3032	0.1443
1.45	0.69	1.0789	0.8438	0.6661	0.4330	0.1684	0.1263	0.2826	0.1370
1.50	0.67	1.0485	0.8159	0.6439	0.4186	0.1601	0.1201	0.2645	0.1303
1.55	0.65	1.0200	0.7898	0.6232	0.4051	0.1525	0.1143	0.2476	0.1241
1.60	0.63	0.9931	0.7653	0.6037	0.3924	0.1454	0.1090	0.2327	0.1183
1.65	0.61	0.9676	0.7423	0.5854	0.3805	0.1388	0.1041	0.2188	0.1129
1.70	0.59	0.9436	0.7206	0.5682	0.3693	0.1326	0.0995	0.2057	0.1079
1.75	0.57	0.9209	0.7002	0.5519	0.3588	0.1269	0.0952	0.1942	0.1033
1.80	0.56	0.8993	0.6809	0.5366	0.3488	0.1216	0.0912	0.1834	0.0989
1.85	0.54	0.8787	0.6627	0.5221	0.3394	0.1166	0.0874	0.1740	0.0948
1.90	0.53	0.8592	0.6453	0.5084	0.3304	0.1119	0.0839	0.1643	0.0910
1.95	0.51	0.8406	0.6289	0.4953	0.3220	0.1074	0.0806	0.1568	0.0874
2.00	0.50	0.8229	0.6133	0.4830	0.3139	0.1033	0.0775	0.1488	0.0841
2.05	0.49	0.8060	0.5985	0.4712	0.3063	0.0994	0.0745	0.1412	0.0809
2.10	0.48	0.7898	0.5843	0.4600	0.2990	0.0957	0.0718	0.1347	0.0779
2.15	0.47	0.7743	0.5709	0.4493	0.2920	0.0922	0.0692	0.1286	0.0750
2.20	0.45	0.7594	0.5580	0.4390	0.2854	0.0889	0.0667	0.1227	0.0724
2.25	0.44	0.7452	0.5457	0.4293	0.2790	0.0858	0.0643	0.1178	0.0698
2.30	0.43	0.7315	0.5339	0.4200	0.2730	0.0828	0.0621	0.1124	0.0674
2.35	0.43	0.7184	0.5226	0.4110	0.2672	0.0800	0.0600	0.1079	0.0651
2.40	0.42	0.7057	0.5118	0.4025	0.2616	0.0774	0.0580	0.1030	0.0630
2.50	0.40	0.6819	0.4915	0.3864	0.2511	0.0724	0.0543	0.0950	0.0589
2.60	0.38	0.6597	0.4728	0.3715	0.2415	0.0680	0.0510	0.0882	0.0553
2.70	0.37	0.6391	0.4554	0.3577	0.2325	0.0639	0.0479	0.0813	0.0520
2.80	0.36	0.6198	0.4393	0.3450	0.2242	0.0602	0.0451	0.0761	0.0489
2.90	0.34	0.6018	0.4242	0.3331	0.2165	0.0567	0.0426	0.0707	0.0462
3.00	0.33	0.5848	0.4102	0.3113	0.2024	0.0536	0.0402	0.0661	0.0436
3.10	0.32	0.5689	0.3971	0.2916	0.1895	0.0507	0.0380	0.0619	0.0413
3.20	0.31	0.5539	0.3848	0.2736	0.1779	0.0481	0.0360	0.0579	0.0391
3.30	0.30	0.5397	0.3732	0.2573	0.1672	0.0456	0.0342	0.0547	0.0371
3.40	0.29	0.5263	0.3623	0.2424	0.1576	0.0433	0.0325	0.0517	0.0352
3.50	0.29	0.5136	0.3520	0.2287	0.1487	0.0412	0.0309	0.0483	0.0335
3.60	0.28	0.5016	0.3423	0.2162	0.1405	0.0392	0.0294	0.0461	0.0319
3.70	0.27	0.4901	0.3331	0.2047	0.1330	0.0374	0.0280	0.0434	0.0304
3.80	0.26	0.4792	0.3244	0.1940	0.1261	0.0357	0.0267	0.0412	0.0290
3.90	0.26	0.4689	0.3162	0.1842	0.1197	0.0340	0.0255	0.0391	0.0277
4.00	0.25	0.4590	0.3083	0.1751	0.1138	0.0325	0.0244	0.0372	0.0265
4.10	0.24	0.4368	0.2935	0.1667	0.1083	0.0311	0.0233	0.0354	0.0253
4.20	0.24	0.4163	0.2796	0.1588	0.1032	0.0298	0.0224	0.0337	0.0243
4.30	0.23	0.3972	0.2667	0.1515	0.0985	0.0286	0.0214	0.0321	0.0232
4.40	0.23	0.3793	0.2547	0.1447	0.0941	0.0274	0.0205	0.0307	0.0223
4.50	0.22	0.3626	0.2435	0.1384	0.0899	0.0263	0.0197	0.0294	0.0214
4.60	0.22	0.3470	0.2330	0.1324	0.0861	0.0252	0.0189	0.0281	0.0205
4.70	0.21	0.3324	0.2232	0.1268	0.0824	0.0242	0.0182	0.0269	0.0197
4.80	0.21	0.3187	0.2140	0.1216	0.0790	0.0233	0.0175	0.0258	0.0190
4.90	0.20	0.3058	0.2053	0.1167	0.0759	0.0224	0.0168	0.0248	0.0182
5.00	0.20	0.2937	0.1972	0.1121	0.0729	0.0216	0.0162	0.0238	0.0176

Table 4.2. Tabulation of Spectral Shapes (cont'd)

PERIOD (SECOND)	Frequency (Hz)	SA/PGA							
		REG. GUIDE 1.60, HOR.	REG. GUIDE 1.60, VERT.	NUREG/CR-0098, HOR.	NUREG/CR-0098, VERT.	CEUS, HOR. ROCK	CEUS, VERT. ROCK	CEUS, HOR. SOIL	CEUS, VERT. SOIL
5.10	0.20	0.2823	0.1895	0.1077	0.0700	0.0208	0.0156	0.0229	0.0169
5.20	0.19	0.2716	0.1823	0.1036	0.0674	0.0200	0.0150	0.0220	0.0163
5.40	0.19	0.2518	0.1690	0.0961	0.0625	0.0186	0.0140	0.0204	0.0151
5.60	0.18	0.2342	0.1571	0.0893	0.0581	0.0173	0.0130	0.0190	0.0141
5.80	0.17	0.2183	0.1464	0.0833	0.0541	0.0162	0.0121	0.0177	0.0132
6.00	0.17	0.2040	0.1368	0.0778	0.0506	0.0151	0.0114	0.0165	0.0123
6.20	0.16	0.1910	0.1281	0.0729	0.0474	0.0142	0.0106	0.0155	0.0115
6.40	0.16	0.1793	0.1202	0.0684	0.0445	0.0133	0.0100	0.0145	0.0108
6.60	0.15	0.1686	0.1130	0.0643	0.0418	0.0125	0.0094	0.0137	0.0102
6.80	0.15	0.1588	0.1065	0.0606	0.0394	0.0117	0.0088	0.0129	0.0096
7.00	0.14	0.1499	0.1005	0.0572	0.0372	0.0111	0.0083	0.0121	0.0090
7.20	0.14	0.1417	0.0949	0.0540	0.0351	0.0104	0.0078	0.0115	0.0085
7.40	0.14	0.1341	0.0899	0.0512	0.0333	0.0098	0.0074	0.0109	0.0080
7.60	0.13	0.1271	0.0852	0.0485	0.0315	0.0093	0.0070	0.0103	0.0076
7.80	0.13	0.1207	0.0809	0.0461	0.0299	0.0088	0.0066	0.0098	0.0072
8.00	0.13	0.1147	0.0769	0.0438	0.0285	0.0083	0.0062	0.0093	0.0068
8.50	0.12	0.1016	0.0681	0.0388	0.0252	0.0073	0.0055	0.0082	0.0059
9.00	0.11	0.0907	0.0607	0.0346	0.0225	0.0064	0.0048	0.0073	0.0052
9.50	0.11	0.0814	0.0545	0.0310	0.0202	0.0057	0.0043	0.0066	0.0046
10.00	0.10	0.0734	0.0491	0.0280	0.0182	0.0050	0.0038	0.0060	0.0041

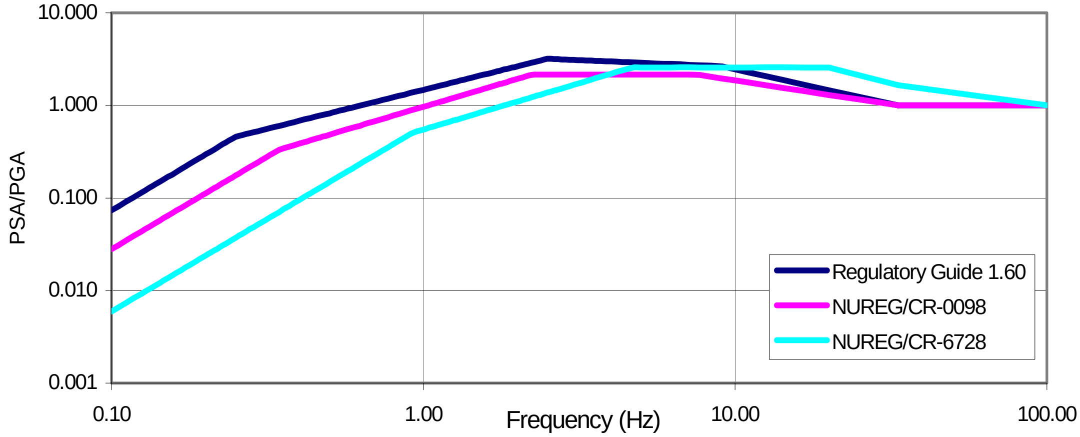

(a) Spectral Shapes for Horizontal Motion

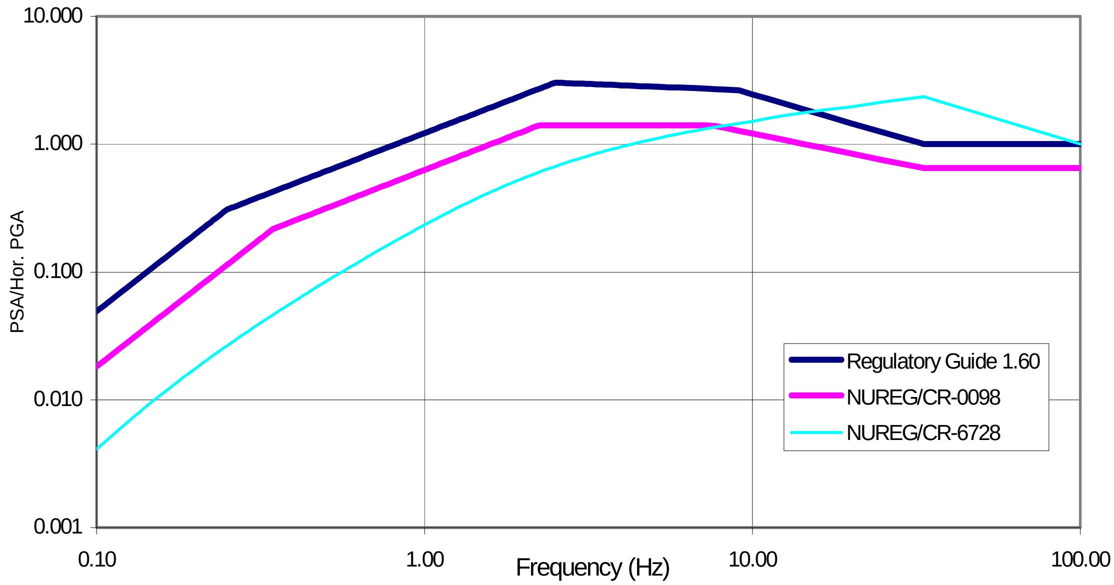

(b) Spectral Shapes for Vertical Motion

Figure 4.2: Plots of Horizontal and Vertical Spectral Shapes In Terms of Frequency (Logarithmic Scales)

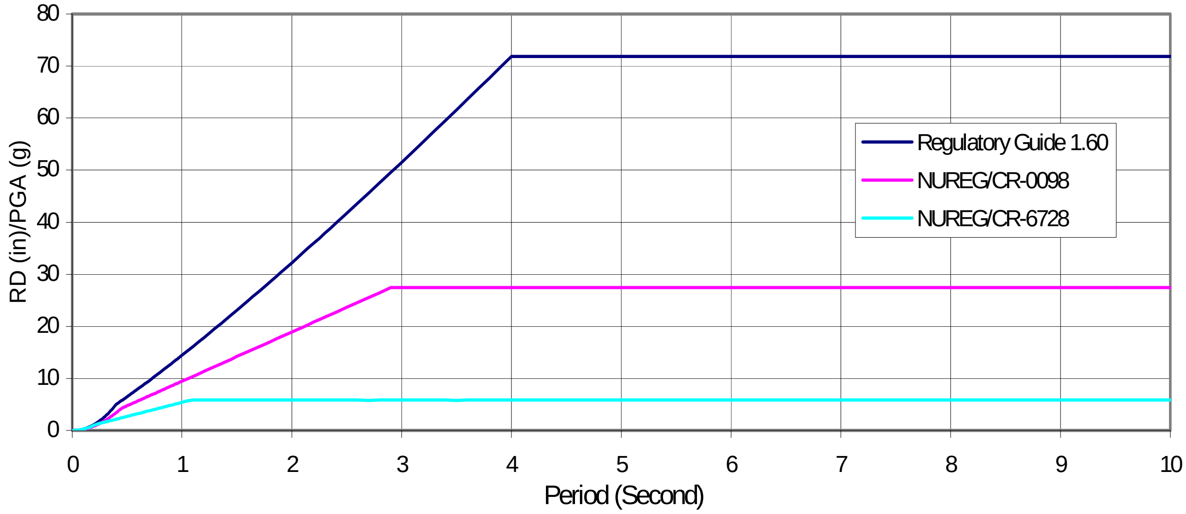

(a) Spectral displacement vs. period

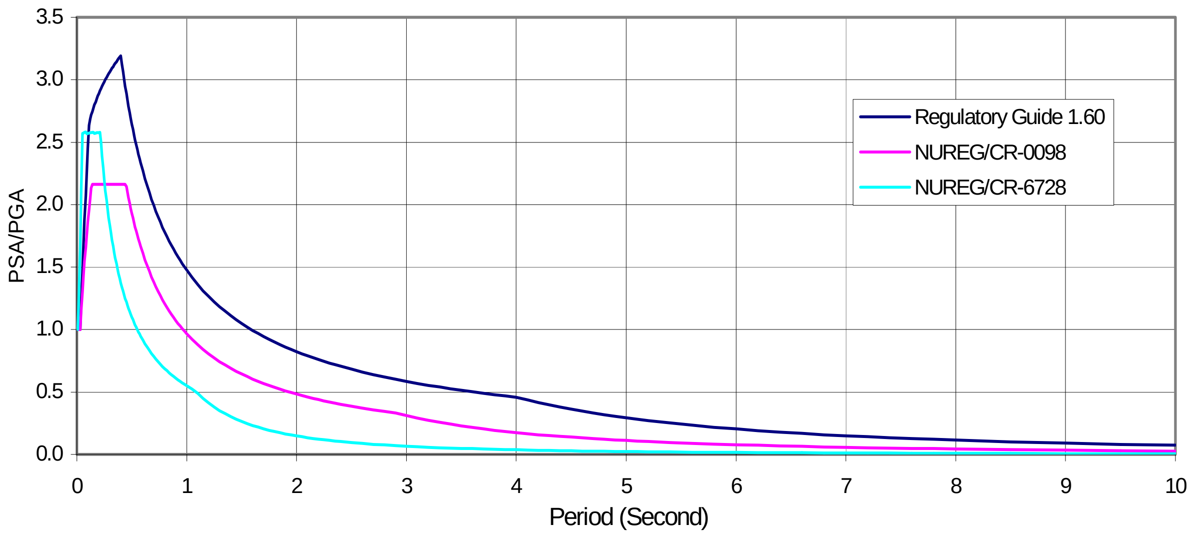

(b) Spectral acceleration vs. period

Figure 4.3: Plots of Horizontal Spectral Shapes In Terms of Period (Linear Scales)

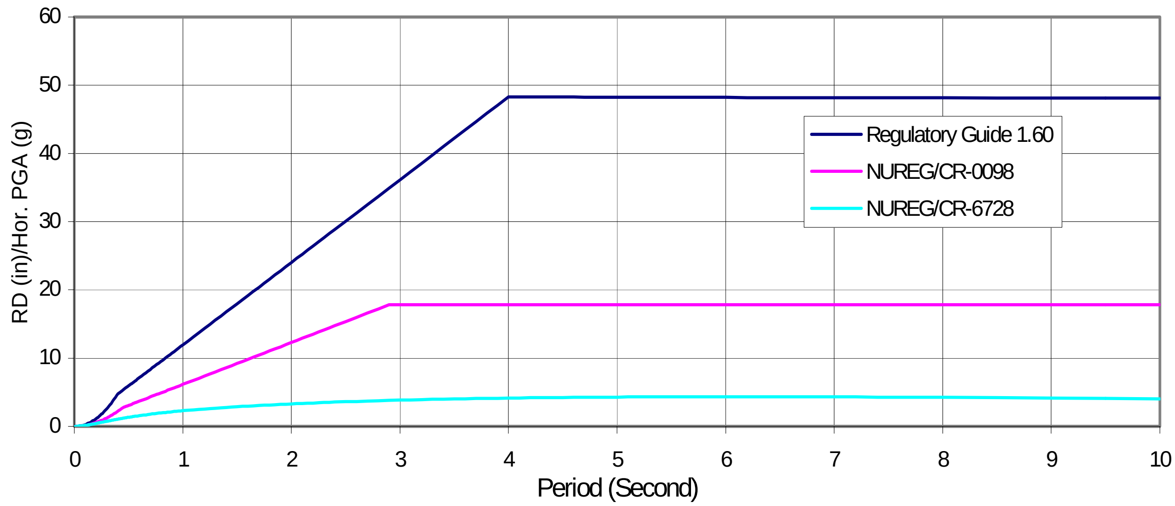

(a) Spectral displacement vs. period

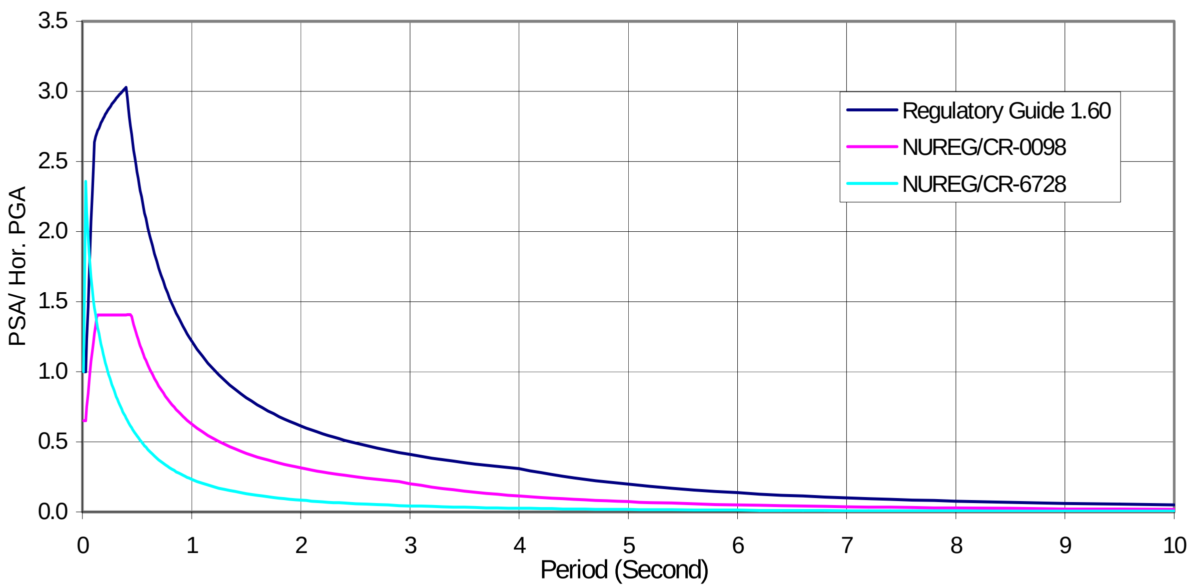

(b) Spectral acceleration vs. period

Figure 4.4: Plots of Vertical Spectral Shapes In Terms of Period (Linear Scales)

4.1.1 NUREG/CR-0098 Spectral Shape

The NUREG/CR-0098 spectral procedure, which was originally developed by Newmark based on actual strong-motions recorded in western US earthquakes, was followed to develop the horizontal spectral shape. The procedure has been widely used in the industry in other sectors besides the nuclear industry and probably considered as the best-estimated ground-motion characteristics for WUS, reflecting the empirical strong motion database. Hidden conservatism, inherent in most design procedures, has been deliberately avoided for this adopted spectral shape. The median spectral amplification factors, which represent the 50th percentile, were used rather than the 84% spectral amplification factors.

According to NUREG/CR-0098, a Peak Ground Velocity to PGA (PGV/PGA) of 36 in/s per g should be used to develop the PGV parameter to anchor the PGV period range. A PGD*A/(PGV^2) coefficient of 6 should be used to develop the peak ground displacement (PGD) parameter for anchoring constant displacement range, where consistent units should be used for PGD (in L), A (in LT^{-2}) and PGV (in LT^{-1}). These listed velocity and displacement parameters were selected so that the spectral shapes would be compatible to a median earthquake (e.g., Magnitude 6.5) range that was considered to be the typical condition for designs of many plant sites, especially outside California, which likely require more special site-specific studies.

4.1.1.1 NUREG/CR-0098 Vertical Motion Spectral Shape

The NUREG/CR-0098 recommends that the vertical response spectrum be equal to 2/3 of the horizontal response spectrum uniformly at all periods.

4.1.2 Regulatory Guide 1.60 Spectral Shape

The Regulatory Guide 1.60 spectral procedure was selected in the parametric analyses because it has been widely used for designing many of the existing nuclear power plants. However, the Regulatory Guide 1.60 spectral procedure has been found to be unrealistically conservative when compared with the empirical strong motion data from several recent studies sponsored by the NRC (see discussions in NUREG/CR-6728). This procedure might become obsolete for future nuclear power projects, as more updated procedures are implemented with more up-to-date studies by geoscientists. Nevertheless, it is believed that this approach can serve as an upper bound evaluation case along with its merits in terms of past applications.

4.1.2.1 Regulatory Guide 1.60 Vertical Motion Spectral Shape

The Regulatory Guide 1.60 spectral procedure was followed in developing the vertical motion spectral shape. It should be noted that at the zero period, the Regulatory Guide 1.60 assumes the same PGA for both horizontal and vertical component motions, but the V/H ratios are period dependent.

4.1.3 NUREG/CR-6728 Spectral Shape

For the parametric analyses in this project, it was decided to follow the recommendations in the NUREG/CR-6728 spectral procedure to reflect the state-of-the-art practice toward ground motion hazards in the CEUS sites. Randomized site response analyses were performed in searching and evaluating potential candidate generic CEUS spectral shapes for both rock and soil sites. Eventually, a M-6.5 generic CEUS soil site spectral shape was selected. The rationale of selecting the CEUS spectral shape is that this CEUS spectral shape, along with the two WUS spectral shapes represented by the NUREG/CR-0098 and the Regulatory Guide 1.60 spectral shape procedures, provides for a reasonable range of variation in long period shaking intensities. In addition, the collection of cask response results arising from the response analyses would provide a comprehensive set of parametric response results for cross comparison to applicant submittals.

The comparison of the CEUS spectral shapes between generic rock and generic soil sites showed relatively small differences. Therefore, the CEUS generic soil site spectral shapes can provide reasonable representations for the CEUS generic rock site conditions in regards to the expected ground-surface shaking demand. As discussed earlier, the relatively low long-period contents in the adopted CEUS spectral shape could also provide coverage of generic rock site response conditions for both CEUS and WUS sites.

4.1.3.1 CEUS Generic Vertical Motion Spectral Shape

The NUREG/CR-6728 spectral procedure was followed in developing the vertical motion spectral shapes. The report presented three sets of period dependent V/H ratios as a function of the PGA levels. A PGA at 0.25 g would represent typical design conditions of most of the non-western US sites, and the vertical motion spectral shape for the V/H ratios for PGA at 0.2–0.5 g from the report was chosen to develop the spectral shape for the generic CEUS spectral shape.

4.1.4 Time Histories for the Three Spectral Shapes

Time histories of seismic accelerations were input to the coupled cask/pad/foundation model. After developing the three target spectral shapes, the next step involved generating a suite of input ground motions that would have shaking characteristics matching the target spectral shapes. These ground motions were then scaled to yield earthquakes with varying values of PGA to apply to the analysis models.

There are various ways for generating input time histories for dynamic response analyses. One includes scaling historical earthquake records by a constant scaling factor (i.e., uniform factor for all periods). Another modifies recorded motions by period-dependent scaling factors so that the resulting records would match the intended smooth spectral shape throughout the entire period range. There are relative merits in either approach. Whereas the first approach might result in theoretically more correct solutions (because of its ability to preserve inherent variations in strong ground motion data), this method requires a prohibitively large number of sets of input motions (probably over 20) to obtain a statistically stable set of response solutions. In recognition of the fact that this approach is impractical, the second approach of spectrum-compatible motions was chosen for the parametric analyses.

As discussed earlier, the stochastic nature of earthquake response of structures needs to be respected, and a design decision should not be based on a single analysis. The parametric analyses were expected to develop a meaningful set of statistical parameters describing the expected cask response, which could then be used to develop guidelines for reviewing cask design submittals. Logically, a larger number of time history inputs might be more appropriate to develop statistically stable response measures. However, in practice, it is very rare that adequate resources are available to support a sufficiently large number of input motion characteristics to meet the theoretical objective. The number of input motions for establishing statistically stable response measures depends on the complexity of the structural model and the degree of nonlinearity in the structural response. Common design practice involves inherent conservatism in the design criteria to compensate for the insufficient number of input motions. For example, in designing major bridges, enveloping the calculated demands for all the motion sets is rather common for applying up to three sets of input motion. Developing statistical parameters to design for a specified confidence level would generally require a minimum of seven to ten sets of input motions. For this project, it was decided as a compromise to conduct analyses for five sets of three component motions for each of the three adopted spectral shapes. Furthermore, the spectral compatible motion approach was adopted to maximize the chance that the resultant solutions be statistically stable (i.e., that the mean and standard deviation be meaningful) for the limited five sets of input motions.

This project used startup motion records contained in the strong motion database recommended by the NUREG/CR-6728. Five earthquake records for the WUS sites appropriate for the NUREG/CR-0098 and the Regulatory Guide 1.60 spectral shapes were selected:

1) 1978 Iran Tabas
2) 1999 Taiwan Chi-Chi
3) 1992 Landers
4) 1994 Northridge
5) 1979 Imperial Valley

Likewise, five different earthquake records for the CEUS sites appropriate for the NUREG/CR-6728 spectral shape were also selected:

A) 1985 Nahanni
B) 1988 Saguenay
C) 1979 Imperial Valley
D) 1989 Loma Prieta
E) 1994 Northridge

Table 4.3 tabulates the startup motion records selected for developing the needed spectrum-compatible motions for the cask response parametric study. The steps in modifying the selected strong motion records for spectrum compatibility are listed below:

(1) Find principal major and minor horizontal shaking directions.

(2) Rotate startup motion to the principal directions.

(3) Transform each component motion to frequency domain.

(4) Based on the response spectra of startup motion and the target spectrum, adjust the Fourier amplitudes for each frequency but keep the phase angle unchanged. Repeat this process iteratively (typically no more than 5 iterations) for convergence to target spectrum.

(5) Conduct baseline corrections of spectrum-compatible motion.

(6) Recheck for spectrum compatibility and repeat (3) through (5) if necessary.

(7) Check the cross correlation of the two orthogonal horizontal component motions and repeat (1) through (6) if necessary.

The three right columns in Table 4.3 tabulate the peak accelerations, velocity and displacement values of each component motion after modifications for spectrum compatibility. The peak values presented in Table 4.3 have been normalized for a horizontal PGA of 1 g. The appropriate horizontal PGA can be used as a uniform scaling factor applied to each of the component motion records to develop a three component input motion for design analyses. For the dry cask parametric studies, the ground motions shown in Table 4.3 were scaled to a variety of horizontal PGA values at ranging from 0.25 g to 1.25 g to calculate the cask response at various shaking levels.

As discussed earlier, for each of the ground surface spectrum-compatible motion records, deconvolution analyses were conducted using three profiles (as presented in Figure 3.5) to provide startup motion records at the foundation base in the coupled response model. These analyses allowed for variations of potential coefficient of restitution implied by different soil conditions. Appendix III has been included to document each set of the generated input motions. In the course of the project, some questions have been raised regarding how soil properties (e.g., strain-compatible properties) affect the selected ground motions. Appendix I is provided to offer some information on these issues. The following paragraphs provide a brief summary of the procedure.

As discussed earlier, it was intended that the three spectral shapes be scaled to various PGA levels. The resulting spectra could then be compared against the ground surface design spectrum documented by dry cask applicants to determine the appropriate dry cask response cases in terms of the relevant level of input motion intensity. While the PGA was used as a parameter to scale the ground motion records, it is important to remember that this parameter only characterizes the response of a zero period structure. The cask response is more sensitive to the spectral acceleration at other frequencies than it is to the PGA.

After selecting the input motion records, the next step was to choose soil profiles that represent a wide range of site conditions likely to be found throughout the United States. In the process of selecting ground motion records, the ground motion at the surface is assumed to be independent of the soil profile. The ground motions applied at the base of the foundation differ for the various soil types, but in theory, the resulting surface motions for the same earthquake with different soil types should be the same if no errors were introduced in the deconvolution process or in the foundation model. Thus, the sensitivity of the response with respect to the soil profile is primarily due to soil-structure interaction effects that are most pronounced in the upper layers of the foundation in the vicinity of the cask. Thus, if these analyses are to be applied to a site-specific investigation, the soil properties near the surface at the site should be compared with the properties of the generic soil profiles near the surface to determine which analysis results are most applicable to that site.

Table 4.3-A: Startup Motions for NUREG/CR-0098 Spectral Shape

No.	Earthquake Event	Year	Magnitude	Faulting Mechanism	Station	Distance (Km)	Site Code	Startup Motion Component, File Name	PGA (g)	PGV (cm/s)	PGD (cm)	Modified Motion Component, File Name	PGA (g)	PGV (cm/s)	PGD (cm)
1	Tabas, Iran	1978	7.4	Reverse	Tabas	3.0	Deep narrow	TABAS\TAB-UP	0.688	45.6	17.04	SET-1-H1	-1.000	-90.0	44.6
							Soil Profile	TABAS\TAB-LN	0.836	97.8	36.92	SET-1-H2	-1.000	-78.5	-39.7
								TABAS\TAB-TR	0.852	121.4	94.58	SET-1-UP	0.670	-46.7	-21.4
2	Taiwan, Chi-Chi	1999	7.4	Reverse	WGK	11.1	Deep soil	WGK-V	0.180	25.0	16.28	SET-2-H1	-1.000	-84.8	40.1
							Vs = 180-360 m/s	WGK-E	0.334	69.0	35.70	SET-2-H2	-1.000	67.6	-34.4
							at Upper 30m	WGK-N	0.484	74.4	66.92	SET-2-UP	0.667	44.9	26.7
3	Landers	1992	7.3	Strike/Slip	Joshua Tree #	11.6	Shallow stiff soil	LANDERS\JOS-UP	0.181	15.0	9.39	SET-3 H1	1.000	-96.2	-27.8
								LANDERS\JOS000	0.274	27.5	9.82	SET-3 H2	-1.000	-89.0	33.3
								LANDERS\JOS090	0.284	43.2	14.51	SET-3 UP	-0.667	-53.2	25.4
4	Northridge	1994	6.7	Reverse	Jensen Filter Plant	6.2	Deep soil	NORTHR\JEN-UP	0.300	34.1	8.89	SET-4 H1	1.000	-104.2	-53.4
							Vs = 180-360 m/s	NORTHR\JEN022	0.080	106.2	43.06	SET-4 H2	-1.000	-75.1	37.7
							at Upper 30m	NORTHR\JEN292	0.200	99.3	24.00	SET-4 UP	-0.667	-52.0	21.7
5	Imperial Valley	1979	5.2	Strike/Slip	Calexico Fire Station	15.0	Deep soil	IMPVALL\A-CXO-UP	0.900	0.9	0.05	SET-5 H1	1.000	-91.9	32.8
							Vs = 180-360 m/s	IMPVALL\A-CXO225	0.450	8.0	0.87	SET-5 H2	1.000	-84.9	-42.3
							at Upper 30m	IMPVALL\A-CXO315	0.400	5.2	0.51	SET-5 UP	0.667	-51.2	23.2

Table 4.3-B: Startup Motions for Regulatory Guide 1.60 Spectral Shape

No.	Earthquake Event	Year	Magnitude	Faulting Mechanism	Station	Distance (Km)	Site Code	Startup Motion Component, File Name	PGA (g)	PGV (cm/s)	PGD (cm)	Modified Motion Component, File Name	PGA (g)	PGV (cm/s)	PGD (cm)
1	Tabas, Iran	1978	7.4	Reverse	Tabas	3.0	Deep narrow	TABAS\TAB-UP	0.688	45.6	17.04	SET-1-H1	-1.000	-166.9	124.9
							Soil Profile	TABAS\TAB-LN	0.836	97.8	36.92	SET-1-H2	-1.000	160.3	102.7
								TABAS\TAB-TR	0.852	121.4	94.58	SET-1-UP	0.670	-99.3	-63.2
2	Taiwan, Chi-Chi	1999	7.4	Reverse	WGK	11.1	Deep soil	WGK-V	0.180	25.0	16.28	SET-2-H1	-1.000	-167.8	101.8
							Vs = 180-360 m/s	WGK-E	0.334	69.0	35.70	SET-2-H2	-1.000	130.9	-85.5
							at Upper 30m	WGK-N	0.484	74.4	66.92	SET-2-UP	0.667	93.5	67.1
3	Landers	1992	7.3	Strike/Slip	Joshua Tree #	11.6	Shallow stiff soil	LANDERS\JOS-UP	0.181	15.0	9.39	SET-3 H1	1.000	-156.4	71.2
								LANDERS\JOS000	0.274	27.5	9.82	SET-3 H2	-1.000	-153.8	-94.7
								LANDERS\JOS090	0.284	43.2	14.51	SET-3 UP	-0.667	-110.8	64.7
4	Northridge	1994	6.7	Reverse	Jensen Filter Plant	6.2	Deep soil	NORTHR\JEN-UP	0.300	34.1	8.89	SET-4 H1	1.000	189.2	-136.4
							Vs = 180-360 m/s	NORTHR\JEN022	0.080	106.2	43.06	SET-4 H2	-1.000	-132.1	93.7
							at Upper 30m	NORTHR\JEN292	0.200	99.3	24.00	SET-4 UP	-0.667	-109.8	87.1
5	Imperial Valley	1979	5.2	Strike/Slip	Calexico Fire Station	15.0	Deep soil	IMPVALL\A-CXO-UP	0.900	0.9	0.05	SET-5 H1	1.000	146.8	80.7
							Vs = 180-360 m/s	IMPVALL\A-CXO225	0.450	8.0	0.87	SET-5 H2	1.000	-161.7	-106.5
							at Upper 30m	IMPVALL\A-CXO315	0.400	5.2	0.51	SET-5 UP	0.667	-117.4	63.5

Table 4.3-C: Startup Motions for NUREG/CR-6728 Spectral Shape

No.	Earthquake Event	Year	Magnitude	Faulting Mechanism	Station	Distance (Km)	Site Code	Startup Motion Component, File Name	PGA (g)	PGV (cm/s)	PGD (cm)	Modified Motion Component, File Name	PGA (g)	PGV (cm/s)	PGD (cm)
1	Nahanni	1985	6.8	Reverse/ Oblique	NW Terr, Canada: Mackenzie, St 1	6.0	IZA	S1-Up	2.086	40.5	12.12	SET-1-H1	-1.000	46.5	8.3
								S1-010	0.978	46.0	9.67	SET-1-H2	-1.000	41.7	9.0
								S1-280	1.096	46.1	14.58	SET-1-UP	0.670	20.1	8.1
2	Saquenay	1988	5.9	??	GSC Site-Baie-St. Pau	95.6	CBC	1125S07-V	0.122	2.6	0.28	SET-2-H1	-1.000	42.9	8.9
								1125S07-L	0.122	4.7	0.51	SET-2-H2	-1.000	45.7	5.5
								1125S07-V	0.173	5.7	0.66	SET-2-UP	0.667	21.8	4.5
3	Imperial Valley	1979	6.5	Strike/Slip	El Centro Array #1	15.5	AQD	H-E01-Up	0.164	5.1	2.39	SET-3 H1	1.000	40.6	7.5
								H-E01140	0.280	19.0	6.41	SET-3 H2	-1.000	40.6	8.2
								H-E01230	0.277	11.3	5.44	SET-3 UP	-0.667	19.2	4.6
4	Loma Prieta	1989	6.9	Reverse/ Oblique	Corralitos	6.1	B	CLS-Up	1.300	28.8	9.34	SET-4 H1	1.000	42.6	7.8
								CLS-000	1.328	57.4	7.22	SET-4 H2	-1.000	35.7	6.4
								CLS-090	1.080	49.4	7.43	SET-4 UP	-0.667	20.3	6.5
5	Northridge	1994	6.7	Reverse	Pacoima Dam, Kagel Canyon	8.2	B	PKC-Up	0.559	23.7	9.84	SET-5 H1	1.000	36.4	8.2
								PKC-000	0.752	34.3	11.48	SET-5 H2	1.000	51.2	10.7
								PKC-090	0.978	48.5	8.38	SET-5 UP	0.667	19.3	-5.5

4.2 Frictional Contact at Cask/Pad Interface

A literature search was performed to gather the results of experimental studies investigating the coefficient of friction between steel and concrete. The reports of several relevant studies were identified. There were a variety of goals in the studies. Two studies [21, 22] investigated the bond strength between steel plates and concrete that had been cast against the steel plates, and also measured the coefficient of friction after the bond was broken. Another study [23] investigated the coefficient of friction between wire brush and steel plate skids and concrete at low and high speeds for aircraft landing gear applications. While the wire brush skid data is not directly applicable to this work, the flat plate data proved useful. The study documented in Idun and Darwin [24] was conducted to investigate the effect of an epoxy coating on the coefficient of friction for applications to the bond between reinforcing bars and concrete. The data given for uncoated reinforcing bars is applicable to this work. Bonding of reinforcing bars also motivated the work of Baltay and Gjelsvik [25], where the coefficient of friction was measured over a wide range of normal pressures to investigate the effect of the normal pressure. Finally, an investigation of the coefficient of friction between steel and concrete at low sliding speeds is documented in Olofsson and Holmgren [26]. This investigation was motivated by a design of a natural gas storage room in which a steel plate slides slowly against a concrete surface.

A variety of conditions could potentially exist at the interface between the cask and the pad. It is possible for moisture to accumulate in that region, decreasing the coefficient of friction. It is also possible that the two surfaces could develop a bond over time, effectively increasing the coefficient of friction. The experimental studies referenced here indicate that the coefficient of friction can be influenced by the presence of mill scale on the steel surface, as well as by the normal pressure applied to the interface. The data from the experimental results on a steel/concrete interface has been compiled to obtain an estimate of the statistical variation in the coefficient of friction. All of the relevant data in the referenced experimental results of a coefficient of friction at the steel/concrete interface has been compiled and plotted in the form of a histogram in Figure 4.5. Also shown in this plot is a normal probability distribution fitted to this data.

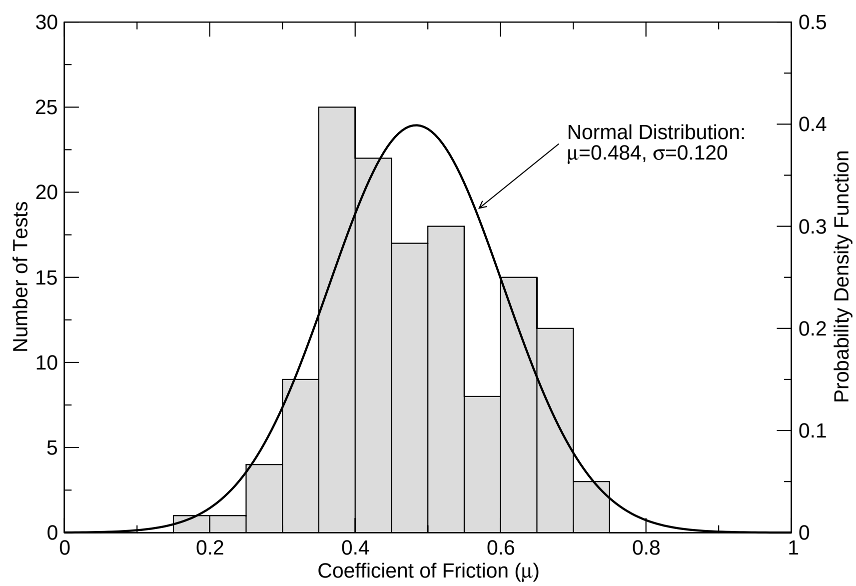

Figure 4.5: Histogram of Steel/Concrete Coefficient of Friction Test Results

The data included in this plot comes from all of the sources referenced above. In some cases, data was excluded because it was not relevant. The epoxy-coated bar data in Idun and Darwin [24] was not included, and the wire brush skid data in Dreher [23] was also not included. Idun and Darwin [24] provide a table showing the averages of 10 experiments of a given type. These averages were each counted as a single data point, but they could arguably be weighted by a factor of 10. The overall statistics are not affected significantly by changing the weighting of these data points. Also, in Baltay and Gjelsvik [25], some low values were obtained for cases with low normal pressure and with mill slag on the plates. The lowest pressures in these experiments were around 6.9 kPa (1 psi). The nominal contact pressure between the cask and pad ranged between 88 kPa (13 psi) and 180 kPa (26 psi). There may be a case for excluding those data points because such conditions would not be observed, but they were included in the plot to represent a wide range of conditions. The cases where the concrete was initially bonded to the steel resulted in higher values for the coefficient of friction, but they were included to give a representation of cases where the cask might develop a bond with the concrete over time.

As noted on the plot, a normal distribution fitted to the data has a mean of 0.484 and a standard deviation of 0.120. The lowest recorded value was 0.2 for a case with mill slag on the steel and a very low normal pressure. The highest recorded value was 0.72. This was from an experiment where the concrete was initially bonded to the steel, and that bond was broken before the coefficient of friction was measured. For the parametric study, the goal was to select an extreme lower bound, an extreme upper bound, and a best estimate value for the coefficient of friction between the cask and pad. Values of 0.2, 0.8, and 0.55 were selected for these cases, respectively. Based on the normal distribution fitted to the experimental data, the lower bound value of 0.2 is about 2.4 standard deviations below the mean, and the upper bound value of 0.8 is about 2.6 standard deviations above the mean. About 99% of all samples fall within these bounds.

The surveyed data is for the coefficient of friction at steel/concrete interfaces. Dry cask storage systems can have either steel or concrete at the base, where contact is made with the concrete pad. The coefficient of friction between concrete and concrete is likely to be somewhat higher than that between steel and concrete, but the upper and lower bounds of 0.2 and 0.8 used for cask with steel bases are judged to still provide useful bounding estimates of the behavior of casks with concrete bases.

5. Analysis Results

Some basic understanding of the mechanics of freestanding dry cask storage systems (DCSS) in response to seismic ground motion is instrumental for interpreting the analysis results of the parametric study. The dynamic response of DCSSs interacting with the underlying soil/rock foundation is of particular interest. Three main response parameters were used to describe the behavior of the analytical cask models: (1) the lateral displacement at the cask base relative to the pad (as a measure of cask sliding), (2) the angular rotation of the cask with respect to the vertical coordinate axis (as a measure of cask tipping angle), and (3) the lateral displacement at the cask top relative to the pad (as a measure of overall lateral movement of the cask). There is considerable scatter in the cask response results. Consequently, linear regression analyses were performed on these results to generate nomograms, which can be used as a practical tool for cask system reviewers and designers to assess the seismic behavior of casks.

5.1 Physics of Cask Behavior and Soil-Structure Interaction Effects

It is instructive to examine the basic physics of the freestanding cask problem before proceeding with the presentation of analysis procedures and results. In this discussion, the behavior of the cask is examined both before and after the onset of cask motion relative to the pad.

5.1.1 Cask Behavior Before Onset of Relative Movement

5.1.1.1 Static Equilibrium Calculations

Figure 5.1 shows a diagram of the cross section of a cask with some essential dimensions. The distance from the base of the cask to the center of gravity is denoted as h_{cg}, and the shortest horizontal distance from the center of gravity to the edge of the cask is denoted as r. In the case of a rectangular module, r is half the shortest base dimension. For an upright cylindrical cask, r is the radius of the cask base.

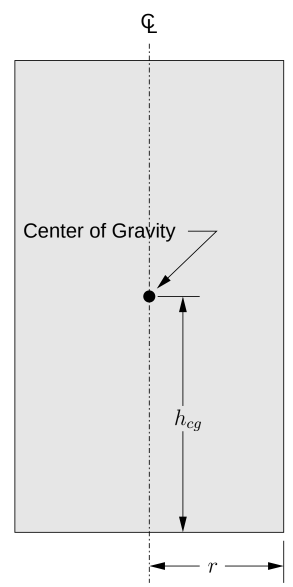

Figure 5.1: Diagram of a Cask

A freestanding cask subjected to a seismic ground motion will not experience any motion relative to the slab upon which it rests if the ground motion is below certain threshold values. It is assumed that the cask/pad interface follows Coulomb's law of friction, where slippage occurs between two surfaces only when the lateral force acting to cause sliding exceeds the product of the friction coefficient, μ, and the compressive normal force on these surfaces.

Principles of statics can be applied to determine the point at which the cask could experience sliding or tipping relative to the pad. Prior to cask tipping or sliding, the cask moves together with the pad as if they were bonded together. If a_h is the magnitude of the horizontal ground acceleration vector during a seismic event and a_v is the vertical ground acceleration at that same time (downward acceleration is positive), one can show that by applying Coulomb's friction law the following condition must be met for sliding to occur:

$$\mu < \frac{a_h}{(g - a_v)} \tag{5.1}$$

where g is the acceleration of gravity.

Equation 5.1 can be adapted to solve for the horizontal acceleration that will cause sliding to initiate. To aid in this, it is useful to introduce a variable, v, which is the ratio of a_v to a_h, at any given time step.

$$v = \frac{a_v}{a_h} \tag{5.2}$$

Substituting Equation 5.2 into Equation 5.1 and solving for a_h results in the following condition for sliding:

$$\frac{a_h}{g} > \frac{1}{(1/\mu) + v} \tag{5.3}$$

In a similar manner, by solving for moment equilibrium, a criterion can also be defined for the initiation of tipping, assuming that the cask has not already begun to slide:

$$\frac{r}{h_{cg}} < \frac{a_h}{(g - a_v)} \tag{5.4}$$

Substituting Equation 5.2 into this and solving for a_h results in a condition for tipping:

$$\frac{a_h}{g} > \frac{1}{(h_{cg}/r) + v} \tag{5.5}$$

By comparing Equations 5.1 and 5.4, it can be seen that if $\mu > \frac{r}{h_{cg}}$, tipping will occur before sliding, whereas if $\mu < \frac{r}{h_{cg}}$, sliding will occur first. For both sliding and tipping, the most critical situation is when there is a large downward vertical acceleration at the same time as a large horizontal acceleration. This situation results in a combination of a high force inducing sliding or tipping, and a low resisting force. In the sign convention employed here, this happens whenever v has a high positive value. Because v is a ratio of two constantly changing quantities, v changes constantly during the seismic event. For simple capacity calculations using the equations presented above, it is reasonable to use a critical value of v, equal to the absolute value of the ratio of the maximum vertical acceleration to the maximum horizontal acceleration. For the earthquake ground motions in this study, the critical v, computed as described above, ranges from 0.67 to 1.0. The above equations are useful for understanding whether the cask is likely to move at all, and if so, whether tipping or sliding is likely to be the dominant type of motion.

For the cylindrical cask in the study, r is 1.68 m (66.25 in), and h_{cg} is 3.00 m (118.2 in). The ratio r/h_{cg} = 0.56 for this design, meaning that if μ is less than 0.56, the cask is dominated by sliding behavior rather than by tipping behavior. In the case of the rectangular module, r is 1.47 m (58.0 in) and h_{cg} is 2.54 m (100.0 in), resulting in a ratio r/h_{cg} of 0.58.

5.1.1.2 Soil-Structure Interaction Effects

If the ground motion is not sufficiently high to cause the cask to lift off the pad or slide relative to the pad, the cask behaves essentially as if it were bonded to the pad. The interaction between the cask and the soil takes place in a manner very similar to typical soil-structure interaction problems involving fixed structures. The deformability of the soil to which the structure is attached reduces the stiffness of the overall system.

The cask itself is a quite rigid structure. The finite element model of the cylindrical cask was modified to determine the effect of the foundation on the fundamental frequency of the cask before uplift or sliding occurs. The contact interactions between the cask and pad, and the pad and soil were changed to bonded surfaces. The nodes at the base and sides of the soil column were constrained against displacement. A horizontal force was applied to the nodes on the top of the cask, and this load was abruptly released. The frequency of the fundamental rocking mode of the cask can be determined from the time history of the cask response after the load is released.

A second model was created in which the elements comprising the soil foundation were removed, leaving only the cask and pad. This is used to determine the fundamental rocking frequency of the cask/pad system without the effect of the soil to determine the effect that the soil foundation has on the fundamental frequency of the system. As before, the cask/pad interface is bonded. The nodes at the bottom of the pad are restrained against displacement. Figure 5.2 shows the deformed shape of this model just before the load is released.

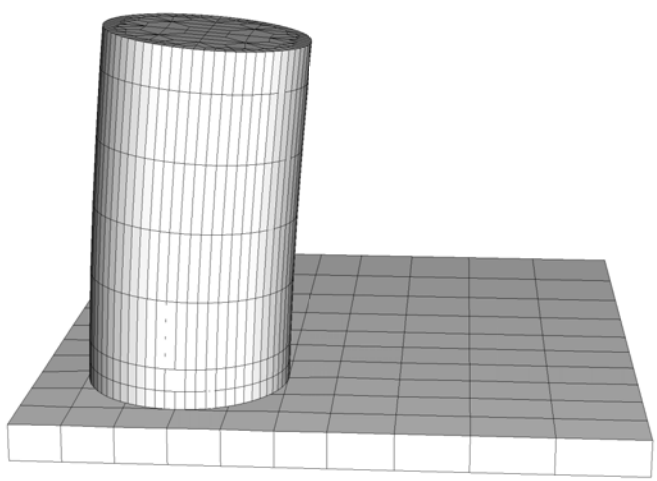

Figure 5.2: Deformed Shape of Cylindrical Cask/Pad Pullback Test (Magnified 100x)

Table 5.1 shows the frequencies of this rocking mode obtained from the various analysis cases in the study. In the soil column investigation, both the elastic cask and the rigid cask models were used to determine the effect of the rigid cask modeling approach on this soil-structure interaction effect. It can be seen that the frequencies of the rigid cask models are slightly lower than those for the elastic cask model, but the difference is relatively minor. The rigid cask was not analyzed for the model with only the cask and pad because the main source of flexibility in that case is the cask, and the results with the rigid cask would not be meaningful.

Table 5.1: Frequency of Cask Rocking Mode

	Elastic Cask	Rigid Cask
Soft Soil	7.7 Hz	7.5 Hz
Stiff Soil	13.6 Hz	12.4 Hz
Rock	14.2 Hz	13.0 Hz
Cask and Pad Only	28.3 Hz	N/A

From this table, it can be seen that the shift in the frequency of the rocking mode due to the presence of the foundation is quite significant, especially for the softer foundations. The difference between the rock and stiff soil foundations is not particularly large due to the presence of the layers of engineered fill and weathered rock at the top of the rock foundation model.

Figure 5.3 shows the spectral shapes of the earthquakes used in this study. These spectral shapes are normalized to the peak ground acceleration (PGA), so the quantity plotted on the *y* axis is the ratio of the pseudo-spectral acceleration (PSA) to the PGA. The periods of the elastic cask model are also shown as vertical lines for the soft soil, stiff soil, and rock foundations, as well as for the fixed base model of the cask and pad only. It can be seen that for the NUREG/CR-0098 and the Regulatory Guide 1.60 earthquakes, the fixed base cask experiences accelerations that are only slightly higher than the PGAs. The decrease in the stiffness due to the foundation significantly increases the acceleration experienced by the cask before uplift or sliding occurs due to the soil-structure interaction effect. The NUREG/CR-6728 spectrum has more high-frequency content, and even the fixed base cask experiences accelerations greater than the PGA.

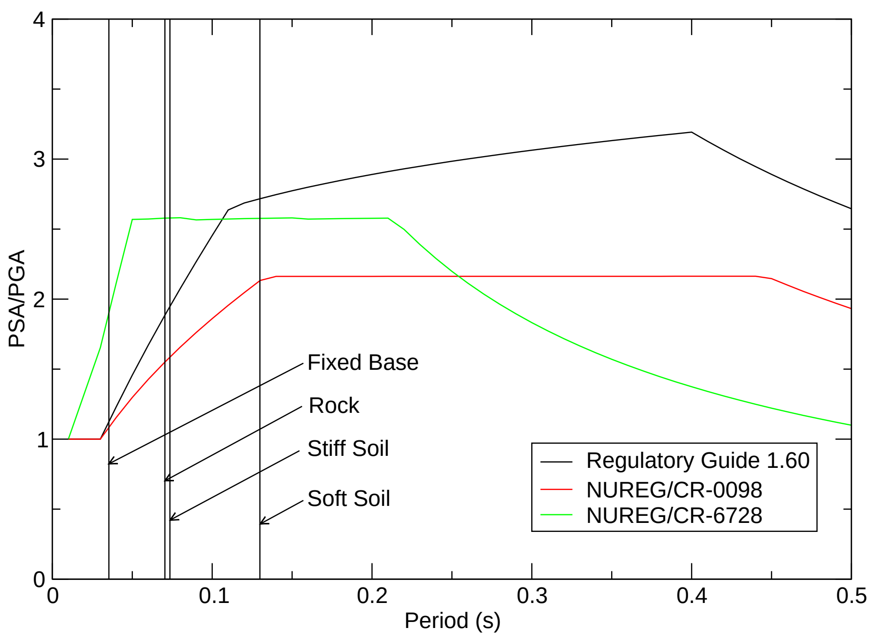

Figure 5.3: Spectral Shapes and Cask Periods with Various Soil Types

The statics-based equations presented in the previous section assumed that the cask system is rigid enough that the peak acceleration experienced by the cask is equal to the PGA. It can be clearly seen from Figure 5.3 that before uplift or sliding, the cask actually can experience accelerations much greater than the PGA. The accelerations used in the equations of the previous section should be multiplied by the ratio of PSA to PGA to account for this. The accelerations that the cask experiences before uplift under a given seismic event can potentially be close to 3 times higher than the PGA if the soil foundation is sufficiently compliant. This highlights the importance of including the foundation in a model of the freestanding cask. If the foundation is not included in the model, the model may significantly under-predict the magnitude of the seismic event required to initiate tipping of the cask.

5.1.2 Cask Behavior After Onset of Relative Movement

After the cask begins to tip, it is no longer valid to assume that the cask is bonded to the pad. Before uplift, the cask has a unique fundamental frequency. The frequency of the free vibration of the cask is independent of the vibration amplitude. Once an edge of the cask lifts up from the pad, the frequency of that rocking motion becomes a highly nonlinear function of the amplitude of that motion. A method to characterize the rocking frequency of the cask as a function of the tipping angle was proposed by Housner [27]. The function resulting from this method shows that the rocking period is zero at a tipping angle of zero, and that the period asymptotically approaches infinity as the tipping angle approaches the angle at which the center of gravity is directly above the corner of the cask.

As the cask rocks back and forth, energy is absorbed every time the cask impacts the pad. This can be a significant energy dissipation mechanism, and the type of soil underlying the pad can have a noticeable effect on the amount of energy dissipated. This mechanism is believed to be the most important soil-structure interaction effect after the cask begins to tip. It is important to note that the cylindrical cask can assume either a rocking motion or a rolling motion. Significant energy is dissipated if the cask is rocking back and forth, but very little energy is dissipated in the rolling motion.

5.1.3 Demonstration of Soil Column Response and Soil-Structure Interaction

As described in Section 3.1.5, the target surface ground motions have been modified using a deconvolution procedure to produce acceleration histories to be applied to the base of the soil column. The deconvolution procedure is based on the assumption that the soil mass behaves as an idealized one-dimensional soil column. If the soil column used in the finite element models perfectly replicates those assumptions, the ground motion measured at the surface of the soil column without the presence of any structures should closely match the original surface motion.

To assess the performance of the model in this project to replicate the original surface ground motion, the cask and pad have been removed from the soil column models, and each of the three soil columns (soft soil, stiff soil, and rock) has been subjected to the five deconvolved base ground-motion records for each of the three spectral shapes in the parametric study. The boundary conditions on the soil column model ensure that the ground motion is nearly identical at any two nodes located on the same vertical layer of the column.

Figure 5.4 shows a representative comparison of the spectral shape of the original surface ground motion with spectral shapes of the surface motion obtained from the analytical models without the presence of the cask and pad. The plots in this figure show the first horizontal component of the ground motion with the Case 1 earthquake conforming to the NUREG/CR-0098 spectral shape. Spectral responses are shown with a 5% damping for the soft soil, stiff soil, and rock columns, as well as for the original surface motion. Plots of the soil column response spectra are provided for all three spectral shapes and all three soil profiles in the first horizontal and vertical directions in Appendix IV. The response of the soil column without the cask and pad matches the original surface motion quite closely at periods above about 0.3 s. At higher frequencies, there are occasionally high peaks in the soil column model response. Once the cask lifts up from the pad, it is believed to respond most to spectral content in the range of 0.5 Hertz (Hz) to 2 Hz, so these high frequency differences likely have a negligible effect on the cask response. If they do have an effect, it would be to increase the response, so the results obtained in this study are believed to be conservative.

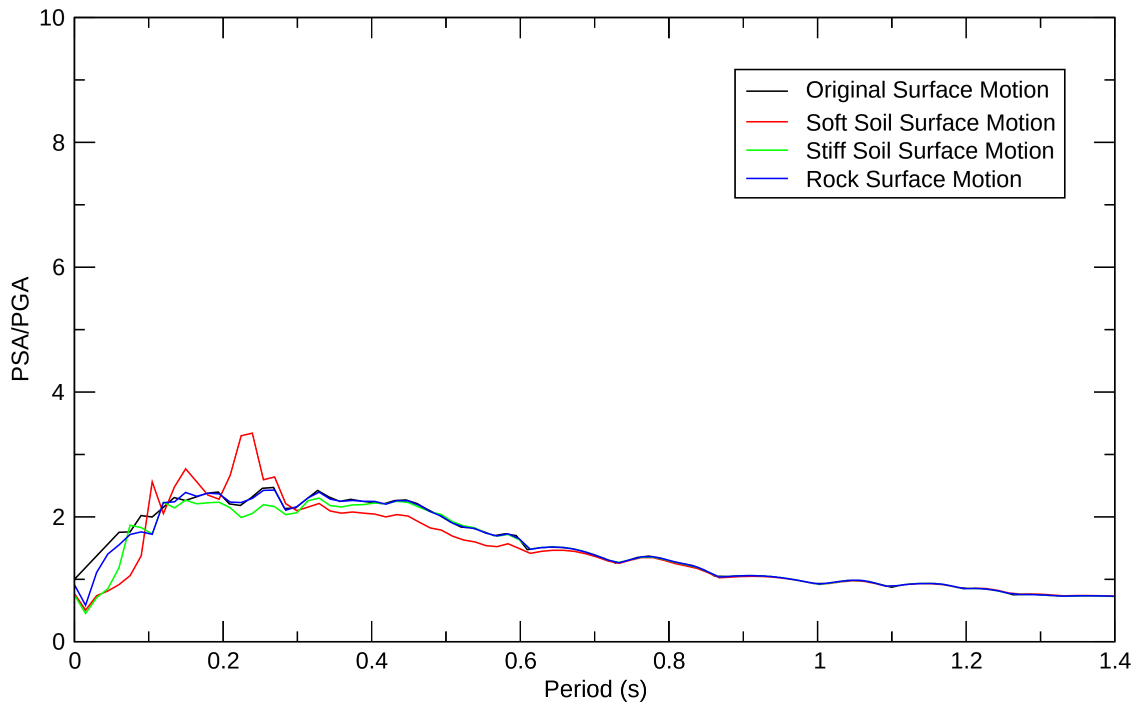

Figure 5.4: Comparison of Original Surface Motion and Motion at Top of Soil Column Model, NUREG/CR-0098 Spectral Shape, Case 1 Earthquake, First Horizontal Component

The spectral shapes in Appendix IV show the response of the soil column without the presence of cask and pad. Since there is no structure present on the surface of the ground and the layers are uniform, the response is not dependent on the horizontal location on the soil mass. When the cask and pad are present, the soil-structure interaction effects cause local disturbances in the soil response. The magnitude of these disturbances increases in regions near the cask and pad.

To demonstrate the local disturbances in the region of the cask and pad in the soil column, spectral shapes have been derived from the acceleration time histories taken at a number of locations in the full analysis model. These are shown for the first horizontal component of the ground motion with the Case 1 earthquake conforming to the NUREG/CR-0098 spectral shape, scaled to 1 g PGA, with the soft soil profile in Figure 5.5. Similar sets of plots are shown for the stiff soil in Figure 5.6, and for the rock profile in Figure 5.7. In all these cases, the cask experienced significant motion but did not tip over. The earthquake ground motions used in these plots are the same as those in Figure 5.4.

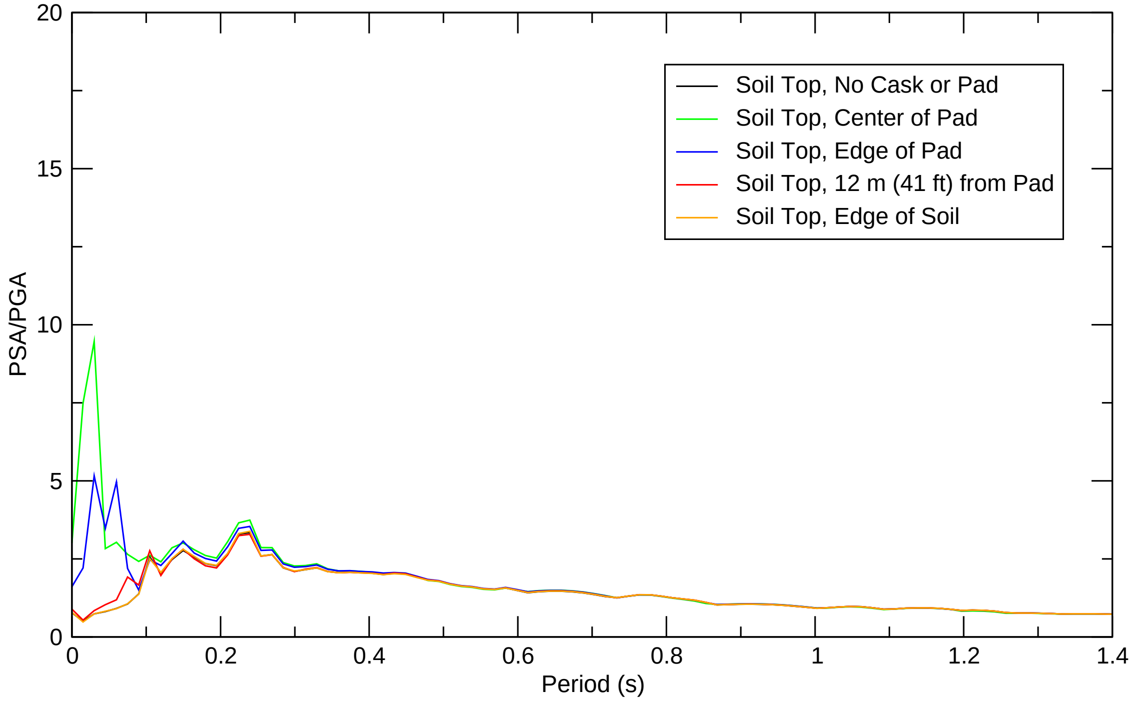

Figure 5.5: Spectral Response at Points on Surface of Soil Column Model, Soft Soil, NUREG/CR-0098 Spectral Shape, Case 1 Earthquake, 1 g PGA, 1st Horizontal Component

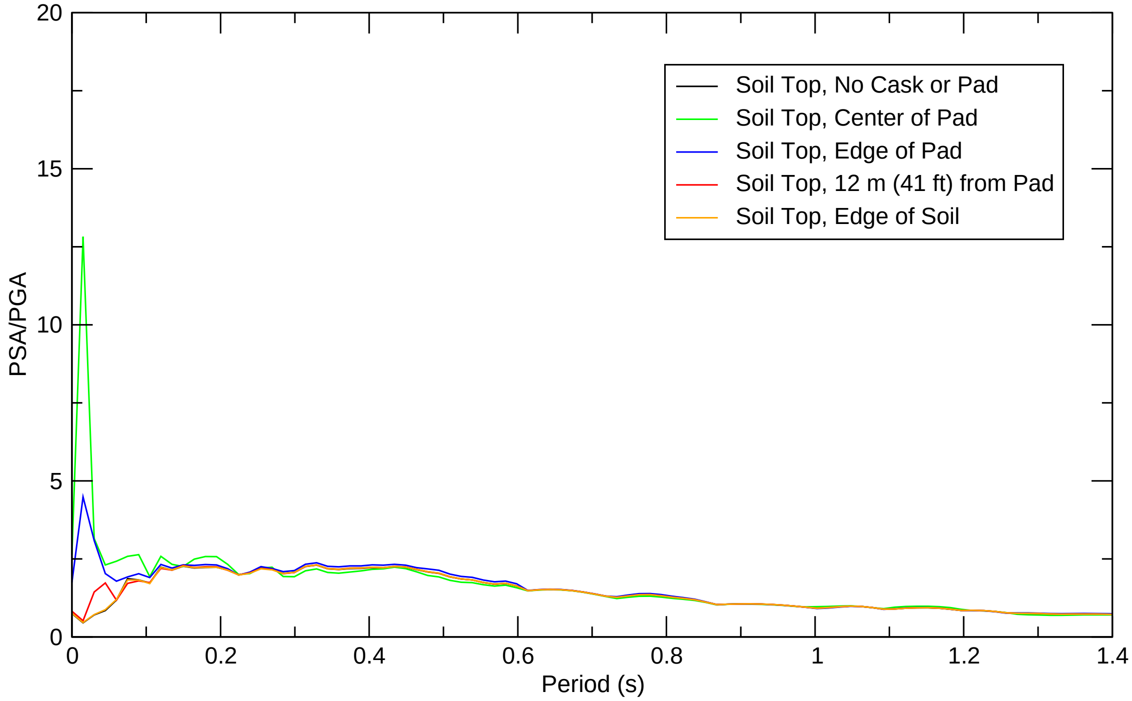

Figure 5.6: Spectral Response at Points on Surface of Soil Column Model, Stiff Soil, NUREG/CR-0098 Spectral Shape, Case 1 Earthquake, 1 g PGA, 1st Horizontal Component

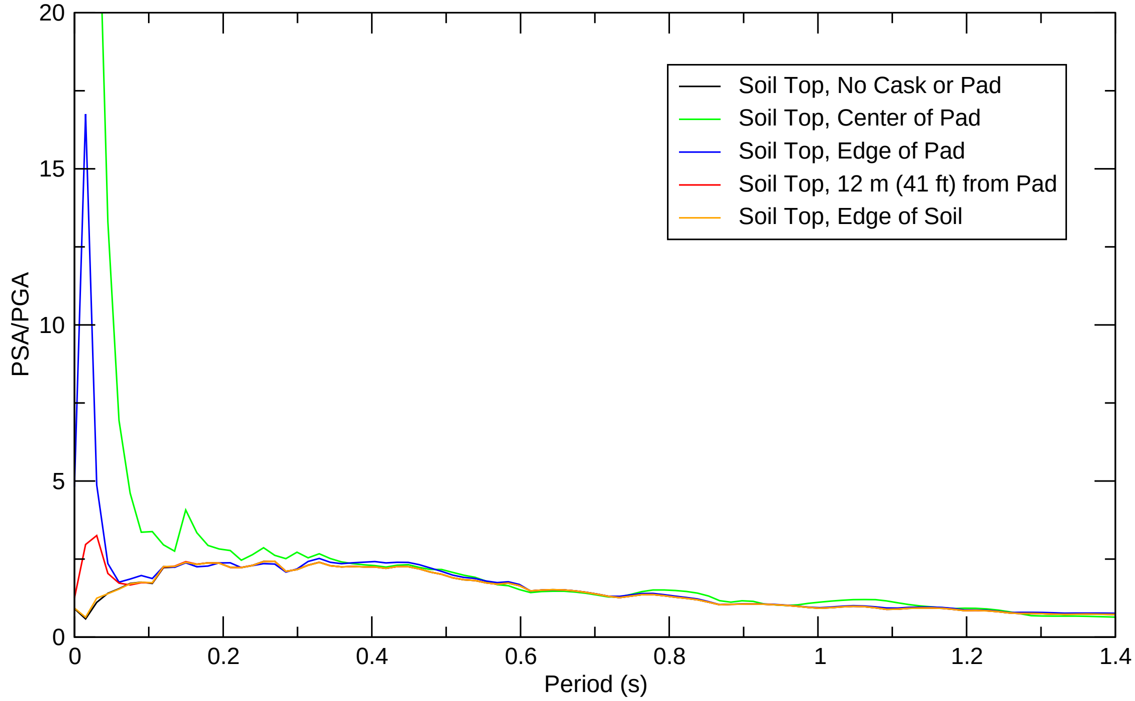

Figure 5.7: Spectral Response at Points on Surface of Soil Column Model, Rock, NUREG/CR-0098 Spectral Shape, Case 1 Earthquake, 1 g PGA, 1st Horizontal Component

The results for all three soil profiles have similar characteristics. Locations immediately below the pad experience extremely high frequency responses. As the recording location is moved away from the pad, the response approaches that of the bare soil column. For all three soil profiles, the response at the far edge of the soil column matches that of the bare soil column almost exactly, and the two lines are indistinguishable. It is interesting to note that the high frequency peaks in the response spectrum for the points directly below the pad increase in magnitude as the stiffness of the foundation increases. In the case of the rock profile, this effect may be caused by the presence of the soft layer of engineered fill.

The plots shown in this section and in Appendix IV demonstrate that the soil column model reasonably replicates the target surface ground motion and still allows for soil-structure interaction effects to occur. As mentioned previously, allowing for soil-structure interaction is important both before and after the cask begins to move relative to the pad. Before the cask begins to move relative to the pad, the reduction in effective frequency of the cask system can cause a significant increase in the accelerations of the pad. After the cask begins to lift off from the pad, the soil-structure interaction effects are primarily evident in the amount of rebound of the cask after impact with the pad.

To demonstrate the effect of soil-structure interaction, a modified version of the model of the cylindrical cask has been created without the soil column. The cask and pad models are exactly the same as in the full model, but the nodes at the base of the pad have an imposed acceleration. The ground motion record applied to the pad base has been adjusted to fit the target spectral shape but has not undergone the deconvolution procedure. Thus, the ground motion at the base of this “rigid” model is equivalent to the ground motion at the surface of the soil column model in the far field away from the cask. This model is useful to demonstrate the behavior of the cask without the soil-structure interaction effects. Comparing the results from the rigid model with those from the coupled models that include the soil or rock foundation can provide insights into the soil-structure interaction effects.

A small subset of the parametric analysis cases has been analyzed using this rigid cask model. The ground motion records applied to this model are the Case 1 records conforming to the Regulatory Guide 1.60 spectral shape. The cask/pad friction coefficient has been set to 0.55. Analyses were performed with the PGA at 0.25g, 0.4g, 0.5g, and 0.6g. The peak cask top lateral displacement magnitudes relative to the pad for analyses with the soft, stiff, and rock profiles, as well as for the rigid model, are reported in Table 5.2. The analyses that include the soil column will be discussed in more detail later in this report.

Table 5.2: Comparison of Peak Top Displacements (m) of a Cylindrical Cask for Rigid Model and Coupled Models with Soil or Rock Foundation (Note: 1 m = 3.28 ft)

PGA (g)	Soft	Stiff	Rock	Rigid
0.25	0.00711	0.00142	0.00309	0.0000289
0.4	0.351	0.206	0.456	0.124
0.5	1.134	1.362	0.856	0.364
0.6	2.46	1.90	2.10	Tips

In an analysis of this nature, it is expected that there should be a large amount of scatter. A larger sampling of analysis cases would be required to provide a rigorous demonstration of the soil-structure interaction effect. However, there are clear trends that can be seen even from this small set of analysis results.

The static threshold of horizontal motion at which tipping would begin to occur is computed using Equation 5.5. For the Regulatory Guide 1.60 ground motion records, the peak vertical acceleration is equal to the peak horizontal acceleration, so it is assumed that v=1.0 for the purposes of this calculation. For the cylindrical cask, this threshold is 0.36 g. As mentioned previously, soil-structure interaction can actually cause the cask to begin tipping at accelerations below this level. Because the rigid model does not include soil-structure interaction, there should be very minimal tipping for horizontal ground motions below 0.36 g.

From Table 5.2, it can be seen that at 0.25 g, all models experience minimal response, but the response of the rigid model is orders of magnitude lower than that of the models with soil. At 0.4 g, which is slightly above the static tipping threshold, the response of the rigid model is roughly half that of the coupled models with soil or rock foundation. This is also true at 0.5 g. At 0.6 g, the cask response in all models is significant, and they are all on the verge of tipping. The rigid model actually tips over, while none of the other models tip.

The soil-structure interaction effects are particularly important if the PGA is below, or slightly above, the static tipping threshold. Soil-structure interaction can cause the cask to begin tipping much earlier than it would without this effect. Once the cask has begun to tip, the soil-structure interaction effects appear to have a reduced influence on the cask response. It is important to keep in mind, however, that accurately modeling the point at which tipping first occurs can have a significant effect on the response later on in an analysis, even in a case where the cask would tip without including soil-structure interaction effects in the model.

5.2 Representative Analysis Results

A large number of analyses were conducted using the parameters outlined in the previous chapter to examine the sensitivity of cask response to these parameters. Because of the large number of analyses, it is not practical to include all results for every analysis in this report. A few key results from each of the analyses are discussed in Section 5.3. Detailed analysis results of some selected cases are presented here to provide an understanding of the key phenomena.

Figure 5.8 provides an illustration of some meaningful measures of cask response that are used in the parametric study. Annotations are made on a deformed mesh plot from an analysis of the cylindrical cask, but the same measures are also used for the rectangular module. At the beginning of an analysis, the cask is upright, and the center of the cask base rests on the initial cask position denoted in the figure. During an earthquake event, the cask can experience very large movements, as illustrated in the figure. These movements potentially consist of a combination of sliding, rocking, and rolling.

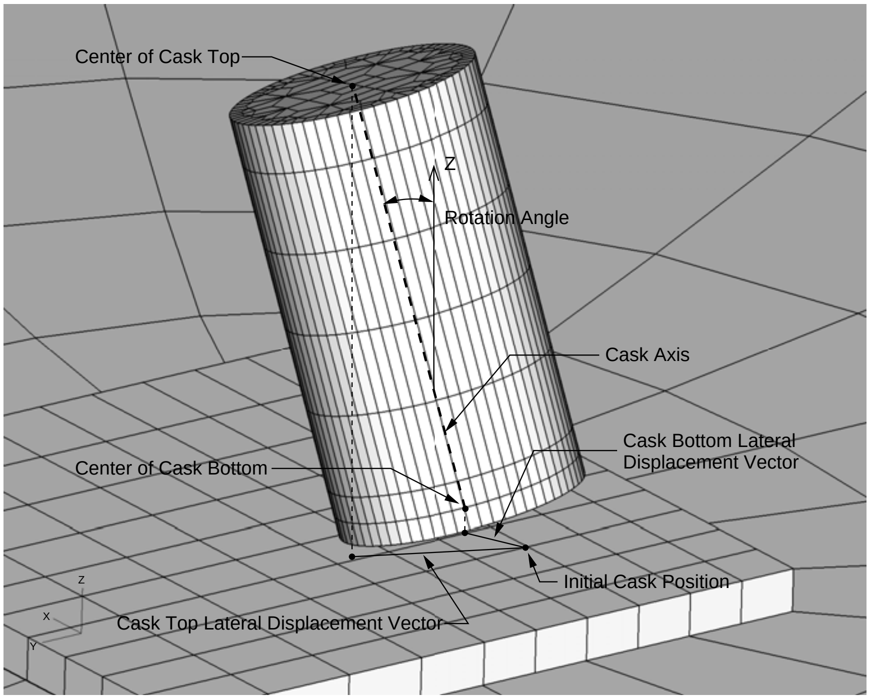

Figure 5.8: Explanation of Key Response Quantities

The three primary measures of cask response used in the parametric study and illustrated in Figure 5.8 are the lateral displacement of the cask base relative to the initial position on the pad, the lateral displacement of the cask top relative to the initial position on the pad, and the angle of rotation from the vertical axis. Magnitudes of the relative displacement vectors are more useful than the values of the components of these vectors in the two lateral directions because the cask could potentially move in any direction. The magnitude of the relative lateral displacement vector between the cask base and pad is a reflection of the amount of cask sliding. It is important to realize, however, that for a cylindrical cask, the cask can also roll along the edge of the base, and that rolling can contribute to the relative lateral base displacement. The rotation angle is the angle between the axis of the cask and the vertical coordinate axis. This is a direct way to assess the amount of rotation at a given time and could be used to determine a factor of safety against tipping. The magnitude of the relative lateral displacement vector between the cask top and the pad is a measure that combines the effects of sliding, rotation, and rolling. This physical quantity is a good overall measure of cask response and can be directly applied to determine whether collision would occur between adjacent casks in an array.

All quantities mentioned above vary significantly in the duration of an analysis. A post-processing program has been developed to extract time histories of these measures from the analysis output file. Time histories of these measures are presented in the next section for a selected set of analyses to provide a basic understanding of the phenomena. The maximum values of these three measures over the duration of the earthquake are reported for the full set of parametric analysis cases.

5.2.1 Representative Analysis Results for Cylindrical Cask

The cylindrical cask has a strong tendency to undergo a rolling motion in preference to a rocking motion if the ground motion is sufficiently high to put the cask into motion and the coefficient of friction is sufficiently high to prevent sliding. Figure 5.9 shows a representative plot of the lateral displacement trajectories of both the cask top and bottom relative to the pad for the cylindrical cask subjected to a high ground motion. In this case, the stiff soil profile is used, the coefficient of friction between the cask and pad is 0.55, and the Iran Tabas earthquake (Case 1) is used, fitted to the NUREG/CR-0098 spectral shape and scaled for a PGA of 1.0 g.

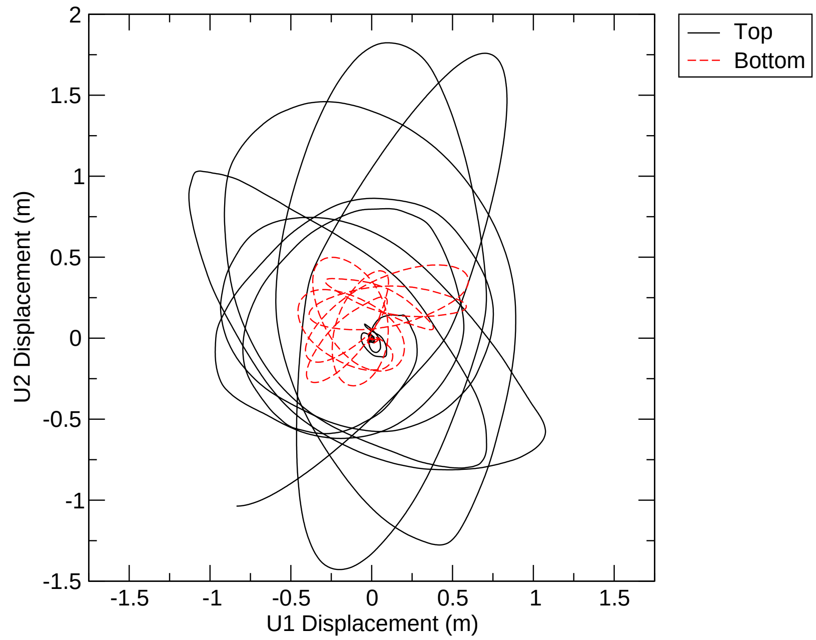

Figure 5.9: Lateral Displacement Trajectories for Cylindrical Cask Top and Bottom, Iran Tabas Earthquake, NUREG/CR-0098 Spectral Shape, PGA=1.0 g, Stiff Soil Profile, Cask/Pad μ=0.55

When the lower bound friction coefficient of 0.2 between the cask and pad is used, a sufficiently high lateral force to initiate rocking or rolling motion cannot be developed, and the cask slides on the pad. The displacement of the cask top is nearly identical to that of the cask base. Figure 5.10 shows plots of the time histories of the magnitudes of the top and bottom lateral displacements relative to the pad for the cylindrical cask with the stiff soil profile and the cask/pad μ=0.2. Plots are shown for all five of the earthquakes conforming to the NUREG/CR-0098 spectral shape, and the earthquakes are all scaled so that the PGA is equal to 1.0 g. It can be seen that the plots of cask top and base displacement are nearly identical because the cask experiences only minor rotation. When the top and bottom displacements are almost the same, only the red line shows in the plots.

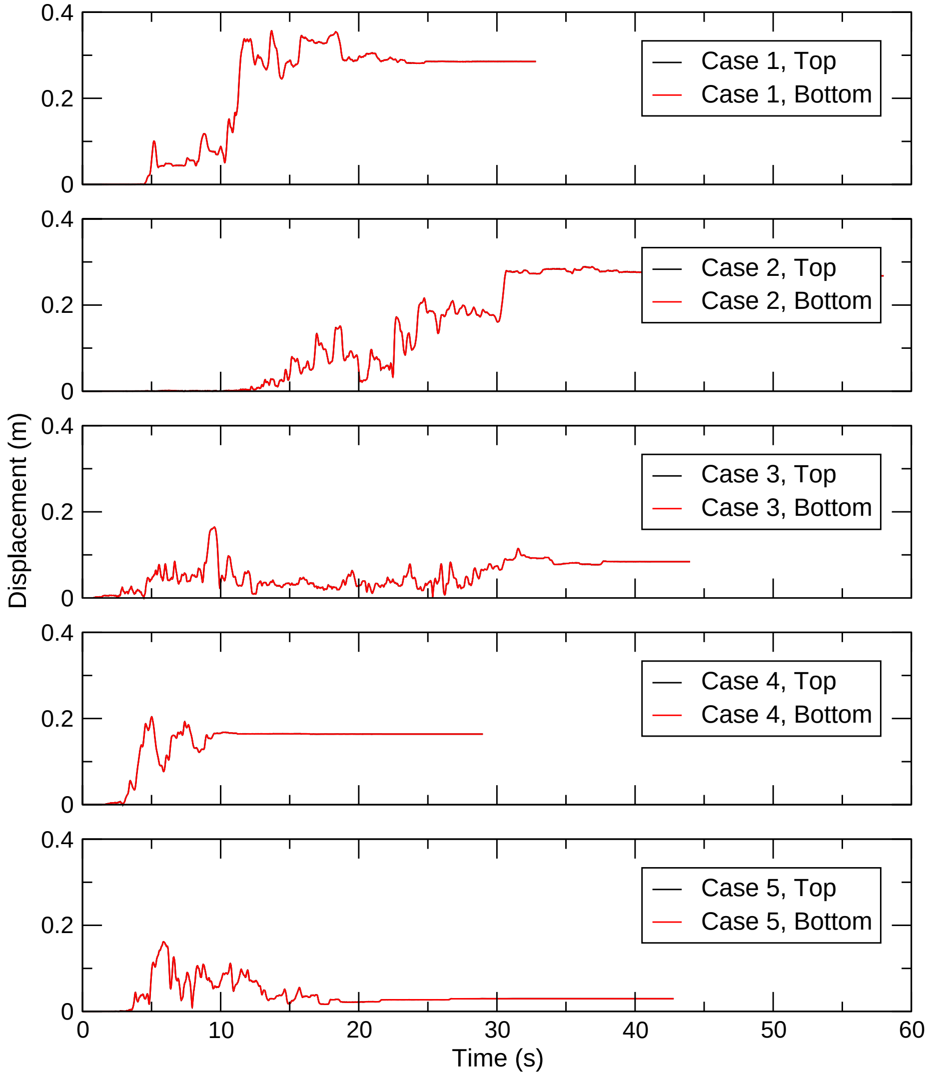

Figure 5.10: Time Histories of Cask Displacement Relative to Pad for Cylindrical Cask, Stiff Soil Profile, Cask/Pad μ=0.2, All 5 Earthquakes, NUREG/CR-0098 Spectral Shape, PGA=1.0 g

Figure 5.11 shows a similar plot for all five earthquake records, but with a cask/pad coefficient of friction of 0.55. Here it can be seen that the cask base and top displacements significantly deviate from each other in some cases, indicating a relatively high rotational angle. In some cases, the cask undergoes a rolling motion, and the cask top experiences very high displacements relative to the pad. In other cases, the cask has more of a tendency to rock back and forth, and the cask top displacements are typically much smaller. Once the cask begins to move relative to the pad, the response becomes highly nonlinear and highly dependent on the phasing of the ground motion with respect to the phasing of the cask response.

As the ground motion increases, the cask response tends to increase. If an input ground motion record is scaled linearly, the cask response will not always increase monotonically as a function of the ground motion. Since the cask response is dependent on the state of the cask when subjected to a ground motion pulse, the ground motion could either increase or decrease the motion of the cask. It sometimes occurs that scaling up the ground motion causes the cask to move in such a way so that the pulses that may have previously excited the cask actually decrease the energy in the cask. If the peak responses of the cask subjected to a number of ground motion records are averaged out, the average response will almost always increase monotonically as a function of the ground motion.

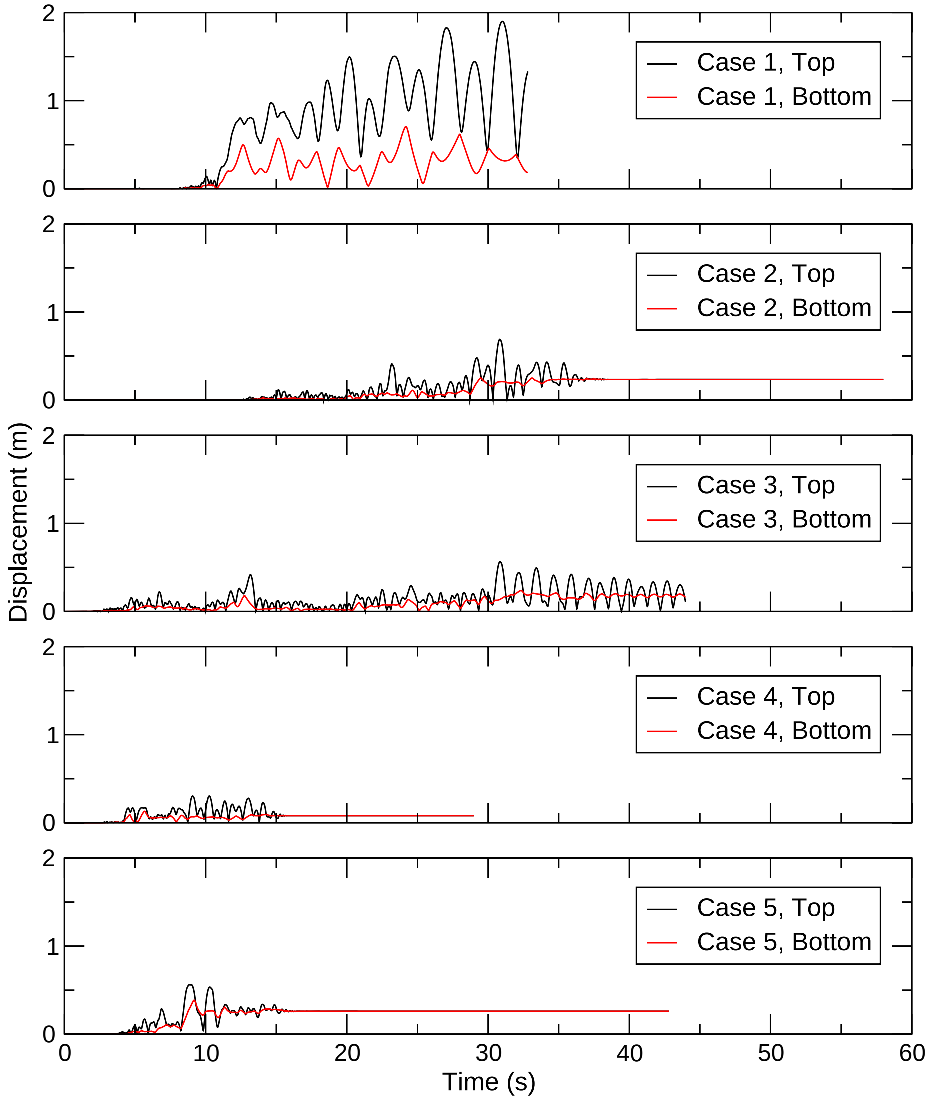

Figure 5.11: Time Histories of Cask Displacement Relative to Pad for Cylindrical Cask, Stiff Soil Profile, Cask/Pad μ=0.55, All 5 Earthquakes, NUREG/CR-0098 Spectral Shape, PGA=1.0 g

Figure 5.12 shows a series of cask displacement histories similar to those shown in the previous two figures, but with a coefficient of friction of 0.8 between the cask and pad. The responses are in general quite similar to those with μ=0.55, but they are slightly larger. It is interesting to note that in Case 2, the cask tips over.

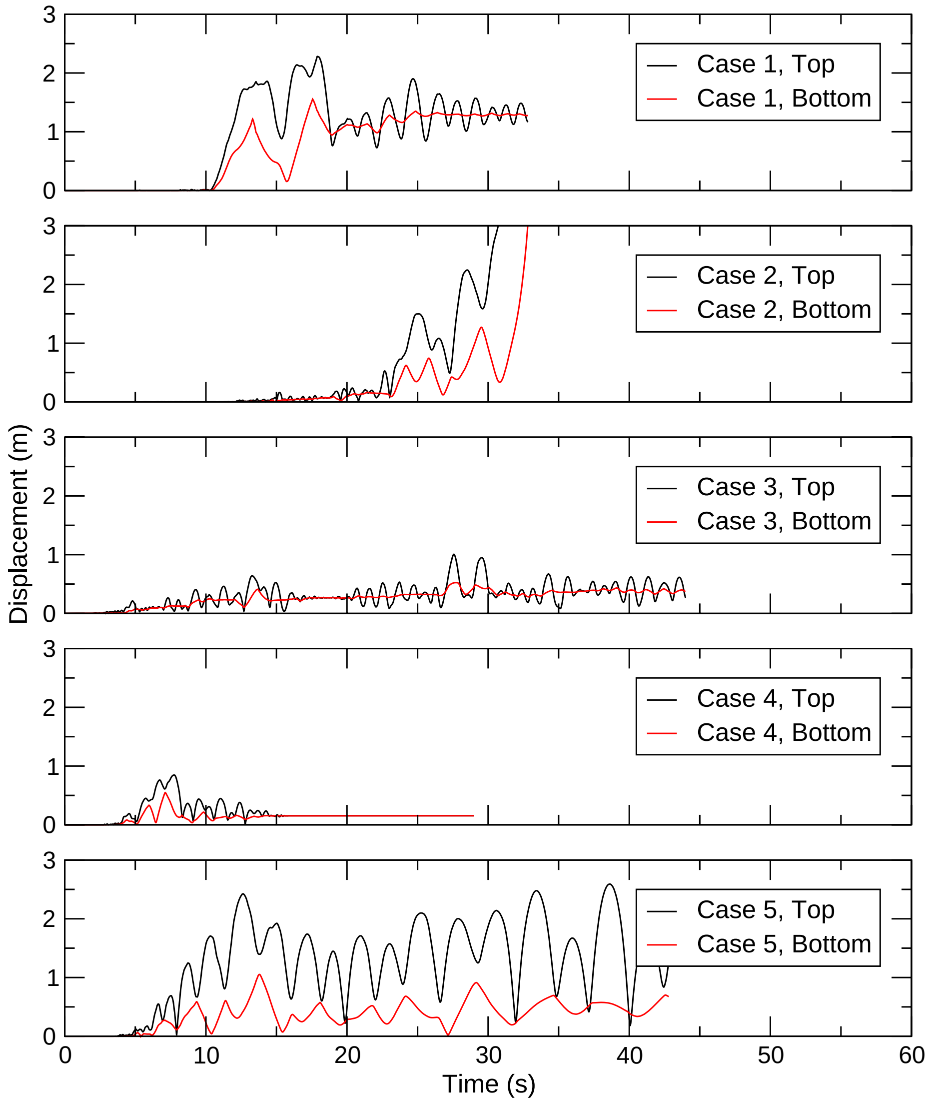

Figure 5.12: Time Histories of Cask Displacement Relative to Pad for Cylindrical Cask, Stiff Soil Profile, Cask/Pad μ=0.8, All 5 Earthquakes, NUREG/CR-0098 Spectral Shape, PGA=1.0 g

5.2.2 Representative Analysis Results for Rectangular Module

Because of the rectangular shape of the module base, this type of module generally exhibits much lower response than that experienced by a cylindrical cask subjected to the same ground motion. The rectangular module base prevents it from assuming a rolling motion. The module is forced to either rock about one of the edges or slide. Since one of the edges is significantly longer than the other, it always tends to rock about the shorter edge. Figure 5.13 shows an example of the relative lateral displacement trajectories for the module top and base for a case in which the coefficient of friction is 0.55. The stiff soil profile was used, and the ground motion came from the Iran Tabas earthquake record fitted to the NUREG/CR-0098 spectra, scaled to PGA=1.0. These are the same conditions used to generate the plot in

Figure 5.9, but it can be seen that the response is much lower in this case. The motions of the top and base are nearly identical to each other, and the module experiences minimal sliding.

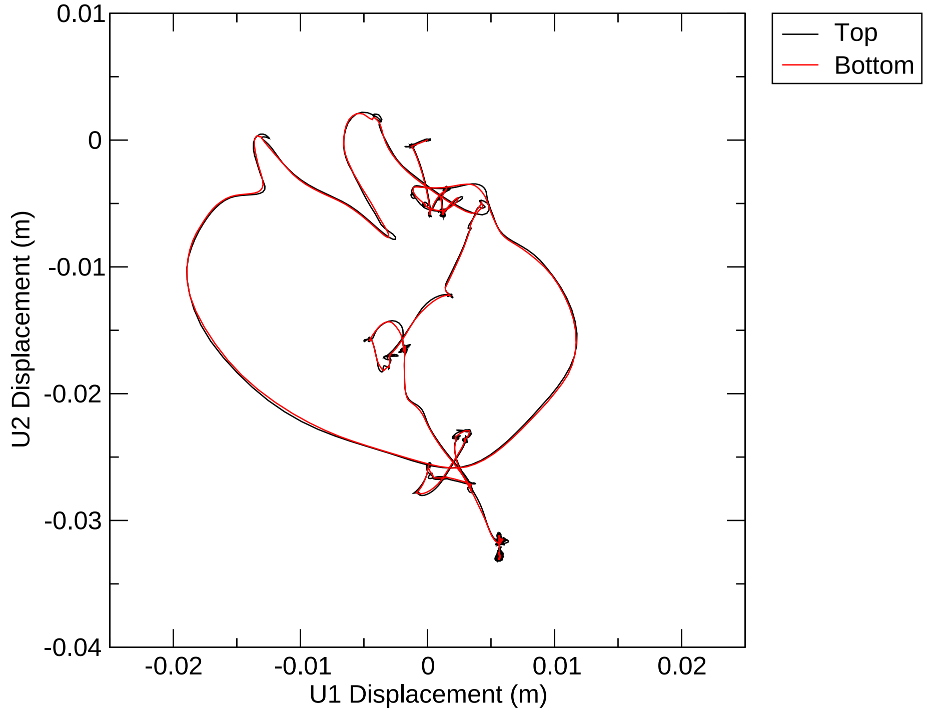

Figure 5.13: Lateral Displacement Trajectories for Rectangular Module Top and Base, Iran Tabas Earthquake, PGA=1.0 g, Stiff Soil Profile, μ=0.55

Plots similar to those provided in Figure 5.10, Figure 5.11, and Figure 5.12 are provided for the rectangular module. Figure 5.14 shows the response of the module subjected to 5 earthquake records with μ=0.2. Figure 5.15 shows the same series of plots for μ=0.55, and Figure 5.16 shows them for μ=0.8. The plots for μ=0.2 are nearly identical to those for the cylindrical cask. This is to be expected because the response consists of nearly pure sliding, so geometric details of the cask do not affect the response. The response is lower when μ=0.55 because the sliding is limited. There is still sufficient sliding to limit rocking. When μ=0.8, the sliding is further limited, and the cask exhibits some rocking motions. The overall response, however, is still quite small, even at the peak ground acceleration of 1.0 g used to generate these plots.

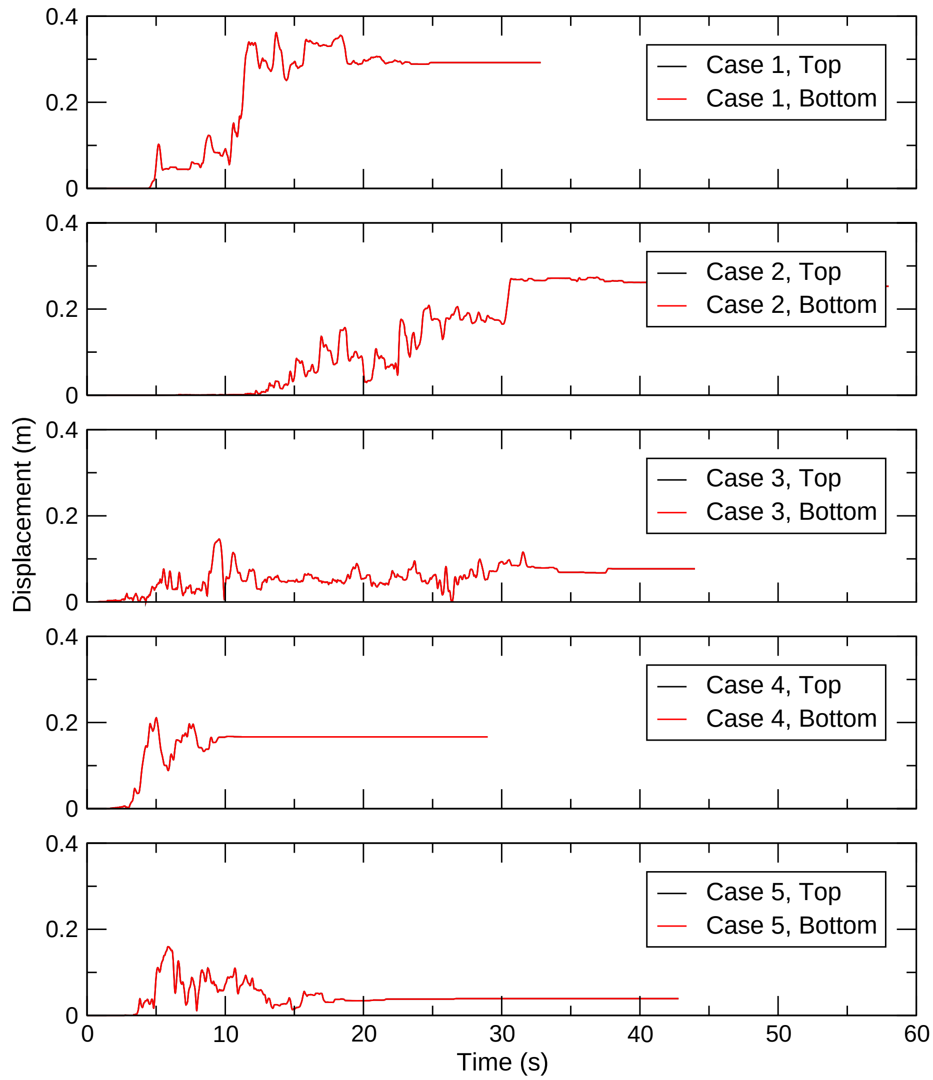

Figure 5.14: Time Histories of Cask Displacement Relative to Pad for Rectangular Module, Stiff Soil Profile, Cask/Pad μ=0.2, All 5 Earthquakes, NUREG/CR-0098 Spectral Shape, PGA=1.0 g

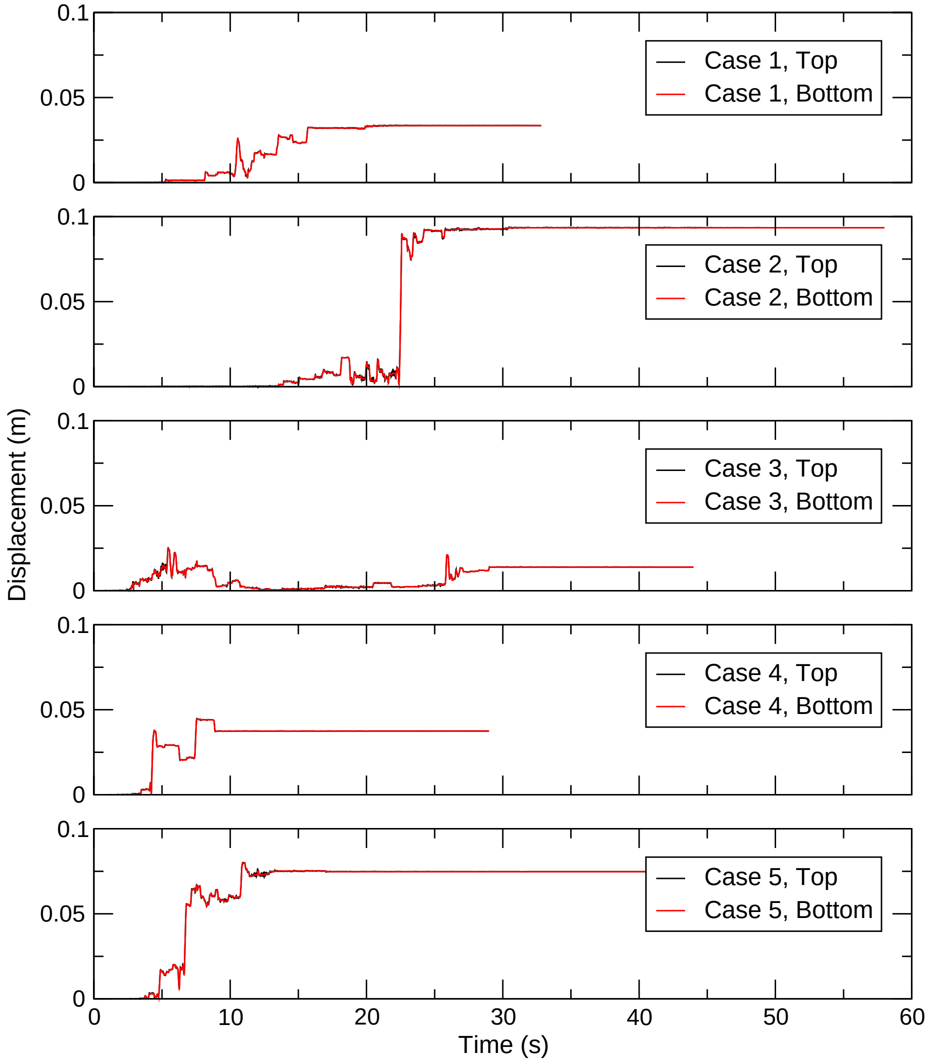

Figure 5.15: Time Histories of Cask Displacement Relative to Pad for Rectangular Module, Stiff Soil Profile, Cask/Pad μ=0.55, All 5 Earthquakes, NUREG/CR-0098 Spectral Shape, PGA=1.0 g

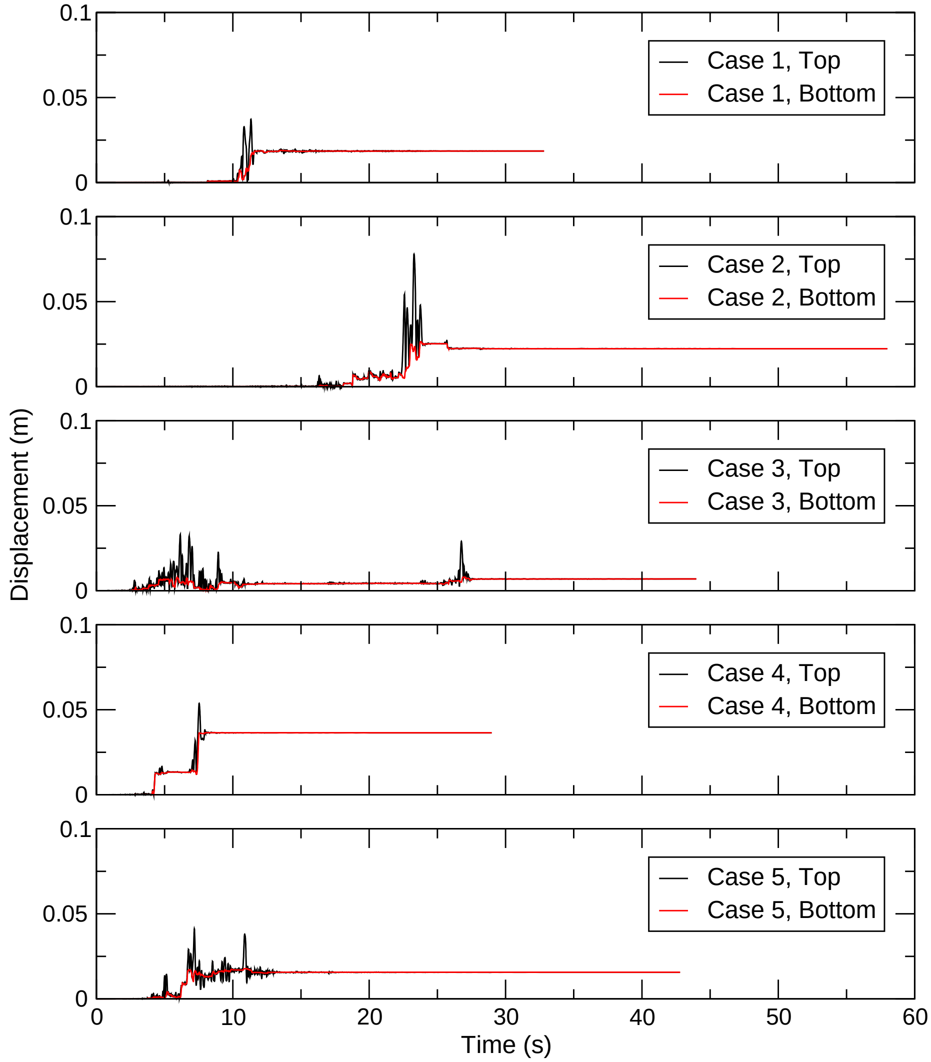

Figure 5.16: Time Histories of Cask Displacement Relative to Pad for Rectangular Module, Stiff Soil Profile, Cask/Pad μ=0.8, All 5 Earthquakes, NUREG/CR-0098 Spectral Shape, PGA=1.0 g

5.3 Presentation of Analysis Results

A total of 1165 analyses were performed in completing the set of parametric analyses outlined in Table 4.1 for the cylindrical cask and the rectangular module. Due to the large number of analyses, the complete time histories of all of these analysis cases are not presented here. Instead, the three key quantities used to characterize the analysis results as outlined in Section 5.2 and illustrated in Figure 5.8 are reported for each case. These quantities are the peak magnitude of the lateral displacement vectors at the cask top and bottom relative to the pad and the peak cask rotation from the vertical. These results are tabulated for all analysis cases in Appendix V.

In the tables of analysis results in Appendix V, there are cases labeled as “Tips”, which designate cases when the cask system tips over. Since cask displacements and rotations carry very little meaning in these “Tips” cases, they are omitted in the tables. In parametric cases for the cylindrical casks subjected to earthquake ground motions conforming to the Regulatory Guide 1.60 spectral shape, the higher cask responses were observed at a given level of PGA. Almost all analyses with PGA=1.0 g resulted in the cask tipping over, so the analyses were not run with PGA=1.25 g. To provide more data points for plotting results, these analyses were run with PGA=0.4 g and PGA=0.5 g.

Relatively coarse increments in ground motion intensity were used to provide a broad coverage of a wide range of potential events. The undesirable consequence of this is that if a cask tips over at a given level of ground motion, it is difficult to identify the level of ground motion at which the cask is on the threshold of tipping. For example, if a cask tips over at PGA=1.0 g, but it exhibits minimal response under the same conditions but with the ground motion of PGA=0.6 g, the threshold of tipping could be anywhere between 0.6 g and 1.0 g PGA. To decrease the uncertainty in the level of ground motion required to overturn the cask, additional analyses at more refined increments of PGA were performed in the cases when the cask tipped over. The results of these additional analyses are also included in the tables in Appendix V.

In addition to the tabular presentation of the cask response parameters for each of the analysis cases, graphical presentations of a subset of these same results are also provided in Section V.2 of Appendix V. For each combination of cask type, soil type, and spectral shape, plots of peak relative cask top displacement and peak rotation as functions of PGA are provided. These two measures of cask response are likely to be the most useful for assessing the safety of a cask design under given site and seismic conditions. Because the cask motion is often dominated by rocking, the peak displacement of the cask top is almost always greater than the peak displacement of the cask bottom, so this parameter is the most useful for safeguarding against collision of adjacent casks. In only 6 of the 1165 analysis cases, the displacement of the cask bottom was slightly greater than that of the cask top. In all of these cases, the cask response was dominated by sliding rather than tipping. The largest difference between the peak bottom and top displacement within these 6 cases was 7 mm (0.3 in). Because the peak top displacement is almost always greater than the peak bottom displacement, the peak bottom displacement is not included in the plots.

In each of the plots in Appendix V, 15 lines are used to connect the results with a given set of parameters at varying levels of ground motion. There is a separate line for each combination of ground motion record and coefficient of friction between the cask and pad. The ground motion records are denoted as Case 1-5 for the five startup ground motion records fitted to the NUREG/CR-0098 or Regulatory Guide 1.60 spectral shapes. A different set of startup ground motion records was used for the earthquake records that were fitted to the NUREG/CR-6728. To differentiate these, they are denoted as Case A-E. The actual names of the ground motion records corresponding to these identifiers are listed in Section 4.1.4. A total of 18 combinations of cask type, soil type, and spectral shape were studied. Thus, to provide separate plots of the three key cask response quantities, 54 plots are required. The first 18 plots show the relative cask top displacement results, the second 18 plots show the cask rotation results, and the final 18 plots show the relative cask bottom displacement results.

5.4 Discussion of Analysis Results

The analysis results presented in Appendix V demonstrate the wide range of responses that the cask could potentially exhibit under a variety of conditions. It can be seen that in many cases, there is a large amount of scatter in the results when five different time histories are used for the seismic input with other parameters held constant. These are expected results because of the nonlinearities present in the analysis models.

As expected, the cask response tends to increase as the ground motion increases. In some cases, however, the cask response under a given set of input parameters is lower with a higher level of ground motion than with a lower level. The cask response is very sensitive to the timing of the ground motion pulses. The earthquake records are scaled linearly in this study, but the cask response is not expected to increase linearly as a function of the ground motion scaling. Because the cask response is nonlinear, changing the scaling of the ground motion can dramatically change the timing of the cask motion. At a given level of ground motion, the cask may be in a position that maximizes its response to a critical ground motion pulse. At a higher level of ground motion, the cask may be positioned differently at the time of that same pulse, causing it to exhibit a very minimal response. Although some isolated cases indicate a non-monotonic increase in the response as a function of the ground motion, the mean response of the 15 cases with 5 different ground motion records and 3 cask/pad coefficients of friction always increased monotonically in this study. Due to the randomness in the cask response, it is clearly important to evaluate the cask response under a number of different earthquakes and compute statistics of those results. Basing decisions on an isolated analysis case could be incorrect because of the large scatter in the results.

The parametric analysis results indicate that the cask response is very sensitive to the value of the cask/pad friction coefficient, μ. In most of the plots in Appendix V, the five sets of results using a given value of μ are generally clustered together. As discussed previously, the upper and lower bound values of μ used in this project are extreme values, about 2.5 standard deviations above and below the mean value. The selected range of μ provides useful upper and lower bound measures of response that can be used for design review.

The cylindrical cask tended to result in a much higher response than the rectangular module under the same conditions. Once the vertical cylindrical cask begins to lift up from the pad, it can either begin to rock back and forth, or assume a rolling motion. Much less energy is absorbed in the rolling mode than in the rocking mode. In addition, ground motion pulses in any direction can cause rocking or rolling of cylindrical casks. This is in contrast to rectangular modules, which due to their geometry, tend to only rock about the short dimension. Because of these characteristics, cylindrical casks tend to assume a rolling motion. The cylindrical cask is only slightly more slender than the rectangular module. The ratios of center of gravity height-to-base dimension are nearly the same for these two designs.

At high levels of ground motion, rocking and rolling motions dominate the cylindrical cask response. There is not a marked difference between the responses obtained when μ=0.55 and when μ=0.8 because the lower of these two coefficients of friction is sufficiently high to cause the cask to favor tipping over sliding. Further increasing μ above this level does little to change the response. The lower bound cases (μ=0.2) produced the highest response only in some cases when low levels of ground motion (PGA=0.25 g) were applied to the cask.

The opposite of the above statements about the effect of the cask/pad coefficient on the cask response can generally be stated for the rectangular module analyses. Due to the geometry of this module, it does not assume a rolling motion. The cask top displacement is generally higher when a lower bound coefficient of friction is used than with higher values. It should be noted that the lower bound coefficient of friction of 0.2 is sufficiently low that neither of the cask designs investigated here exhibit any significant tipping. As a result, when μ=0.2, the response of the rectangular module is generally very close to that of the cylindrical cask under the same conditions.

The response of both cask designs is highly dependent on the spectral shape of the ground motion. The ground motion records conforming to the NUREG/CR-6728 spectral shape produced the lowest response. The NUREG/CR-0098 earthquakes produced a medium response, and the Regulatory Guide 1.60 earthquakes resulted in the highest response levels. The cylindrical cask never tipped over under the NUREG/CR-6728 ground motion, even with PGA=1.25 g. At that level of ground motion, the highest observed peak lateral displacement of the cask top relative to the pad is 0.83 m (33 in). Under the NUREG/CR-0098 ground motion records, the highest observed cask top displacement is 1.63 m (64 in) with PGA=0.6 g. When these records are scaled up so that the PGA=1.0 g, 2 of 45 cases result in the cask overturning. When the cylindrical cask is subjected to earthquakes conforming to the Regulatory

Guide 1.60 spectra with PGA=0.5 g, the peak observed cask top displacement is 2.42 m (95 in). Scaling up these records to PGA=0.6 g results in overturning for 2 of 45 cases.

Similar trends were observed for the rectangular module, although the response is lower and the cask never overturns. The highest observed peak top displacement with the NUREG/CR-6728 spectral shape earthquakes is 0.26 m (10 in) at PGA=1.25 g. Under the NUREG/CR-0098 earthquakes at the same PGA, this increases to 0.52 m (21 in). When subjected to the Regulatory Guide 1.60 earthquakes at PGA=1.25 g, the peak top displacement of a rectangular module is 1.7 m (67 in).

5.5 Compilation of Analysis Results in Nomograms

5.5.1 Nomograms for Specific Spectral Shapes

As mentioned previously, there is a large amount of scatter in the cask response results. The cask typically responds quite differently to the five different ground motion records fitted to the same spectral shape. This scatter is to be expected and is analogous to the scatter that would be observed in the response of identical casks subjected to various actual earthquakes. To facilitate evaluation of cask designs, it is useful to consolidate these results in a statistical manner. To this end, least squares regression curve fits have been performed on the cask analysis results, providing equations that describe the cask response as a function of the ground motion intensity.

The cask response as a function of ground motion intensity has been found to be fit reasonably by an exponential equation of the form:

$$y = A x^B \tag{5.6}$$

where y is a variable describing the cask response, A and B are parameters of the fitted curve, and x is a variable describing the ground motion intensity. Taking the natural logarithm of both sides of this equation yields the following:

$$\ln(y) = \ln(A) + B\ln(x) \tag{5.7}$$

It can be seen that an equation of this form appears as a linear function when x and y are both plotted on logarithmic scales. Thus, standard linear regression procedures can be used to compute the values of A and B. Pairs of data points, x_i and y_i, from each analysis case, i, are transformed by taking their natural logarithms, and linear regression is performed on the transformed values: $\ln(x_i)$ and $\ln(y_i)$.

In linear regression, there is an implicit assumption that the distribution of y with x held constant ($Y|x$) conforms to a normal probability distribution. The best-fit line thus represents the mean or expected value of the random variable. Because the linear regression is performed on data that have undergone a logarithmic transformation in this case, the distribution of y with x held constant is implicitly assumed to follow a lognormal distribution. The best-fit line thus represents the median value, and the mean is greater than the median.

Once the linear regression is performed, two parameters describing the scatter of the data and the quality of the fit are computed. These parameters are computed based on the transformed data and the transformed fitted function using the standard methods as described in Ang and Tang [28]. $S_{Y|x}$ is the conditional standard deviation and is a measure of the dispersion of the data points about the fitted function. In this case, it is the conditional standard deviation of the underlying normal distribution, and is computed using the following equation:

$$S^2_{Y|x} = \frac{1}{n-2}\sum_{i=1}^{n}(\ln(y_i) - y'_i)^2 \tag{5.8}$$

where n is the number of data points and y'_i is the value of the transformed fitted function evaluated at x_i:

$$y'_i = \ln(A) + B\ln(x_i) \tag{5.9}$$

The parameter r^2 provides a measure of the ability of the fitted curve to represent the data and can vary from 0 to 1. Higher values of this parameter indicate better fits. This parameter is also based on the transformed data, and is computed with the formula:

$$r^2 = 1 - \frac{S^2_{Y|x}}{S_Y^{\ 2}} \tag{5.10}$$

where S_Y^2 is computed from the transformed data as:

$$S_Y^{\ 2} = \frac{1}{n-1}\sum_{i=1}^{n}\left(\ln(y_i) - \frac{1}{n}\sum_{i=1}^{n}\ln(y_i)\right)^2 \tag{5.11}$$

The conditional standard deviation can be used to produce functions representing envelopes of the data. For the exponential equation employed here, an equation for a confidence band at the median plus m standard deviations is expressed as:

$$y = Ax^B \exp\left(m\, S_{Y|x}\right) \tag{5.12}$$

All of the plots of the regression fits of the response data shown in this section show the equation for the median fitted curve, including the values of the *A* and *B* parameters. The values of $S_{Y|x}$ and r^2 are reported in the legend of the plot next to the equation for the median response. In addition, the 84% and 16% confidence bands are shown in the regression plots along with the equations for these functions. These represent the median plus and minus one standard deviation, respectively, and were computed using Equation 5.12.

Figure 5.17 shows a representative plot of the function obtained to fit a series of analysis results using least squares to compute the values of *A* and *B* in a way that minimizes the residual error. The fitted curve provides functions describing the peak cask top displacement as a function of PGA for earthquakes conforming to the NUREG/CR-0098 spectral shape with a cask/pad friction coefficient of 0.55 and the soft soil profile. This plot is shown using linear scales, while Figure 5.18 shows the same data and fitted curves plotted on logarithmic scales. These plots show three fitted curves along with points that represent individual analysis results. The median curve is the function that minimizes the residual error. The equation for that function is shown in the legend of the plot.

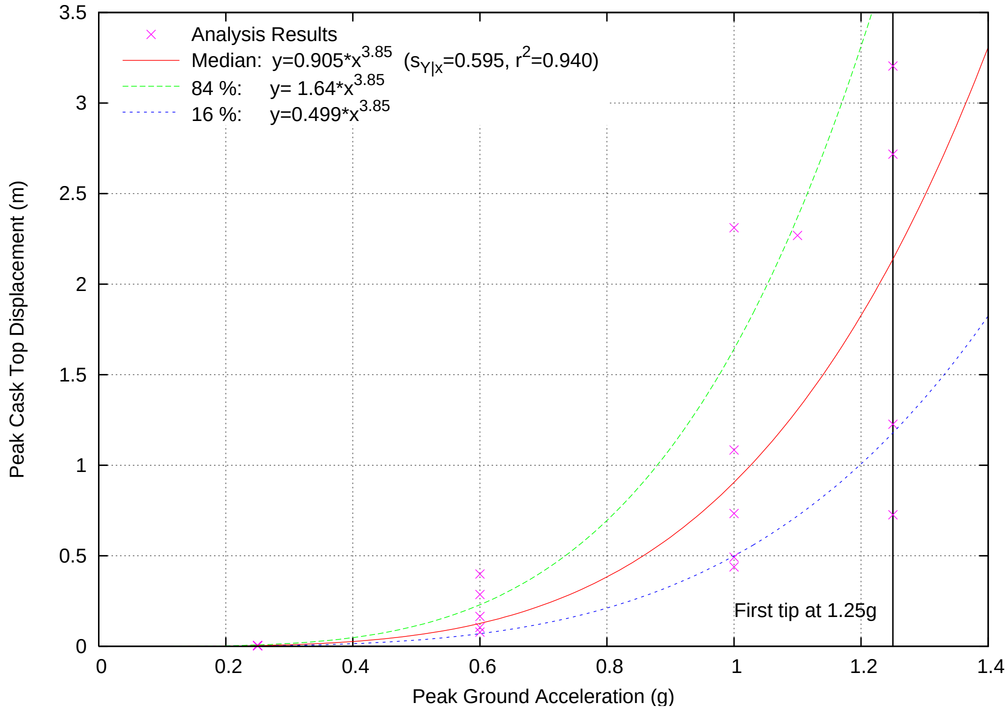

Figure 5.17: Peak Top Displacement Regression Fit, Linear Scale, Cylindrical Cask, NUREG/CR-0098 Earthquakes, Cask/Pad μ=0.55, Soft Soil Profile

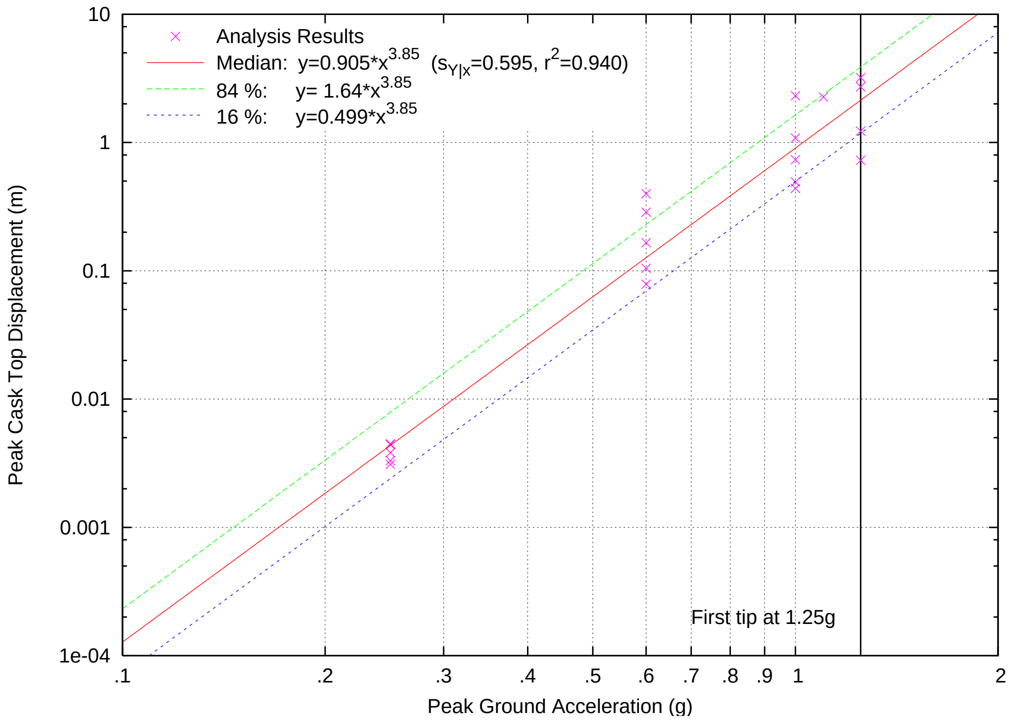

Figure 5.18: Peak Top Displacement Regression Fit, Logarithmic Scale, Cylindrical Cask, NUREG/CR-0098 Earthquakes, Cask/Pad μ=0.55, Soft Soil Profile

A note should be made of the heavy vertical line that appears at 1.25 g PGA on these plots. In the regression plots developed in this study, a heavy vertical line is used to denote the lowest ground motion intensity at which a cask tipped over in that set of results. The results of the analyses in which the cask tipped over are not included in the plots. In some cases, analyses at higher ground motion levels indicated that a cask that tipped over at a lower level of ground motion does not tip over at a higher ground motion level. This is to be expected sometimes because of the nonlinear nature of the cask response. These results are not, however, included in the regression fits.

The plots provided in Figure 5.17 and Figure 5.18 show regression fits of the peak cask top displacement as a function of PGA for one cask design, one spectral shape, one coefficient of friction, and one soil profile. It is desirable to group together the results that are not particularly sensitive to input parameters. As mentioned before, the cask results are very sensitive to the cask design due to the fact that the behavior of the cylindrical cask is fundamentally different from that of the rectangular module. The cask response is also quite sensitive to the spectral shape and the coefficient of friction. In the analysis cases run here, the cask response does not appear to be particularly sensitive to the soil profile. There are certainly differences in the results obtained using the different soil profiles, but relative to the overall amount of scatter seen in the results, the differences due to the soil profile are quite small.

To demonstrate the similarities in the trends of the results with differing soil profiles, plots of the regression fits of the peak cask top displacement as a function of PGA are provided for the cylindrical cask subjected to the NUREG/CR-0098 earthquakes with the cask/pad μ=0.55 for the stiff soil and rock profiles in Figure 5.19 and Figure 5.20, respectively. These are provided on logarithmic scales and can be compared with Figure 5.18, in which everything else is the same as in these plots except that the soft soil profile is used.

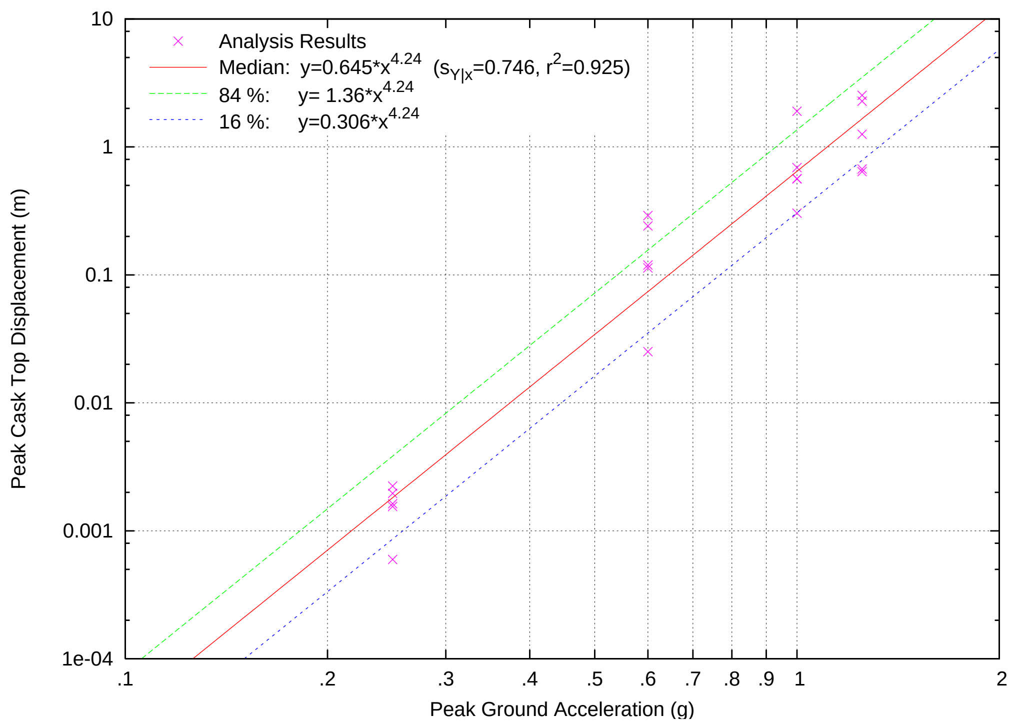

Figure 5.19: Peak Top Displacement Regression Fit, Logarithmic Scale, Cylindrical Cask, NUREG/CR-0098 Earthquakes, Cask/Pad μ=0.55, Stiff Soil Profile

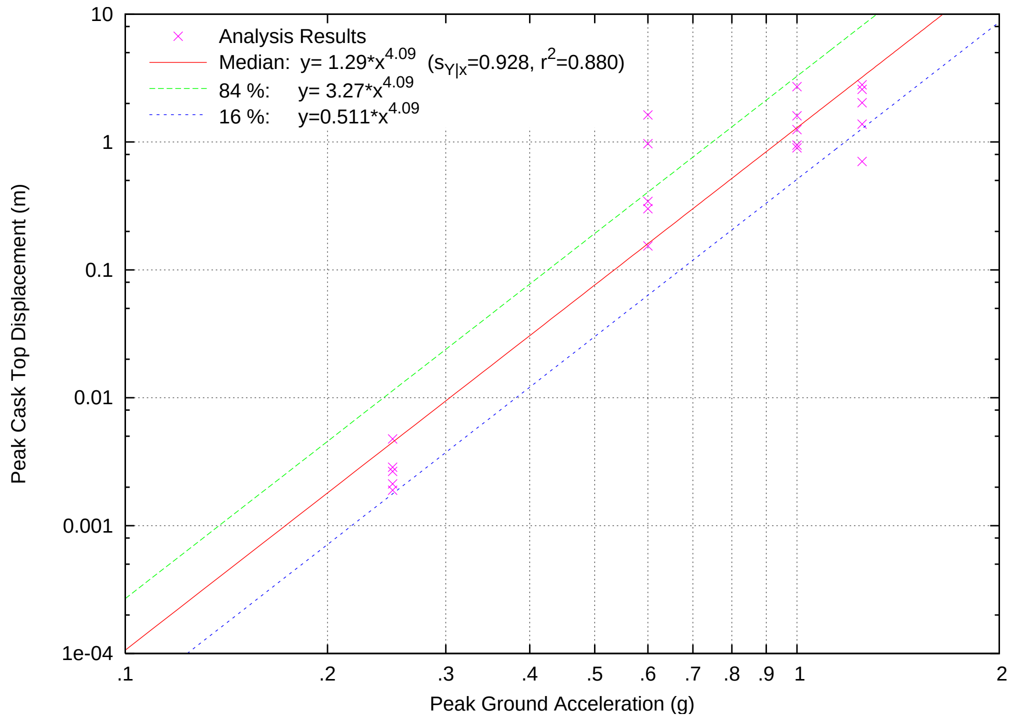

Figure 5.20: Peak Top Displacement Regression Fit, Logarithmic Scale, Cylindrical Cask, NUREG/CR-0098 Earthquakes, Cask/Pad μ=0.55, Rock Profile

There are differences in the regression fits for these data sets, but in general, these differences are minor. Because the soil type does not have a significant effect on the response, the data points for all three soil profiles can be grouped together for regression fitting. Figure 5.21 shows a regression fit of the peak cask top displacements with the soft soil, stiff soil, and rock profile results grouped together for the cylindrical cask with the NUREG/CR-0098 spectral shape and μ=0.55. Different types of symbols are used to denote the results from the three soil profiles. It can be seen that there is not a large difference in the response with the different soil types. Combining these results provides more data points for a fitted curve that can be applied to a broad range of soil types.

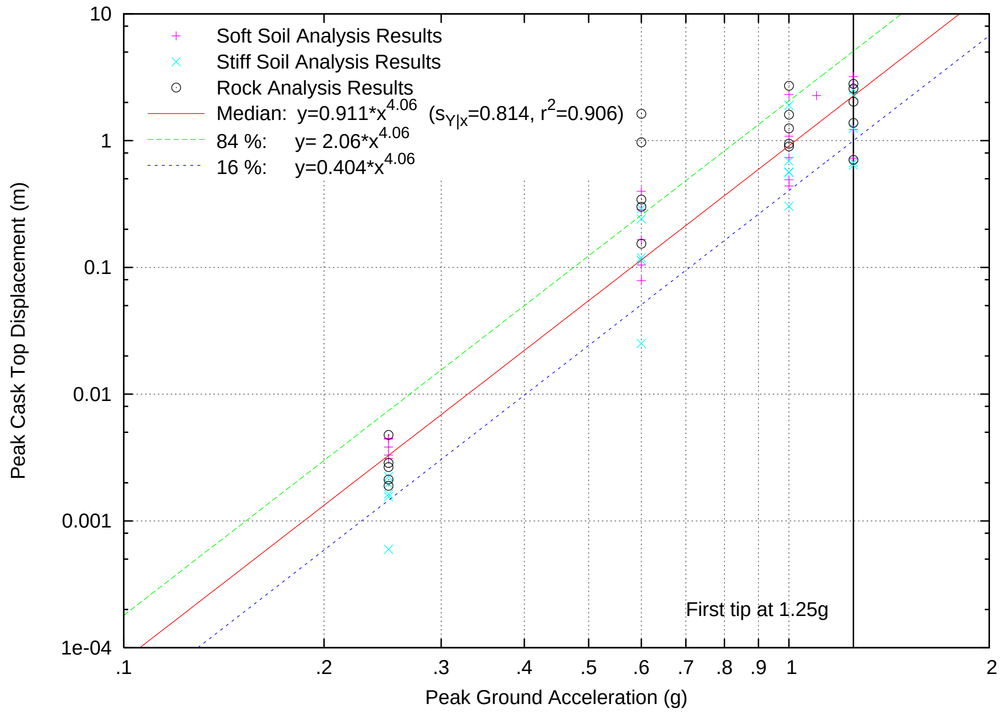

Figure 5.21: Peak Top Displacement Regression Fit, Logarithmic Scale, Cylindrical Cask, NUREG/CR-0098 Earthquakes, Cask/Pad μ=0.55, All Soil Profiles

Plots similar to those shown in Figure 5.21 are provided in Appendix VI for both cask designs, all three spectral shapes, and all three values of the cask/pad friction coefficient used in this study. These plots are provided for both the peak cask top displacement as well as the peak cask rotation as functions of PGA. They can be used as nomograms for evaluating the response of these cask designs subjected to earthquakes conforming to the spectral shapes used here. The conditional standard deviation for a given fitted curve can be used in conjunction with the equation of the fitted curve to develop the probability distribution of the response of a given cask with a given friction coefficient subjected to an earthquake conforming to one of the three spectral shapes used in this study. Functions are provided for the median response and the 84% and 16% confidence bands, but the response at a different degree of confidence can be easily computed using Equation 5.8.

It is important to note that in general, the quality of the fitted curves, as indicated by the r^2 value, is quite good, but there are some data sets that are not fit very well. In general, the regression fits of the peak cask rotations are not as good as those for the peak cask displacements. For the cases where the cask response is dominated by sliding, the rotation angles are quite low, and the regression fits are not very good because of the large amount of noise in this data. In these cases, the angles of rotation are low, so the poor fitting of the data is not likely to have serious consequences for cask design review. Even if the required level of confidence for design purposes were increased significantly in these cases to account for the poor fits, the cask rotations would still be quite low in general.

It is very important to point out that all parametric analyses were performed for specific designs of a cylindrical cask and a rectangular module, freestanding on selected foundation types subjected to earthquake excitations conforming to selected spectral shapes. The principal objective of the parametric analyses is to compile analysis results in nomograms to provide meaningful and practical interpretation of seismic behavior of dry cask systems to cask designers and reviewers. The users of these nomograms are reminded to compare the design details of their dry cask storage systems and site-specific seismicity to those used in the parametric analyses. Any significant differences in these comparisons may limit the applicability of the nomograms of analysis results to specific cask design cases.

5.5.2 Combination of Spectral Shape Nomograms

Up to this point, the parameter used to describe the magnitude of the ground motion has been the PGA. If the ground motion at a given site is expected to conform to one of the three spectral shapes used in this study, the spectrum-specific nomograms can be used to find the expected cask response at a given level of PGA. As is clearly evident by the large differences in the response as a function of PGA for the three spectral shapes studied here, the cask response is clearly not a direct function of PGA. Peak ground acceleration is simply a measure of the response of an infinitely stiff structure. The cask's fundamental period is a highly nonlinear function of the tipping angle, but it is more sensitive to the spectral content of the ground motion in the 0.5-s to 2-s period range than to the high frequency content.

For useful comparisons of results from different spectral shapes, it is necessary to use a parameter to describe the ground motion that is more indicative of the cask response than is the PGA. Two parameters that appear to have promise for this purpose are the peak ground velocity (PGV) and the pseudo-spectral acceleration (PSA) at 5% damped 1 Hz. The PGV, which is not a direct function of the spectral shape, is influenced by the spectral accelerations across the middle of the spectrum in the period range likely to be important to the cask response.

Table 5.3 shows the peak ground acceleration, velocity, and displacement for the surface motion records conforming to the NUREG/CR-0098 spectral shape used in the parametric study. These are all scaled so that the PGA is equal to 1.0 g. The peak ground accelerations reported are in the two orthogonal horizontal directions in which the earthquake ground motion is defined. The ground motions in both of these directions are scaled so that their peak accelerations are equal. The acceleration in the orthogonal direction is typically very low at the time of the peak acceleration in one direction, so that the peak magnitude of the horizontal acceleration vector is very close to that of the peak acceleration components in the two directions. Thus, the peak accelerations reported in the table are for the two directions. The reported peak ground velocity and displacement, on the other hand, are the peak magnitudes of the horizontal velocity and displacement vector, respectively. These are typically significantly higher than the peak velocity and displacements in the two directions in which the ground motion is defined. Similar data is shown for the Regulatory Guide 1.60 spectral shape earthquakes in Table 5.4, and Table 5.5 shows this information for the NUREG/CR-6728 earthquakes. The average of these quantities for the five records is also shown in these tables.

Table 5.3: Peak Ground Acceleration, Velocity, and Displacement for Surface Ground Motion Records Conforming to NUREG/CR-00098 Spectral Shape

Ground Motion Record	Peak Ground Acceleration (g)	Peak Ground Velocity (m/s)	Peak Ground Displacement (m)
1	1.0	1.08	0.478
2	1.0	1.03	0.411
3	1.0	1.02	0.346
4	1.0	1.06	0.538
5	1.0	0.919	0.424
Average	1.0	1.02	0.439

Table 5.4: Peak Ground Acceleration, Velocity, and Displacement for Surface Ground Motion Records Conforming to Regulatory Guide 1.60 Spectral Shape

Ground Motion Record	Peak Ground Acceleration (g)	Peak Ground Velocity (m/s)	Peak Ground Displacement (m)
1	1.0	1.88	1.36
2	1.0	1.70	1.05
3	1.0	1.62	0.947
4	1.0	1.94	1.37
5	1.0	1.69	1.08
Average	1.0	1.77	1.16

Table 5.5: Peak Ground Acceleration, Velocity, and Displacement for Surface Ground Motion Records Conforming to NUREG/CR-6728 Spectral Shape

Ground Motion Record	Peak Ground Acceleration (g)	Peak Ground Velocity (m/s)	Peak Ground Displacement (m)
A	1.0	0.465	0.0999
B	1.0	0.486	0.100
C	1.0	0.507	0.0879
D	1.0	0.429	0.0781
E	1.0	0.561	0.115
Average	1.0	0.490	0.0963

Least squares regression fits of the response in terms of the PGV have been developed for the combined data for all three spectral shapes and all soil types for a given cask design and friction coefficient. The PGA used for each analysis was multiplied by the average ratio of PGV to PGA as presented in Tables 5.1–5.3 for the appropriate spectral shape. These results are then combined into a single, larger data set for regression fitting. These plots have been developed for the peak cask top displacement and peak cask rotation. Regression fits of the peak cask top displacement and rotation for the cylindrical cask and rectangular module in terms of PGV for all spectral shapes with μ=0.55 are provided on linear plots in Figures 5.22 through 5.25.

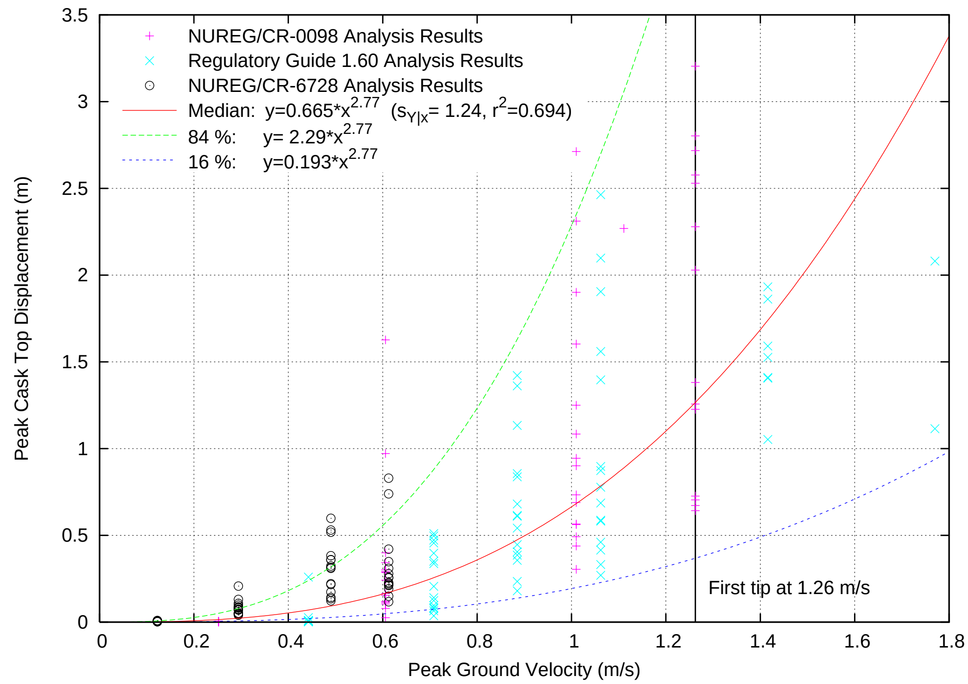

Figure 5.22: Peak Top Displacement Regression Fit in Terms of Peak Ground Velocity, Linear Scale, Cylindrical Cask, All Earthquakes, Cask/Pad μ=0.55, All Soil Profiles

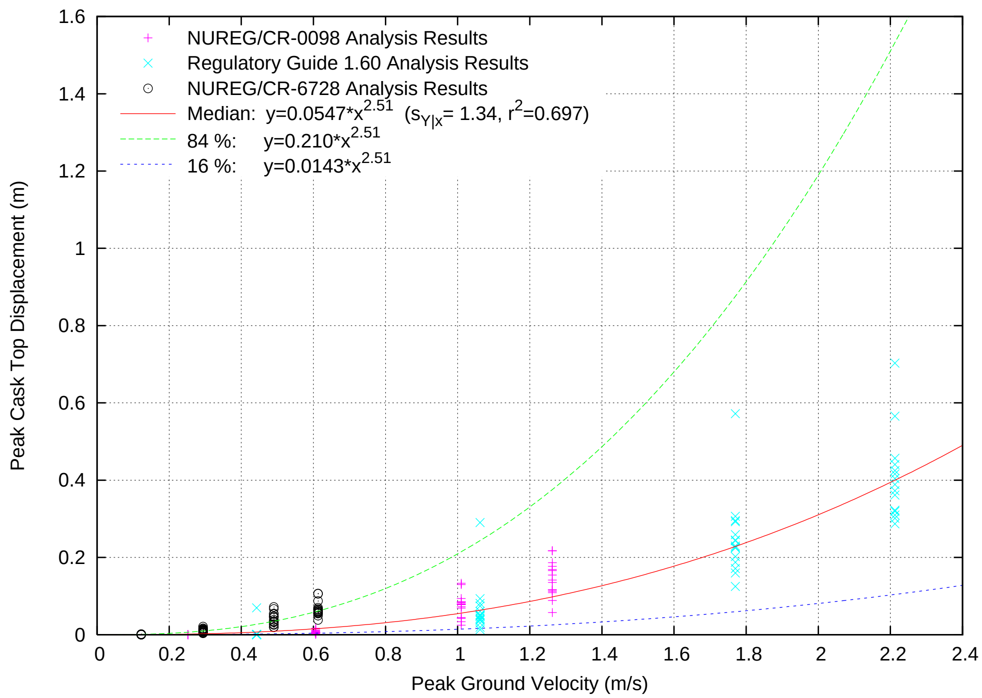

Figure 5.23: Peak Top Displacement Regression Fit in Terms of Peak Ground Velocity, Linear Scale, Rectangular Module, All Earthquakes, Cask/Pad μ=0.55, All Soil Profiles

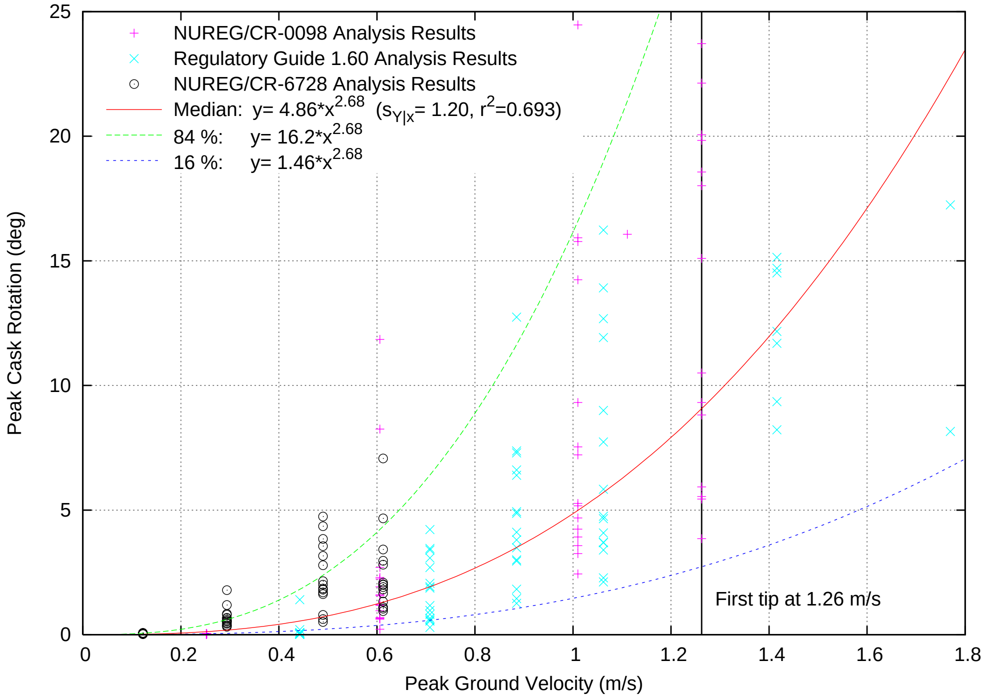

Figure 5.24: Peak Rotation Regression Fit in Terms of Peak Ground Velocity, Linear Scale, Cylindrical Cask, All Earthquakes, Cask/Pad μ=0.55, All Soil Profiles

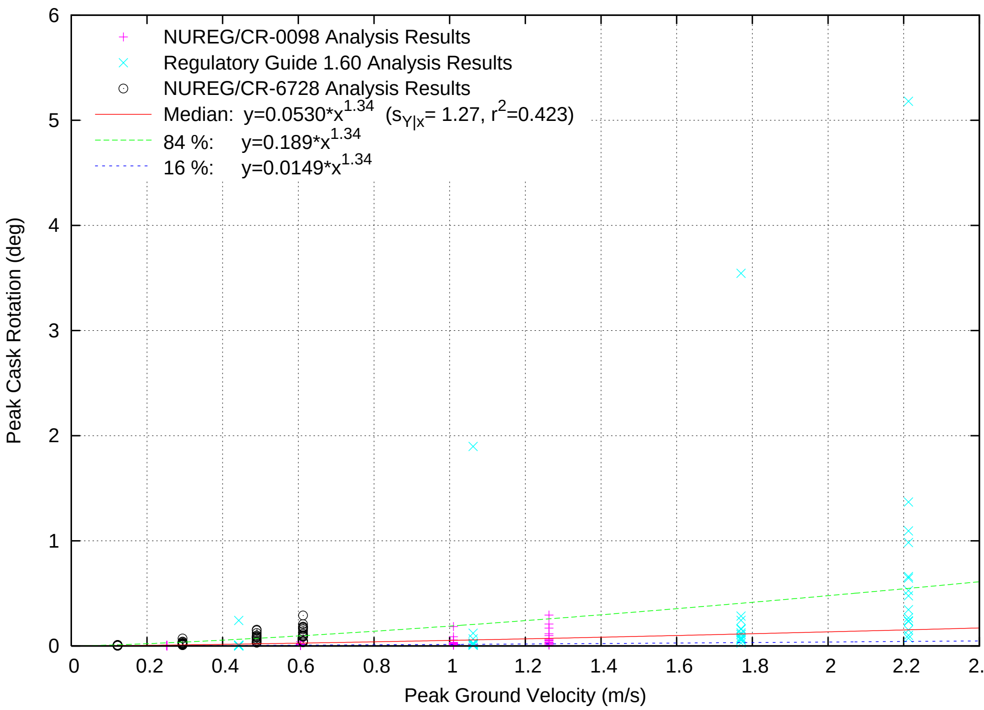

Figure 5.25: Peak Rotation Regression Fit in Terms of Peak Ground Velocity, Linear Scale, Rectangular Module, All Earthquakes, Cask/Pad μ=0.55, All Soil Profiles

A methodology similar to that used to perform regression analysis on the cask response results using PGV as the ground motion parameter can also be applied to provide fitted curves for the cask response in terms of the PSA at 1 Hz. Table 5.6 shows the ratios of the 5% damped 1 Hz PSA to the PGA for the three spectral shapes used here. The value of PGA used for each analysis was multiplied by this factor for the appropriate spectral shape, and the analysis results for all three spectral shapes were plotted together as was done for the plots in terms of PGV. Plots of the data and regression fits on linear scales for the top displacement and rotation in terms of the 1 Hz PSA are provided in Figure 5.26 through Figure 5.29 for the analyses with μ=0.55.

Table 5.6: Ratio of 5% Damped 1 Hz PSA to PGA for Spectral Shapes Used in Current Study

Spectral Shape	1Hz PSA/PGA
NUREG/CR-0098	1.475
Regulatory Guide 1.60	0.966
NUREG/CR-6728	0.550

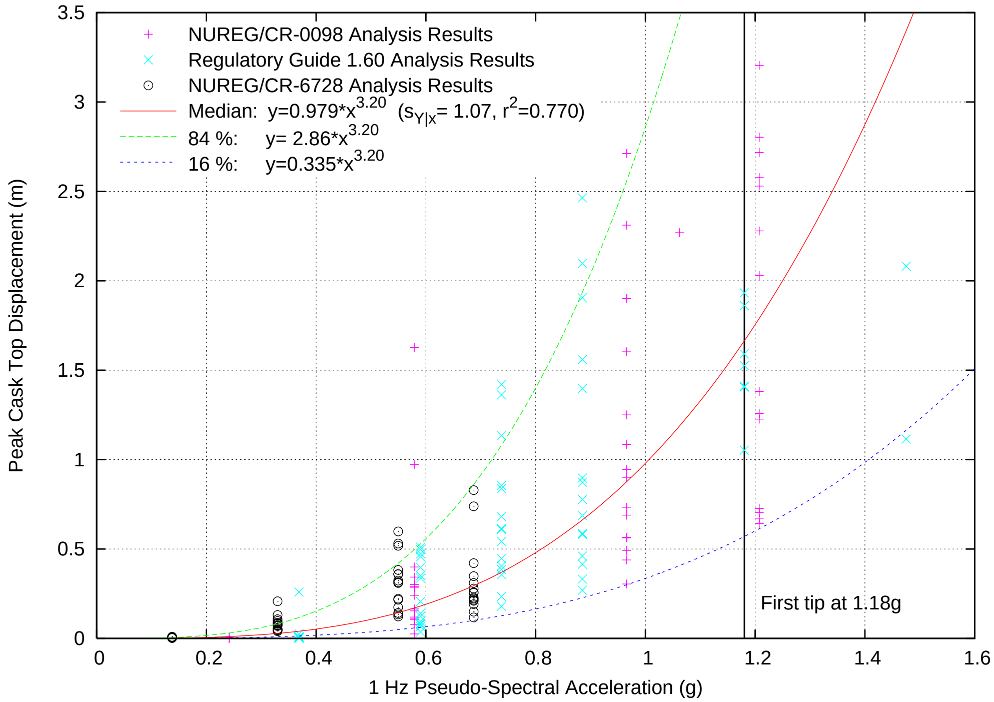

Figure 5.26: Peak Top Displacement Regression Fit in Terms of 1 Hz PSA, Linear Scale, Cylindrical Cask, All Earthquakes, Cask/Pad μ=0.55, All Soil Profiles

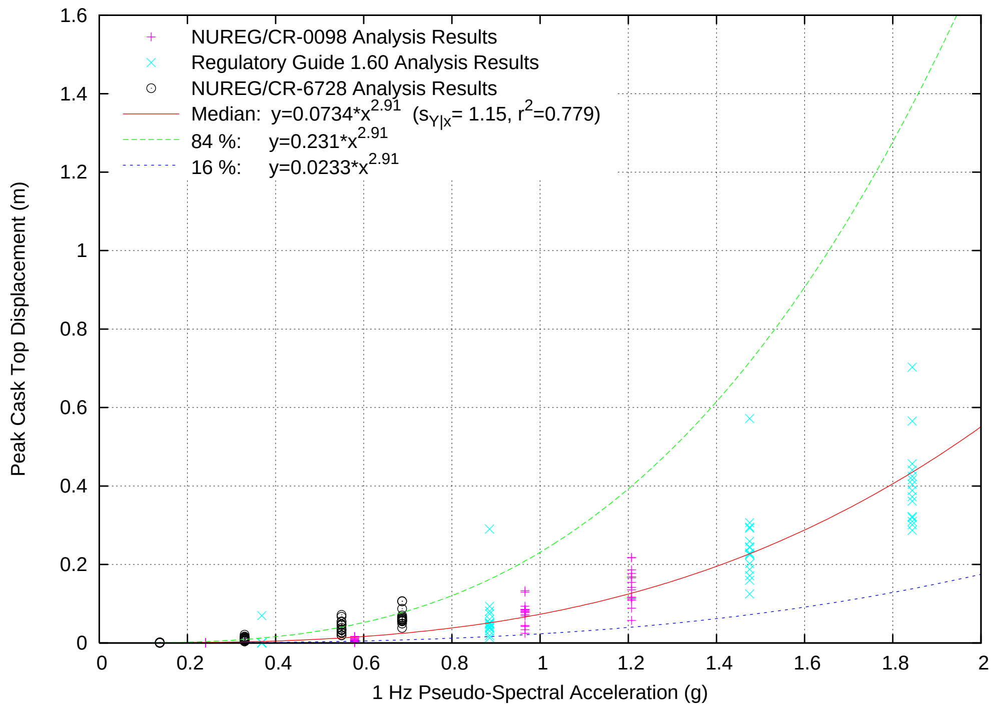

Figure 5.27: Peak Top Displacement Regression Fit in Terms of 1 Hz PSA, Linear Scale, Rectangular Module, All Earthquakes, Cask/Pad μ=0.55, All Soil Profiles

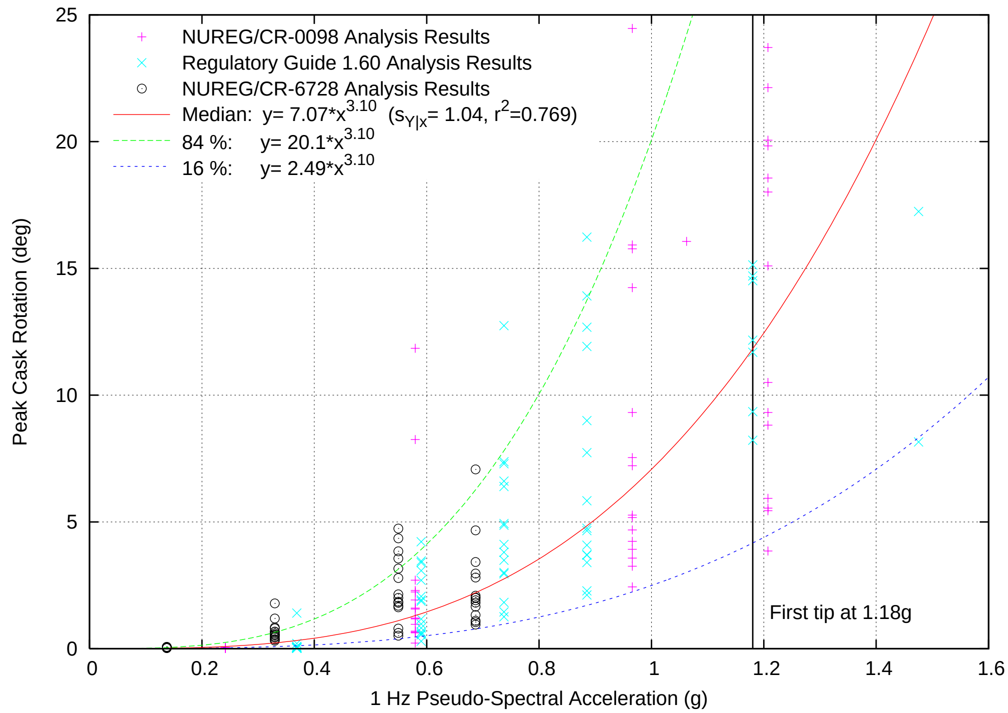

Figure 5.28: Peak Rotation Regression Fit in Terms of 1 Hz PSA, Linear Scale, Cylindrical Cask, All Earthquakes, Cask/Pad μ=0.55, All Soil Profiles

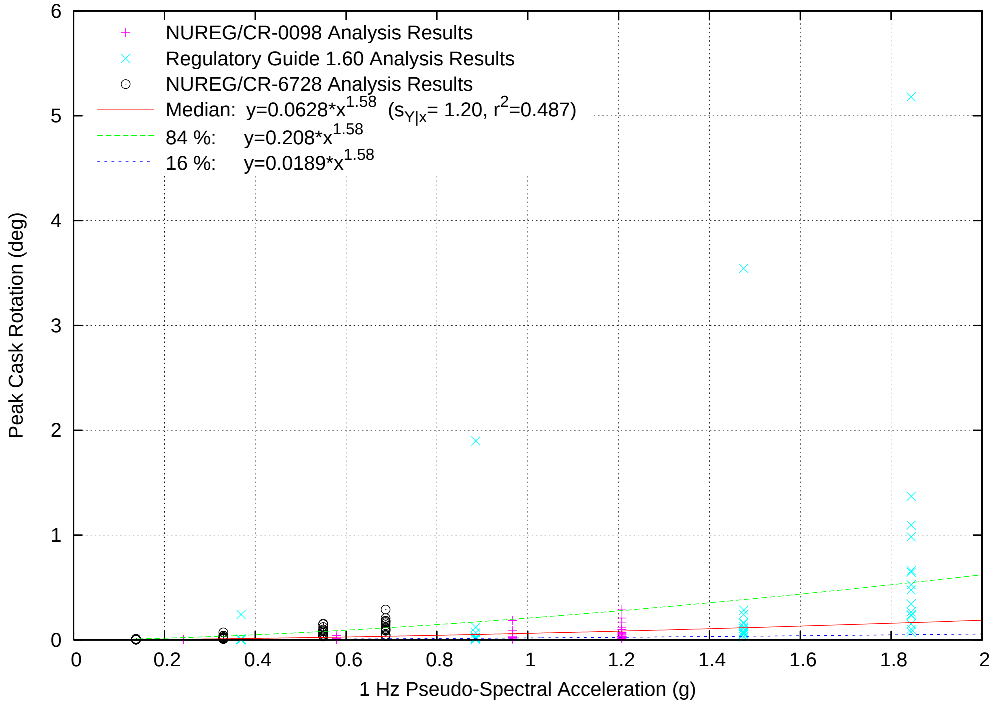

Figure 5.29: Peak Rotation Regression Fit in Terms of 1 Hz PSA, Linear Scale, Rectangular Module, All Earthquakes, Cask/Pad μ=0.55, All Soil Profiles

The quality of the regression fits using the 5% damped 1 Hz PSA as the ground motion parameter is consistently higher than that of the fits where the PGV was used. The r^2 parameter is consistently higher, and the confidence bands are consistently narrower for the fits produced using the 1 Hz PSA. Because of this, and the fact that using a pseudo-spectral acceleration at a given frequency provides a much more direct path from a design spectrum to determine the cask response, the 1 Hz PSA appears to be the most suitable parameter to characterize the ground motion for these general nomograms. A complete set of fitted curves for each of the cask designs and friction coefficients is provided in Appendix VI, plotted on both logarithmic and linear scales. These can be used as nomograms to evaluate the response of casks subjected to earthquakes that conform to response spectra that may differ from those used in this study. The curve fitting coefficients for these nomograms are tabulated in Appendix VII, and example problems are provided to illustrate the application of these nomograms to a site-specific application.

5.5.3 Discussion and Limitations of Nomograms

The fitted curves describing the cask response in terms of the PGV or 1 Hz PSA are based on the three selected spectral shapes. While these ground motion parameters are both far better indicators of the cask response under an arbitrary spectral shape than the PGA, they are still both simple measures of very complex phenomena. If it is desired to apply the results of this study to a different spectral shape with similar characteristics, one could determine the pseudo-spectral acceleration at 1 Hz and use the fitted curves presented in Appendix VI to apply the results of this study to that application.

The curve fits for the peak cask top displacements are of reasonable quality, although not as good as the separate fits for the individual spectral shapes. Since the quality of the fitted curves is lower when the three spectral shapes are combined, the fitted curves for the individual spectral shapes in terms of PGA should be used if the desired ground motion conforms to one of the spectral shapes.

It should be noted that there is more scatter in the peak cask rotation results, especially for the rectangular module. The curve fits are sometimes quite poor for the rotation results, especially in cases where the response is dominated by sliding rather than by tipping. The rotation response is generally quite low in these cases, but in many of these cases, there are several outlying analysis results that are significantly higher than the 84% confidence curve. While this is certainly a concern, it is important to keep in mind that the rotations are still generally quite low in these cases. Requiring a higher confidence level in the design would not likely be a significant penalty in these cases because the response would still be quite low.

The three spectral shapes used in this study are the NUREG/CR-0098, Regulatory Guide 1.60, and NUREG/CR-6728 spectral shapes. Plots of these spectral shapes were provided for the lateral motion in Figure 4.2 and Figure 4.3, and the spectral shape of the vertical component of the motion was provided in Figure 4.4. This strategic selection of spectral shapes provides a reasonable representation of their practical range of application. Based on the results from these spectra, the 5% damped 1 Hz PSA appears to be a reasonable parameter to characterize the effect that an earthquake would have on a cask system. Series of analyses using a much broader range of spectra would be required to validate this approach for spectral shapes that deviate significantly from those used in this study. Judgment is certainly required in applying these results to site-specific spectra that have different shapes than those used in this study. The degree of confidence required for a specific application should be increased as a function of the amount of deviation of the shape of the response spectrum from the shape of those used in this study.

The results represented by these regression fits are for two specific cask designs having the characteristics outlined in Section 3.2.1.1 for the vertical cylindrical cask and Section 3.2.2.1 for the rectangular module. These casks have characteristics fairly typical of those designs in common use. The aspect ratio, defined here as ½ of the shortest dimension of the base divided by the height of the center of gravity (CG) from the base, is one of the most important parameters affecting the stability of the cask. For cylindrical casks, the ½ base width dimension is simply the radius of the cask base. Table 5.7 provides a listing of the ½ base width, CG height, and aspect ratio for storage casks approved by the NRC as of September 2004. The properties are not listed for the Advanced NUHOMS 24PT1 because it is a special case. That system, which was designed for regions of high seismicity, employs multiple horizontal modules, which are attached together, significantly increasing the effective aspect ratio. As a result, sliding would be a greater concern than tipping for seismic evaluations of that system.

From Table 5.7, it can be seen that the aspect ratio of the NRC-approved storage cask designs ranges from 0.43 to 0.68. The cylindrical casks and rectangular modules used in this parametric study have aspect ratios of 0.56 and 0.58, respectively, so they are approximately midway between the extreme upper and lower bounds of the NRC-approved casks. Because stability increases as the aspect ratio increases, it would be conservative to apply the results of this study to casks with higher aspect ratios. Applying these results to casks with lower aspect ratios might be nonconservative and should be done only with extreme care.

Table 5.7: NRC-Approved DCSS (September 2004) – General Use

Vendor	Model Name	Certificate of Compliance Issue Date (Docket)	½ Base Width, *r* m (in)	Height of CG, h_{cg} m (in)	Aspect Ratio, r/h_{cg}
General Nuclear Systems, Inc.	CASTOR V/21	08/17/1990 (72-1000)	1.20 (47.25)	2.44 (96.2)	0.49
NAC International, Inc.	NAC S/T	08/17/1990 (72-1002)	1.19 (47.0)	2.26 (88.8)	0.53
NAC International, Inc.	NAC-C28 S/T	08/17/1990 (72-1003)	1.19 (47.0)	2.26 (88.8)	0.53
BNFL Fuel Solutions Corp.	VSC-24	05/07/1993 (72-1007)	1.68 (66.0)	2.79 (109.9)	0.60
Transnuclear Inc.	TN-24	11/04/1993 (72-1005)	1.20 (47.4)	2.23 (87.8)	0.54
Transnuclear, Inc.	NUHOMS-24P NUMOMS-52B NUHOMS-61BT NUHOMS-24PHB NUHOMS-32PT	01/23/1995 (72-1004)	1.47 (58.0)	2.54 (100.0)	0.58
Holtec International	HI-STAR 100	10/04/1999 (72-1008)	1.22 (48.0)	2.79 (109.9)	0.44
NAC International, Inc.	NAC-MPC	04/10/2000 (72-1025)	1.63 (64.0)	2.50 (98.5)	0.65
Transnuclear, Inc.	TN-32	04/19/2000 (72-1021)	1.24 (49.0)	2.41 (94.9)	0.52
Transnuclear, Inc.	TN-68	05/28/2000 (72-1027)	1.07 (42.25)	2.47 (97.2)	0.43
Holtec International	HI-STORM 100	06/01/2000 (72-1014)	1.68 (66.25)	3.00 (118.2)	0.56
NAC International, Inc.	NAC-UMS (Stg.)	11/20/2000 (72-1015)	1.73 (68.0)	2.94 (115.7)	0.59
BNFL Fuel Solutions Corp.	FuelSolutions WSNF-220 WSNF-221 WSNF-223	02/15/2001 (72-1026)	1.75 (69.0) 1.75 (69.0) 1.75 (69.0)	2.96 ~ 3.05 (116.4 ~ 120.1) 2.61 (102.9) 2.58 (101.6)	0.59 ~ 0.57 0.67 0.68
Transnuclear, Inc.	Advanced NUHOMS-24PT1	02/05/2003 (72-1029)	N/A	N/A	N/A

INTENTIONALLY LEFT BLANK

6. Summary

This research project investigated the seismic response of freestanding spent fuel dry cask storage systems in earthquake events. Since the dry cask system is freestanding on a concrete pad, a significant portion of the modeling effort has been focused on examining the nonlinear frictional contact algorithm at the cask/pad interface. Three-dimensional finite element coupled models of the cask/pad/foundation using the ABAQUS/Explicit code were developed to incorporate this nonlinear interfacial contact as well as the soil-structure interaction effect when evaluating the dynamic nonlinear responses of dry cask systems subjected to prescribed seismic ground motions.

The principal objective of the research project was to perform parametric analyses, using the coupled response models and a selected group of input parameters, to provide to cask design licensing reviewers and applicants a set of generic responses of dry cask systems. Prior to conducting the parametric study, the coupled response models were closely examined and evaluated through performing three site-specific analyses including the three-module rectangular Transnuclear West module/cask, and HI-STORM 100 casks at Hatch Nuclear Power Station and at Private Fuel Storage Facility. Since the relevancy and usefulness of the parametric analysis results depend very much on the input parameters, an elaborate procedure was adopted in identifying them and in selecting their appropriate ranges of variation.

Key input parameters include cask designs, foundation types, coefficients of friction at cask/pad interface, and earthquake ground motions at different PGA (peak ground acceleration) levels conforming to selected spectral shapes. There is a huge matrix of input variables for the pool of input parameters, and a finite subset of this matrix was chosen in the parametric study for practical reasons. The chosen parameters include:

- 2 cask designs: A cylindrical cask with an aspect ratio of 0.56 and a rectangular module with an aspect ratio of 0.58. (The aspect ratio is defined as ½ the base diameter (for a cylindrical cask) or ½ the shorter width (for a rectangular module) divided by the height of the center of gravity from the base.)
- 3 foundation types: Soft soil, stiff soil, and rock
- 3 coefficients of friction at cask/pad interface: 0.20, 0.55, and 0.80
- 3 spectral shapes: NUREG/CR-0098, Regulatory Guide 1.60, and NUREG/CR-6728
- 5 earthquake records: NUREG/CR-0098 and Regulatory Guide 1.60:
  - 1) 1978 Iran Tabas
  - 2) 1999 Taiwan Chi-Chi
  - 3) 1992 Landers
  - 4) 1994 Northridge
  - 5) 1979 Imperial Valley

  NUREG/CR-6728:
  - A) 1985 Nahanni
  - B) 1988 Saguenay
  - C) 1979 Imperial Valley
  - D) 1989 Loma Prieta
  - E) 1994 Northridge
- 4 PGA levels: 0.25, 0.60, 1.00, and 1.25 g

Various individual studies were performed to examine the sensitivity of model results to different model details such as element types, mesh sizes, number of nodes at the edge of cask base, and friction models at the cask/pad interface. A very careful procedure was undertaken in selecting the lateral dimension and the depth of the foundation submodel with properly assigned lateral boundary conditions to demonstrate the appropriateness of using a finite submodel to simulate a semi-infinite foundation. Both explicit and implicit time integration methods were investigated in analyzing the coupled response models, and the explicit time integration method was eventually chosen because it provides very small time increments to assure the solution convergence of the highly dynamic nonlinear cask responses.

The selection of five different earthquake records conforming to the three spectral shapes and three foundation types provides a reasonable variation range of dynamic characterization of seismic ground motions. It is very important for the cask design licensing reviewers and applicants to cross compare the dynamic characterization of site-specific ground motions to those used in the parametric study. In cases with favorable comparisons, the analysis results from the parametric study could be used to guide design and review activities. Otherwise, site-specific cask response analyses might be needed to obtain results in demonstrating the adequacy of cask designs.

The parametric analysis results were examined closely to demonstrate the existence of the dynamic coupling between the dry cask system and the foundation due to the soil-structure interaction, which is one of the primary rationales for the development of coupled response models. In addition, the analysis results in free-field surface motions almost duplicate the prescribed input ground motions. These findings indicate that a reasonably proper modeling procedure has been developed in simulating a semi-infinite foundation using a finite model with appropriately prescribed boundary conditions, and in performing deconvolution analyses of surface-defined ground motions by preserving their dynamic characteristics of amplitudes and frequency contents.

The analysis results from the parametric study are expressed in terms of the peak lateral displacements at cask top and base and the peak cask angular rotation. In general, the cylindrical casks exhibit a higher amount of movements than the rectangular modules when subjected to the same level of seismicity and coefficient of friction at the cask/pad interface. This is because the base of the cylindrical cask is prone to a highly nonlinear rolling motion in an earthquake event resulting in its rather randomized trace on the concrete pad. On the other hand, the rectangular module can undergo only a rocking motion, which is inherently more stable, because of its rectangular base. In conclusion, the analysis results indicate a wide scatter of cask responses, in particular with the cylindrical casks.

Least squares regression curve fits on the cask analysis results as a function of the ground motion intensity have been performed to consolidate the widely scattered cask response results. The curve fitting plots are provided for both the peak cask top displacement and the peak cask rotation for the two cask designs, all three spectral shapes, and all three values of the cask/pad friction coefficient used in this study. The regression curve fits are plotted in terms of median cask response as well as median cask response plus and minus one standard deviation, representing 84% and 16% confidence bands, respectively. These plots are used as nomograms for evaluating the response for selected designs of casks subjected to earthquakes conforming to the spectral shapes used in the study.

The peak ground velocity (PGV) and the pseudo-spectral acceleration (PSA) at 5% damped 1 Hz frequency are the two parameters used to plots nomograms. The PGV, which is not a direct function of the spectral shape, is influenced by the spectral accelerations across the middle of the spectrum in the period range relevant to the cask response. Since the quality of the regression fits using the PSA at 1 Hz frequency as the ground motion parameter is consistently higher than that of the fits with the PGV, the PSA at 5% damped 1 Hz frequency was chosen to characterize the ground motion for the nomograms.

7. Conclusions

After an in-depth evaluation of parametric analysis results and nomograms, the following conclusions are made:

1. The cylindrical cask is less seismically stable than the rectangular module. The cylindrical cask is vulnerable seismically after it starts to roll at its base while the rectangular module is limited to a rocking motion because of its rectangular base.

2. The seismic response of cask/module is very sensitive to the coefficient of friction at the cask/pad interface, μ. In cases with low coefficients of friction such as $\mu = 0.20$, the seismic response of cask/module is governed by sliding displacement. The angular rotation of cask/module increases with μ, and it becomes a dominating contributor to the seismic response of the cask/module when $\mu = 0.80$.

3. The aspect ratio of a cask, defined here as ½ of the shortest dimension of its base divided by the height of its center of gravity, is one of the most important parameters affecting the stability of the cask. The cylindrical casks and rectangular modules used in the parametric study have aspect ratios of 0.56 and 0.58, respectively. Since cask stability increases as the aspect ratio increases, it would be conservative to apply the results of this study to casks with higher aspect ratios. Applying these results to casks with lower aspect ratios might not be conservative and should be done only with extreme care.

4. The linear elastic model is used to simulate the foundation in the coupled finite element model. Therefore, these models are not intended to provide results to address soil failure, in particular, underneath the edges of concrete pad.

5. The cask/module is seismically stable at low levels of peak ground accelerations (PGA) such as 0.25 g, as evidenced from the parametric analysis results.

6. The seismic response of cask/module is quite sensitive to foundation types at low PGA levels such as 0.25 g. However, this sensitivity diminishes with increasing PGA, as evidenced from the parametric analysis results with PGA = 0.6 g.

7. Nomograms of parametric analysis results are compiled for median response of cask/module +/- one standard deviation at a 5% damped 1 Hertz frequency (1 second period) of pseudo-spectral acceleration (PSA) after performing linear regression analyses on the pool of analysis results generated from earthquake ground motions conforming to a given spectral shape and all three foundation types. These nomograms provide seismic responses of the cask/module in term of maximum cask top sliding displacements relative to concrete pad and maximum angular rotations within the ranges of 16 and 84 percentiles.

INTENTIONALLY LEFT BLANK

8. References

1. Code of Federal Regulations, *Title 10*. January 1, 2004.

2. ABAQUS, Inc. “ABAQUS User’s Manual, Version 6.4.” 2003.

3. Luk, V. K., J. A. Smith, D. A. Aube, and R. A. Dameron. “NRC Project on Seismic Behavior of Spent Fuel Storage Cask Systems - Final Report on Seismic Analysis of Three-Module Rectangular Transnuclear West Module/Cask.” December 21, 2001.

4. Luk, V. K., J. A. Smith, D. A. Aube, R. A. Dameron, and I. P. Lam. “NRC Project on Seismic Behavior of Spent Fuel Storage Cask Systems - Final Report on Seismic Analysis of HI-STORM 100 Casks at Hatch Nuclear Power Plant.” June 28, 2001.

5. Luk, V. K., J. A. Smith, D. A. Aube, R. A. Dameron, and I. P. Lam. “NRC Project on Seismic Behavior of Spent Fuel Storage Cask Systems – Seismic Analysis Report on HI-STORM 100 Casks at Private Fuel Storage Facility, Rev 1.” March 31, 2002.

6. Newmark, N. M. and W. J. Hall. NUREG/CR-0098, “Development of Criteria for Seismic Review of Selected Nuclear Power Plants.” U.S. Nuclear Regulatory Commission: Washington D.C. May 1978.

7. Regulatory Guide 1.60, “Design Response Spectra for Seismic Design of Nuclear Power Plants.” U.S. Atomic Energy Commission, Directorate of Regulatory Standards. 1973.

8. McGuire, R. K., W. J. Silva, and C. J. Costantino. NUREG/CR-6728, “Technical Basis for Revision of Regulatory Guidance on Design Ground Motions: Hazard- and Risk-considered Ground Motion Spectra Guidelines.” U.S. Nuclear Regulatory Commission: Washington D.C. October 2001.

9. Moore, D. P., G. S. Bjorkman, and R. P. Kennedy. “Seismic Analysis of Plant Hatch ISFSI Pad and Stability Assessment of Dry Casks.” Proceedings of ICONE 8, Paper # 8499. Baltimore, MD, USA. April 2-6, 2000.

10. Hsu, P., G. V. Jones, D. P. Moore, T. H. Springfield, and D. S. Walden. “Design of Plant Hatch Independent Spent Fuel Storage Installation Pads.” Proceedings of ICONE 8, Paper # 8498. Baltimore, MD, USA. April 2-6, 2000.

11. The Final Safety Analysis Report for the Standardized NUHOMS® Horizontal Modular Storage System for Irradiated Nuclear Fuel, Rev. 6. October 2001.

12. Stevenson & Associates, Inc. “SUPER SASSI/PC User’s Manual.” May 1996.

13. Idriss, I. M. and J. I. Sun. User's Manual for SHAKE91, “A Computer Program for Conducting Equivalent Linear Seismic Response Analysis of Horizontally Layered Soil Deposits.” Program modified based on the original SHAKE program published in December 1972 by Schnabel, Lysmer, and Seed. University of California, Davis: Davis, CA. November 1992.

14. Singh, K. P., A. I. Soler, and M. G. Smith. “Predicting the Structural Response of Free-Standing Spent Fuel Storage Casks under Seismic Events.” 16th Conference on Structural Mechanics in Reactor Technology (SMiRT 16). Washington, D.C. August 12-17, 2001.

15. Holtec Proprietary Computer code DYANMO, QA Validation Manual, HI-91700. 1991.

16. Idriss, I. M. and H. B. Seed. "Seismic Response of Horizontal Layers. " *Journal of the Soil Mechanics and Foundation Division*. ASCE, Vol. 94, No. SM 4. July 1968.

17. Schnabel, P. B., J. Lysmer, and H. B. Seed. "SHAKE: A Computer Program for Earthquake Response Analysis of Horizontally Layered Sites." Report No. UCB/EERC-72/12. Earthquake Engineering Research Center, University of California: Berkeley, CA. December 1972.

18. Prevost, J. H. "DYNAFLOW: Finite Element Analysis for the Static and Transient Response of Linear and Nonlinear Two and Three Dimensional System." Princeton University: Princeton, NJ. 1996.

19. US Army Corps of Engineers. Engineer Technical Letter No. 1110-2-339. March 1993.

20. American Society of Civil Engineers (ASCE). "Seismic Analysis of Safety-Related Nuclear Structures and Commentary." ASCE: New York, NY. 1998.

21. Tennessee Valley Authority. "All Projects, Steel to Concrete Coefficient of Friction Preliminary Tests." Report No. CEB 77-46. December 5, 1977.

22. Rabbat, B. G. and H. G. Russell. "Friction Coefficient of Steel on Concrete or Grout." *Journal of Structural Engineering*. American Society of Civil Engineers, Vol. 111, No. 3, pp. 505-515: March 1985.

23. Dreher, R. C. "Friction and Wear Characteristics of Wire-Brush Skids." NASA Technical Paper 1495. National Aeronautics and Space Administration. 1979.

24. Idun, E. K. and D. Darwin. "Bond of Epoxy-Coated Reinforcement: Coefficient of Friction and Rib Face Angle." *ACI Structural Journal*, Vol. 96, No. 4, pp. 609-615: July-August 1999.

25. Baltay, P. and A. Gjelsvik. "Coefficient of Friction for Steel on Concrete at High Normal Stress." *Journal of Materials in Civil Engineering*. ASCE, Vol. 2, No. 1, pp. 46-49: February 1990.

26. Olofsson, U. and M. Holmgren. "Friction Measurement at Low Sliding Speed Using a Servohydraulic Tension-torsion Machine." *Experimental Mechanics*. Vol. 34, No. 3, pp. 202-207: September 1994

27. Housner, G. W. "The Behavior of Inverted Pendulum Structures During Earthquakes." *Bulletin of the Seismological Society of America*. Vol. 53, No. 2, pp. 403-417: February 1963.

28. Ang, A. H-S. and W. H. Tang. *Probability Concepts in Engineering Planning and Design, Volume I-Basic Principles*. John Wiley & Sons: New York. 1975.